

Characterization of Synaptotagmin 7 function in neurotransmission and its subcellular localization at synapses

By

Mónica C. Quiñones-Frías

B.S. Cellular and Molecular Biology
University of Puerto Rico Río Piedras Campus, 2014

SUBMITTED TO THE DEPARTMENT OF BIOLOGY IN PARTIAL
FULFILLMENT OF THE REQUIREMENTS FOR THE DEGREE OF

DOCTOR OF PHILOSOPHY IN BIOLOGY
AT THE
MASSACHUSETTS INSTITUTE OF TECHNOLOGY

MAY 2020

© 2020 Mónica C. Quiñones-Frías. All Rights Reserved.

The author hereby grants to MIT permission to reproduce and to distribute publicly paper and electronic copies of this thesis document in whole or in part in any medium now known or hereafter created.

Signature of Author: _____
Department of Biology
May 4, 2020

Certified by: _____
Dr. J. Troy Littleton
Menicon Professor of Biology and The Picower Institute for Learning and Memory
Thesis Supervisor

Accepted by: _____
Dr. Stephen P. Bell Professor
Biology Chairman of the Graduate Committee

Acknowledgements

During my time at MIT I've come across many people that have become my lifetime friends and have shaped my experience for the best. First, I want to thank my advisor, Troy, for giving me the opportunity to join his lab and giving me this project. I will forever be indebted to him because he helped me pave the way to achieve my dream of being a scientist. I also want to thank Yulia, without her mentorship every step of the way I would have not been able to do half of the experiments in this thesis. I want to thank Dina for her tireless efforts to keep our lab in the best shape and deeply caring for every single one of us. Dina is the best lab manager in the world! I also want to thank Shirley for being my mentor and friend. To the rest of the lab, I want to thank you for all the good times we've had throughout the years.

Above all, I want to thank my family and friends for their love and support because when times were hard they were always there for me. I want to thank my parents and sister for always given me unconditional support. They've always believed in my potential and encouraged me to never give up to achieve my dreams. I want to give a special thanks to my friends, Gal and Shaul, for countless hours of backgammon and eating udon. Finally, I want to thank my fiancé Josh. He's my best friend and I love him with all my heart. After a long day in lab, the best part was that I got to hang out with you.

Characterization of Synaptotagmin 7 function in neurotransmission and its subcellular localization at synapses

By Mónica C. Quiñones-Frías

Synaptic vesicle (SV) fusion is dependent on proteins that can sense Ca^{2+} and trigger fusion with the plasma membrane. Neurotransmitter release occurs during a rapid synchronized phase of SV fusion mediated by the Ca^{2+} sensor Synaptotagmin 1 (SYT1). A slower SYT1-independent asynchronous phase is also present at many synapses and has been hypothesized to be mediated by another Synaptotagmin, SYT7. To determine if SYT7 plays an evolutionarily conserved role as an asynchronous Ca^{2+} sensor, we used the CRISPR-Cas9 system to generate mutations in the *Syt7* locus and introduced tags to label the endogenous protein in *Drosophila*. Electrophysiology, FM1-43 analysis and quantal imaging revealed that release probability is elevated 2-fold at larval neuromuscular junctions (NMJs) in *Syt7* mutants. No structural changes were identified that could contribute to the elevated evoked response. *Syt1/Syt7* double mutants also display more release than *Syt1* mutants alone, indicating SYT7 is not the asynchronous release Ca^{2+} sensor. *Syt7* mutants display a larger pool of releasable vesicles during high frequency stimulation and a faster recovery of releasable SVs following stimulation, suggesting SYT7 is likely to regulate SV trafficking. Endogenously-tagged SYT7 localizes to a presynaptic membrane compartment called the peri-active zone that has been implicated in SV endocytosis and recycling. SYT7 forms an internally connected presynaptic membrane compartment that surrounds and contacts a host of other intracellular compartments, including endosomes, ER and lysosomes.

In addition to regulating asynchronous release, SYT7 is also known to regulate facilitation and vesicle replenishment. Heterogeneity of SYT7 functions across neurons could arise from posttranslational modification of SYT7 at synapses or differential expression of SYT7 across different neuronal populations. The *Drosophila* NMJ serves as an ideal model synapse to study how SYT7 regulates SV fusion in different neuronal types because muscle contraction is regulated by two glutamatergic motor neuron populations that exhibit tonic and phasic electrophysiological properties. Preliminary data suggests that SYT7 levels might differentially regulate release probability in tonic and phasic neurons at NMJs. In addition, initial structure function studies of SYT7's C2 domains suggest they redundantly aid in trafficking SYT7 to nerve terminals, but are also required for normal stability of the protein.

Advisor: J. Troy Littleton, Menicon Professor of Biology and The Picower Institute for Learning and Memory

Table of Contents

Cover page	1
Acknowledgments	3
Abstract	5
Chapter 1: Introduction	9
Neurotransmission	10
SV fusion	13
Synaptotagmins are calcium sensors for SV fusion.....	17
The Drosophila Neuromuscular Junction as a model synapse to study the role of SYT7 in neurotransmission	24
References	26
Figures	36
Chapter 2: Drosophila Synaptotagmin 7 negatively regulates synaptic vesicle release and replenishment in a dosage-dependent manner.....	43
Introduction	44
Results	49
Discussion	67
Materials and Methods	75
References	86
Figures	97
Chapter 3: Characterization of differential SYT7 expression in tonic versus phasic neurons and the trafficking properties of mutant C2 domain SYT7 proteins.....	129
Introduction	130
Results	133
Discussion	137
Materials and Methods	140
References	143
Figures	145
Chapter 4: Conclusions and Future Directions.	151
Main Conclusion	152
Future Directions	153
References	159
Appendix: Increasing in vivo fluorescence of endogenous SYT7 using the Split-GFP system.	161

Results	162
References	164
Figures	165

Chapter 1: Introduction

Mónica C. Quiñones-Frías

I. Neurotransmission

1.1 Synapses are sites of neuronal communication in the nervous system

The nervous system relies on the regulated secretion of neurotransmitter molecules to transfer information across excitable cells through a process known as neurotransmission. This takes place at specialized junctions called synapses where neurotransmitters are released from the axon terminal of the presynaptic neuron to activate the postsynaptic cell (Südhof and Rizo, 2011) (**Figure 1**). In the presynaptic axon terminal, neurotransmitters are packaged into synaptic vesicles (SVs) that subsequently fuse with the plasma membrane following an action potential (Rizzoli, 2014). SV fusion leads to the release of neurotransmitters into the synaptic cleft that diffuse to the plasma membrane of the postsynaptic compartment to bind ligand-gated receptors that regulate the activity of the downstream neuron (Smart and Paoletti, 2012). Neurons can also form a different kind of junction that allows the passive flow of ions and small molecules to regulate the activity of excitable cells called electrical synapses (Pereda, 2014). The plasma membranes of the presynaptic and postsynaptic compartments at electrical synapses are linked together through gap junctions. The main focus of this thesis is on how SV trafficking and release is regulated in the presynaptic terminal at *Drosophila melanogaster* neuromuscular junctions (NMJs) by a member of the Synaptotagmin superfamily, Synaptotagmin 7 (SYT7).

1.2 SV pools

Depending on the species and synapse in question, presynaptic terminals can contain from ~100 SVs to many thousands, but only a small fraction of the SV population fuse during an evoked response (Rizzoli and Betz, 2005). SVs that are available to fuse during evoked stimuli form part

of the readily releasable pool (Rizzoli and Betz, 2005) (**Figure 2**). SVs in the readily releasable pool are docked and primed at fusion sites called active zones until release is triggered during an evoked response (Kaeser and Regehr, 2017; Sühof, 2012). As nerve stimulation depletes the readily releasable pool, it is replenished by SVs in the recycling pool (Rizzoli and Betz, 2005). Together, the readily releasable pool and the recycling pool comprise 10-20% of all SVs at nerve terminals. The other 80-90% of SVs is known as the reserve pool (Rizzoli and Betz, 2005). This pool is recruited for fusion when the recycling pool is depleted during periods of long stimulation (Denker and Rizzoli, 2010; Rizzoli and Betz, 2005). Defining each pool gives the illusion that they are physically separated from each other but increasing evidence suggests that the reserve and recycling pools are intermixed (Alabi and Tsien, 2012; Denker and Rizzoli, 2010).

The recruitment of SVs into each pool relies on interactions with proteins associated with active zones and the actin cytoskeleton. Active zone proteins interact with SVs to molecularly dock and prime them for fusion. In particular, the active zone protein Munc-13 is essential for rendering SVs fusion competent. Munc-13 mutants lack neurotransmission even though SVs are found near the membrane, suggesting priming is impaired in these mutants (Aravamudan et al., 1999; Imig et al., 2014). It is thought that Munc-13 is crucial for establishing the SV population that form the readily releasable pool (Kaeser and Regehr, 2017). In addition to Munc-13, other active zone proteins have been found to affect the size of the readily releasable pool though to a lesser extent (Körber and Künér, 2016). Recruitment of SVs into the readily releasable pool is dependent on actin polymerization and the phosphorylation state of Synapsin (Körber and Künér, 2016; Rizzoli, 2014). Synapsin is a small cytosolic protein that tethers SVs to the actin

cytoskeleton and becomes phosphorylated to release SVs to replenish the readily releasable pool and recycling pool during nerve stimulation (Denker and Rizzoli, 2010; Rizzoli, 2014).

1.3 Neurotransmission is modulated by short-term plasticity

Neurons can modulate the number of SVs that fused during stimulation by enhancing or decreasing their synaptic strength through a phenomenon called short-term plasticity. Different patterns of nerve stimulation can induce short-term plasticity that may last from milliseconds to minutes. Facilitation is a type of synaptic enhancement induced by paired stimuli occurring within milliseconds of each other that results in a transient increase of neurotransmitter release that decays after ~100 milliseconds. Sustained nerve stimulation can trigger longer forms of synaptic enhancement known as augmentation and post-tetanic potentiation that decay after 5-10 seconds and 30-60 seconds, respectively. A decrease in synaptic strength can be observed at some synapses after paired stimuli or longer periods of nerve stimulation that collectively is termed depression (Catterall and Few, 2008; Zucker and Regehr, 2002).

Neurons possess intrinsic properties that favor facilitation or depression. This is observed in phasic and tonic neurons of NMJs in crayfish, *Drosophila* and mammals (Hennig and Lømo, 1985; Kennedy and Takeda, 1965a, 1965b; Kurdyak et al., 1994). Upon train stimulation, phasic neurons depress while tonic neurons facilitate. Phasic neurons depress because SV fusion sites have a high release probability resulting in less SVs available for fusion during the second stimulus response. In contrast, tonic neurons facilitate because they have a low release probability resulting in more SVs available for fusion during the second stimulus (Regehr, 2012; Zucker and Regehr, 2002). Even though synapses typically exhibit tonic or phasic properties, the initial release

probability at most synapses is not fixed and can be adjusted by altering extracellular calcium concentrations to manipulate the initial release probability, allowing the same synapse to exhibit either facilitation or depression (Jorquera et al., 2012; Mallart, 1993; Regehr, 2012).

Synaptic enhancement and depression are primarily regulated by intrinsic properties in the presynaptic compartment that establish the release probability of release sites. Facilitation can result from calcium channel facilitation, saturation of calcium buffers, activation of a calcium sensor that regulates the fusion of a specific SV population and increased residual calcium. In addition to these presynaptic changes, augmentation and post tetanic potentiation can result from an increased readily releasable pool and vesicle to vesicle fusion to increase neurotransmitter release (Catterall and Few, 2008; Fioravante and Regehr, 2011; Jackman and Regehr, 2017; Regehr, 2012; Zucker and Regehr, 2002). In contrast, depression can result from calcium channel inactivation, depletion of the readily releasable pool, active zone inactivation and slow replenishment of SVs (Catterall and Few, 2008; Fioravante and Regehr, 2011; Regehr, 2012; Zucker and Regehr, 2002). In some neurons, synaptic depression has also been associated with postsynaptic changes such as desensitization of ligand-gated receptors (Zucker and Regehr, 2002).

II. SV fusion

2.1 Evoked SV fusion

To trigger SV fusion after an evoked response, the plasma membrane of the presynaptic terminal must become permeable to calcium ions (Katz and Miledi, 1967). Depolarization of the presynaptic terminal opens voltage-gated calcium channels in the plasma membrane to allow

extracellular calcium into the cell (Catterall and Few, 2008; Stanley, 1993). Voltage-gated calcium channels are concentrated at active zones in the plasma membrane. Active zones cluster calcium channels and prime SVs for fusion to ensure fast neurotransmitter release (Sühof, 2012). Once a SV fuses, lipids and proteins from the SV are endocytosed adjacent to the active zone in the periaxial zone to replenish the SV pool and prepare for the next round of fusion (Saheki and De Camilli, 2012).

The duration of an evoked response can last up to 100-200 milliseconds that is divided in two kinetic phases known as **synchronous** and **asynchronous release** (Kaeser and Regehr, 2014) (**Figure 3**). The synchronous phase accounts for most of the neurotransmitter released and decays within a few milliseconds. The asynchronous phase (also known as the delayed response) is much slower and decays after 100-200 milliseconds (Goda and Stevens, 1994; Katz and Miledi, 1969). In most neurons, asynchronous release makes up less than 10% of the total neurotransmitter release at low frequency stimulation although in some synapses asynchronous release can account for 80% of total release (Hefft and Jonas, 2005; Kaeser and Regehr, 2014). In synapses where asynchronous release is not predominant, it can be enhanced by periods of high frequency stimulation, temperature and nerve stimulation in the presence of strontium (Atluri and Regehr, 1998; Hubbard, 1963; Huson and Regehr, 2020; Lu and Trussell, 2000; Rahamimoff and Yaari, 1973).

2.2 Spontaneous SV fusion

SVs can also fuse in the absence of nerve stimulation (Fatt and Katz, 1952). Spontaneous events were discovered at the frog neuromuscular junction and were initially dismissed as

electrophysiological noise from tears in the muscle after improper dissection. Further study of spontaneous events led to the proposal of the quantal hypothesis of neurotransmission that suggests spontaneous events represent the fusion of a single “quanta”, while an evoked response is the fusion of many of these quanta at the same time (del Castillo and Katz, 1954; Fatt and Katz, 1952). Later it was discovered that these quanta are neurotransmitter-filled SVs at axon terminals (De Robertis and Bennet, 1955; Palay, 1956). Like evoked release, spontaneous release plays important physiological roles in neurons, such as regulating synapse formation, homeostatic plasticity and activating different forms of synaptic plasticity (Kaeser and Regehr, 2014; Ramirez and Kavalali, 2011). In contrast to evoked release, spontaneous events have been found to be both calcium-dependent and independent (Kaeser and Regehr, 2014). Differences in the spatial segregation and recycling pathways have also been found between SVs that fuse through evoked or spontaneous release (Fredj and Burrone, 2009; Kavalali, 2015; Sabeva et al., 2017; Sara et al., 2005). This suggests that the SVs that fuse during evoked and spontaneous release may be molecularly distinct. More work is required to define the molecular signatures that define SVs that fuse during evoked or spontaneous release.

2.3 The SNARE complex is the molecular machine that drives SV fusion

The SNARE complex is a molecular machine formed by a group of proteins in the plasma membrane and SV membrane that drives bilayer fusion. The SNARE complex is composed of the vesicle (v)-SNARE, Synaptobrevin (nSYB), and the target membrane (t)-SNAREs, Syntaxin1a (SYX1a) and SNAP-25 (for “Synaptosomal-Associated Protein, 25kDa”) (**Figure 4**). They were identified as the cleavage targets that blocked neurotransmitter release after treatments with clostridial botulinum and tetanus toxins (Blasi et al., 1993a, 1993b; Link et al., 1992; Schiavo et

al., 1992). nSYB is tethered to the SV by a single pass transmembrane domain. At the plasma membrane, SYX1a is tethered by a single pass transmembrane domain and SNAP-25 is tethered intracellularly through a palmitoyl side chain (Rizo and Rosenmund, 2008; Südhof and Rizo, 2011). Together they form a stable four helix bundle assembled from a helix provided by nSYB, a helix from SYX1a and two helices from SNAP-25. Formation of this complex is thought to drive full fusion of the SV with the plasma membrane to release their neurotransmitter contents into the synaptic cleft (Rizo and Rosenmund, 2008; Südhof and Rizo, 2011).

Primed SVs are predicted to contain a “partially zippered” trans-SNARE complex prior to fusion that can quickly assemble into the full coiled-coil bundle as release is triggered. During bilayer fusion, the SNARE complex initiates the formation of a fusion pore made from proteins and lipids in the SV and the plasma membrane (Bao et al., 2016). Both membranes are partially merged by the pore to allow diffusion of neurotransmitter molecules from the lumen of the SV into the synaptic cleft (Chang et al., 2017; Rizo and Rosenmund, 2008). If the fusion pore closes rapidly, a form of release known as kiss and run occurs and full collapse of the SV is not observed (Alabi and Tsien, 2013). However, it is thought that the major mode of SV fusion occurs when expansion of the fusion pore leads to the complete fusion and collapse of the SV membrane into the plasma membrane (Chang et al., 2017; Rizo and Rosenmund, 2008). Once fusion is completed the fully zippered cis-SNARE complex is dissociated by an ATPase called NSF (for “N-ethylmaleimide sensitive factor”). Once disassembled, chaperones bind to each dissociated SNARE to prevent re-formation of the cis-SNARE complex until the next round of fusion (Rizo and Rosenmund, 2008; Südhof and Rizo, 2011).

III. Synaptotagmins are calcium sensors for SV fusion

3.1 SYT1 regulates synchronous SV fusion

At active zones, calcium builds up to micromolar concentrations to activate calcium sensing proteins to trigger SV fusion on a millisecond timescale (Llinás et al., 1992; Regehr, 2012). The SNARE complex can promote the fusion of membranes *in vitro*, but the complex itself does not possess intrinsic calcium sensitivity and fusion rates mediated solely by the SNAREs are much slower than those observed in neurons (Weber et al., 1998). Synaptotagmin 1 (SYT1) is the primary calcium sensor activated during an evoked response that couples calcium influx to the zippering of the SNARE complex to drive SV fusion in neurons and some neurosecretory cells (Chapman, 2008) (**Figure 4**). Neurotransmission is acutely reduced in *Syt1* mutants because the synchronous component of neurotransmitter release is abolished (Fernández-Chacón et al., 2001; Geppert et al., 1994; Littleton et al., 1994; Yoshihara and Littleton, 2002) (**Figure 5C**). *Syt1* mutants exhibit higher rates of spontaneous fusion suggesting it also serves as a molecular clamp to prevent fusion of docked SVs in the absence of nerve stimulation and calcium influx (Chicka et al., 2008; Littleton et al., 1993; Xu et al., 2009). However, asynchronous release is elevated in *Syt1* mutants suggesting that SYT1 is not the sole calcium sensor that drives SV fusion during an evoked response. SYT1 is enriched in the brain and found on SVs, and is highly conserved across evolution (Adolfson et al., 2004; Perin et al., 1991b, 1991a, 1990). SYT1 contains a single-pass transmembrane domain, a short linker and two calcium sensing C2 domains, termed C2A and C2B (Perin et al., 1991a). Each C2 domain is composed of a beta barrel formed from 4 antiparallel beta strands with protruding loops that contain 5 negatively charged residues that bind calcium ions (Adolfson et al., 2004; Chapman, 2008; Shao et al., 1996) (**Figure 5A-B**). The loops in each C2

domain of SYT1 creates a calcium binding pocket that binds 3 calcium ions in C2A and 2 calcium ions in C2B.

To drive bilayer fusion, SYT1 interacts with the plasma membrane and the SNARE complex in a calcium-dependent manner. In the absence of calcium, SYT1 has low affinity for the plasma membrane but can bind to PIP2 present in the plasma membrane through a polybasic stretch found in C2B, which is predicted to “steer” SYT1 to the correct location and increase its membrane penetration during an evoked response (Bai et al., 2004; Chapman, 2008; Chapman and Davis, 1998; Chapman and Jahn, 1994; Davletov and Sudhof, 1993; Fernandez et al., 2001; Li et al., 1995; Ubach et al., 1998; S. Wang et al., 2016; Zhang et al., 1998). Once SYT1 binds calcium, the calcium binding loops in each C2 domain penetrate the plasma membrane to bring the SV closer for bilayer fusion (Chapman, 2008; Chapman and Davis, 1998; Fernández-Chacón et al., 2001; Pang et al., 2006a; Shin et al., 2009). At the same time, the C2B domain of SYT1 interacts with t-SNAREs, SYX1a and SNAP-25, to aid in formation of the fusion pore and promote its expansion to drive full collapse of the SV (Das et al., 2020; Wang et al., 2001; Zhou et al., 2015). Structure function studies of SYT1 have revealed that C2B is essential for regulating synchronous release while C2A functions to inhibit asynchronous release (Desai et al., 2000; Guan et al., 2017; Mackler et al., 2002; Schupp et al., 2016; Yoshihara et al., 2010; Zhou et al., 2015). SYT1 is a multifunctional protein that regulates other neuronal processes in addition to regulating evoked release. SYT1 interacts with the endocytic machinery to promote SV retrieval after exocytosis (Grass et al., 2004; Li et al., 2017; Yao et al., 2012; Zhang et al., 1994). SYT1 has also been shown to regulate the delivery of AMPA receptors (a ligand-gated receptor) in the postsynaptic compartment of mammals during long-term potentiation (Wu et al., 2017).

3.2 Synaptotagmins are enriched in the nervous system and regulate membrane trafficking

SYTs are a family of membrane-trafficking proteins mostly expressed in the nervous system although expression in non-neuronal tissues has been observed for some isoforms (Hudson and Birnbaum, 1995; Mittelsteadt et al., 2009; Poser Von and Südhof, 2001; Sugita et al., 2001; Xiao et al., 2010). All SYTs possess a single-pass transmembrane domain, a variable linker and two C2 domains, termed C2A and C2B (Adolfson et al., 2004; Brewer et al., 2015; Fernandez et al., 2001; Sutton et al., 1995; Zhou et al., 2015). There are 16 SYT isoforms in mammals and 7 in *Drosophila* (Adolfson et al., 2004; Bhalla et al., 2005; Craxton, 2010, 2004; Gustavsson et al., 2008). Gene duplication of many mammalian SYT homologs is responsible for the discrepancy in the number of isoforms observed between vertebrates and invertebrates (Craxton, 2010, 2004). For example, SYT1 mediates all forms of synchronous release in *Drosophila* while in mammals SYT1, SYT2 and SYT9 serve this role (Marquhze et al., 1995; Pang et al., 2006b).

SYTs with conserved calcium binding in each C2 domain regulate exocytosis in a calcium-dependent manner. As previously described, SYT1 homologs regulate the synchronous phase during evoked release and dense core vesicle (DCV) fusion in endocrine cells (Chapman, 2008; Fernández-Chacón et al., 2001; Fukuda, 2004; Geppert et al., 1994; Iezzi et al., 2005; Littleton et al., 1994; Xu et al., 2007; Yoshihara and Littleton, 2002). SYT3 is an isoform specific to vertebrates that regulates the internalization of AMPA receptors in a calcium-dependent manner to weaken synaptic strength (Awasthi et al., 2019). In *Drosophila*, SYT4 regulates retrograde signaling to regulate synaptic strength and structure after strong stimulation (Barber et al., 2009;

Cho et al., 2015; Harris et al., 2016; Korkut et al., 2013). SYT7 regulates SV fusion in neurons, and modulates lysosome and DCV fusion in endocrine cells (Bacaj et al., 2013; Chakrabarti et al., 2003; Chen et al., 2017; Fukuda et al., 2004; Gao et al., 2000; Gustavsson et al., 2008; Jackman et al., 2016; Luo et al., 2015; Luo and Südhof, 2017; Martinez et al., 2000; Rao et al., 2004; Reddy et al., 2001; Wen et al., 2010).

SYTs that don't bind calcium are less studied but can also play important roles in neuronal physiology. Mammalian SYT4 does not bind to calcium like the *Drosophila* homolog, suggesting that these isoforms have diverged in how they regulate membrane trafficking (Dai et al., 2004; Wang and Chapman, 2010). Mammalian SYT4 has been shown to control dense core vesicle trafficking and release of the neurotrophic factor BDNF (Bharat et al., 2017; Dean et al., 2009). SYT11 regulates endocytosis and *Syt11* mutants have defects in long-term potentiation (Ferguson et al., 2004; Shimojo et al., 2019; C. Wang et al., 2016). A recent study found that SYT13 delays muscle degeneration in mouse models of ALS (Amyotrophic Lateral Sclerosis) and SMA (Spinal Muscle Atrophy) (Nizzardo et al., 2020).

3.3 The many roles of SYT7 in regulating SV fusion

The discovery that SYT1 regulates synchronous release raised the possibility that other members of the SYT family might act as the asynchronous release calcium sensor. Of the SYT isoforms, SYT7 emerged as an intriguing candidate because it has biochemical features resembling the asynchronous release calcium sensor, such as high affinity to calcium and loose coupling to voltage-gated calcium channels at active zones (Atluri and Regehr, 1998; Bhalla et al., 2005; Cummings et al., 1996; Geppert et al., 1994; Goda et al., 1994; Hui et al., 2005; Rahamimoff and

Yaari, 1973; Van der Kloot and Molgo, 1993). Compared to SYT1, SYT7 has 400x higher affinity to calcium and tighter binding to membranes (Bhalla et al., 2005; Hui et al., 2005; Voleti et al., 2017). These features might allow SYT7 to regulate SV fusion further away from active zones and potentially contribute to asynchronous release (**Figure 6**).

Indeed, several studies suggest that SYT7 regulates asynchronous release while SYT1 regulates synchronous release (Bacaj et al., 2013; Chen et al., 2017; Luo et al., 2015; Luo and Südhof, 2017; Wen et al., 2010). Initial studies in mammals and invertebrates found that SYT7 had no role in asynchronous release (Maximov and Südhof, 2005; Saraswati et al., 2007). The attention was brought back to SYT7 by a study at zebrafish neuromuscular junctions that found asynchronous release was significantly reduced by knocking down SYT7 (Wen et al., 2010). Mammalian SYT7 was later found to regulate asynchronous release at excitatory and inhibitory neurons by knocking down SYT1 and SYT7 (Bacaj et al., 2013). SYT1 deficient neurons have enhanced asynchronous release making it easier to detect changes in this phase of release. SYT7 knockouts have also been shown to selectively impair asynchronous release (Chen et al., 2017; Luo et al., 2015; Luo and Südhof, 2017). However, the role of SYT7 in asynchronous release is still controversial, with several groups finding the kinetics of asynchronous release is altered while the total amount of release remains intact in SYT7 knockouts (Turecek and Regehr, 2019). In addition, the expression of SYT1 and not SYT7 was found to regulate the relative contributions of synchronous and asynchronous release at synapses (Turecek and Regehr, 2019).

Besides asynchronous release, SYT7 has been suggested to play multiple roles in regulating vesicle trafficking in neurons and other cells. SYT7 has been postulated to function as

the facilitation sensor at several mammalian synapses (Chen et al., 2017; Jackman et al., 2016; Luo and Südhof, 2017). Interestingly, it has been suggested that the asynchronous release sensor and the facilitation sensor could be mediated by the same mechanism (Rahamimoff and Yaari, 1973). SYT7 has also been suggested to regulate SV replenishment during high frequency stimulation (Jackman et al., 2016; Liu et al., 2014). The authors argue that the absence of asynchronous release is secondary to reduced replenishment rates observed in *Syt7* mutants because less SVs are available for this slower phase of release. This hypothesis has been challenged by others that detected no changes in SV replenishment (Luo et al., 2015). In addition, changes in the replenishment rate of the recycling and reserve pool have been reported that could lead to defects in the replenishment of the readily releasable pool (Durán et al., 2018). SYT7 along with SYT1 have also been suggested to target SVs to distinct endocytic pathways (Li et al., 2017). Besides neurons, SYT7 regulates fusion of lysosomes and DCVs in non-neuronal cells. (Chakrabarti et al., 2003; Fukuda et al., 2004; Gao et al., 2000; Gustavsson et al., 2008; Martinez et al., 2000; Rao et al., 2004; Reddy et al., 2001).

SYT7's role as the asynchronous release sensor, facilitation sensor and regulator of vesicle replenishment in neurons may not be mutually exclusive. Multiple studies have suggested SYT7 has multiple roles in regulating SV fusion at the same synapse (Chen et al., 2017; Luo and Südhof, 2017). A recent review suggests that different experimental manipulations and intrinsic synaptic properties, such as synapse-specific expression of SYT7 isoforms, could lead to heterogeneity of SYT7 function across synapses (Huson and Regehr, 2020). Although multiple phenotypes have been described, it is poorly understood how SYT7 regulates SV trafficking across synapses and more studies are needed to address this question.

SYT7 localization studies have also given inconsistent results. SYT7 has been suggested to localize to the plasma membrane, dense core vesicles and endo/lysosomal compartments (Adolfson et al., 2004; Martinez et al., 2000; Monterrat et al., 2007; Reddy et al., 2001; Schonn et al., 2008; Sugita et al., 2001). The precise location of SYT7 at synapses could shed light on how it regulates neurotransmission. For example, it would be unlikely that SYT7 is the asynchronous calcium sensor if SYT7 is exclusively found on endosomes. However, it could regulate SV replenishment from this compartment.

3.4 Similarities and differences between SYT1 and SYT7

SYT1 and SYT7 have distinct roles during evoked neurotransmitter release and endocytosis but appear to be functionally redundant in some mechanisms. SYT1 and SYT7 both serve as fusion clamps to suppress spontaneous fusion of SVs and regulate the size of the readily releasable pool (Bacaj et al., 2015, 2013; Luo and Südhof, 2017). Even though SYT1 and SYT7 are largely presynaptic, a recent study found that exocytosis of AMPA receptors during long-term potentiation is redundantly regulated by both (Wu et al., 2017). These studies suggest that SYT1 and SYT7 likely share partners that regulate aspects of vesicle trafficking through common pathways.

C2 domains in SYT1 and SYT7 do not regulate SV fusion in the same way. In contrast to SYT1, C2A in SYT7 plays a major role in regulating SV release while C2B plays a minor role (Bacaj et al., 2013; Jackman et al., 2016). Tight membrane binding occurs through the C2A domain in SYT7 and the C2B domain in SYT1, suggesting these C2 domain differences may be critical in

how the two proteins regulate neurotransmitter release (Voleti et al., 2017). However, the C2 domains from SYT1 and SYT7 are not interchangeable because SYT1/ SYT7 chimeras cannot rescue the *Syt1* mutant phenotype (Xue et al., 2010). Another known difference is that SYT7's C2A domain binds 2 calcium ions while SYT1's C2A domain binds to 3 calcium ions (Voleti et al., 2017). These findings suggest that C2 domains in SYT1 and SYT7 contain intrinsic properties shaped through evolution that provide unique features in each homolog to regulate SV fusion.

IV. The *Drosophila* Neuromuscular Junction as a model synapse to study the role of SYT7 in neurotransmission

My thesis is aimed at elucidating the conserved role of SYT7 in neurotransmission. Here I use the larval *Drosophila* neuromuscular junction (NMJ) as model synapse. This synapse is created by neuronal contacts that form axonal swellings, called boutons, with the muscle. Boutons contain active zones that appose glutamate receptors in the postsynaptic density at the muscle. The highly stereotyped nature of the NMJ makes this glutamatergic synapse a powerful model to characterize the role of SYT7 in neurotransmission. In addition, the *Drosophila* NMJ provides an extensive genetic toolkit, amenability to light and electron microscopy, and accessibility to perform electrophysiology recordings.

In Chapter 2, I describe our studies on the role of SYT7 in neurotransmission at the *Drosophila* neuromuscular junction. We found that SYT7 negatively regulates neurotransmitter release in a dosage dependent manner and resides in the peri-active zone region of the synapse. In addition, we found that *Syt7* mutants have enhanced recovery after high frequency stimulation suggesting that SVs are more fusogenic in the absence of SYT7.

In Chapter 3, I describe our studies that indicate the protein levels of SYT7 differ at tonic and phasic synapses at the *Drosophila* neuromuscular junctions. Our preliminary data suggest SYT7 may be a critical regulator for release probability primarily in tonic neurons. We also observe that mutating the calcium binding sites in the C2A and C2B domains of SYT7 redundantly affects its trafficking to terminals and may be essential for protein stability.

References

1. Adolfsen B, Saraswati S, Yoshihara M, Littleton JT. 2004. Synaptotagmins are trafficked to distinct subcellular domains including the postsynaptic compartment. *J Cell Biol* 166:249–60. doi:10.1083/jcb.200312054
2. Alabi AA, Tsien RW. 2013. Perspectives on Kiss-and-Run: Role in Exocytosis, Endocytosis, and Neurotransmission. *Annu Rev Physiol* 75:393–422. doi:10.1146/annurev-physiol-020911-153305
3. Alabi ARA, Tsien RW. 2012. Synaptic vesicle pools and dynamics. *Cold Spring Harb Perspect Biol* 4. doi:10.1101/cshperspect.a013680
4. Aravamudan B, Fergestad T, Davis WS, Rodesch CK, Broadie K. 1999. Drosophila UNC-13 is essential for synaptic transmission. *Nat Neurosci* 2:965–971. doi:10.1038/14764
5. Atluri PP, Regehr WG. 1998. Delayed release of neurotransmitter from cerebellar granule cells. *J Neurosci* 18:8214–8227. doi:10.1523/jneurosci.18-20-08214.1998
6. Awasthi A, Ramachandran B, Ahmed S, Benito E, Shinoda Y, Nitzan N, Heukamp A, Rannio S, Martens H, Barth J, Burk K, Wang YT, Fischer A, Dean C. 2019. Synaptotagmin-3 drives AMPA receptor endocytosis, depression of synapse strength, and forgetting. *Science* (80-) 363. doi:10.1126/science.aav1483
7. Bacaj T, Wu D, Burré J, Malenka RC, Liu X, Südhof TC. 2015. Synaptotagmin-1 and -7 Are Redundantly Essential for Maintaining the Capacity of the Readily-Releasable Pool of Synaptic Vesicles. *PLoS Biol* 13:1–26. doi:10.1371/journal.pbio.1002267
8. Bacaj T, Wu D, Yang X, Morishita W, Zhou P, Xu W, Malenka RC, Südhof TC. 2013. Synaptotagmin-1 and synaptotagmin-7 trigger synchronous and asynchronous phases of neurotransmitter release. *Neuron* 80:947–59. doi:10.1016/j.neuron.2013.10.026
9. Bai J, Tucker WC, Chapman ER. 2004. PIP 2 increases the speed of response of synaptotagmin and steers its membrane-penetration activity toward the plasma membrane. *Nat Struct Mol Biol* 11:36–44. doi:10.1038/nsmb709
10. Bao H, Goldschen-Ohm M, Jeggle P, Chanda B, Edwardson JM, Chapman ER. 2016. Exocytotic fusion pores are composed of both lipids and proteins. *Nat Struct Mol Biol* 23:67–73. doi:10.1038/nsmb.3141
11. Barber CF, Jorquera RA, Melom JE, Littleton JT. 2009. Postsynaptic regulation of synaptic plasticity by synaptotagmin 4 requires both C2 domains. *J Cell Biol* 187:295–310. doi:10.1083/jcb.200903098
12. Barthet G, Jordà-Siquier T, Rumi-Masante J, Bernadou F, Müller U, Mülle C. 2018. Presenilin-mediated cleavage of APP regulates synaptotagmin-7 and presynaptic plasticity. *Nat Commun* 9:4780. doi:10.1038/s41467-018-06813-x
13. Bhalla A, Tucker WC, Chapman ER. 2005. Synaptotagmin Isoforms Couple Distinct Ranges of Ca²⁺, Ba²⁺, and Sr²⁺ Concentration to SNARE-mediated Membrane Fusion. *Mol Biol Cell* 16:4755–4764. doi:10.1091/mbc.e05-04-0277
14. Bharat V, Siebrecht M, Burk K, Ahmed S, Reissner C, Kohansal-Nodehi M, Steubler V, Zweckstetter M, Ting JT, Dean C. 2017. Capture of Dense Core Vesicles at Synapses by JNK-Dependent Phosphorylation of Synaptotagmin-4. *Cell Rep* 21:2118–2133. doi:10.1016/j.celrep.2017.10.084
15. Blasi J, Chapman ER, Link E, Binz T, Yamasaki S, Camilli P De, Südhof TC, Niemann H, Jahn R. 1993a. Botulinum neurotoxin a selectively cleaves the synaptic protein SNAP-25. *Nature* 365:160–163. doi:10.1038/365160a0

16. Blasi J, Chapman ER, Yamasaki S, Binz T, Niemann H, Jahn R. 1993b. Botulinum neurotoxin C1 blocks neurotransmitter release by means of cleaving HPC-1/syntaxin. *EMBO J* 12:4821–4828. doi:10.1002/j.1460-2075.1993.tb06171.x
17. Brewer KD, Bacaj T, Cavalli A, Camilloni C, Swarbrick JD, Liu J, Zhou A, Zhou P, Barlow N, Xu J, Seven AB, Prinslow EA, Voleti R, Häussinger D, Bonvin AMJJ, Tomchick DR, Vendruscolo M, Graham B, Südhof TC, Rizo J. 2015. Dynamic binding mode of a Synaptotagmin-1-SNARE complex in solution. *Nat Struct Mol Biol* 22:555–564. doi:10.1038/nsmb.3035
18. Cabantous S, Terwilliger TC, Waldo GS. 2005. Protein tagging and detection with engineered self-assembling fragments of green fluorescent protein. *Nat Biotechnol* 23:102–107. doi:10.1038/nbt1044
19. Catterall WA, Few AP. 2008. Calcium Channel Regulation and Presynaptic Plasticity. *Neuron* 59:882–901. doi:10.1016/j.neuron.2008.09.005
20. Chakrabarti S, Kobayashi KS, Flavell RA, Marks CB, Miyake K, Liston DR, Fowler KT, Gorelick FS, Andrews NW. 2003. Impaired membrane resealing and autoimmune myositis in synaptotagmin VII-deficient mice. *J Cell Biol* 162:543–549. doi:10.1083/jcb.200305131
21. Chang CW, Chiang CW, Jackson MB. 2017. Fusion pores and their control of neurotransmitter and hormone release. *J Gen Physiol* 149:301–322. doi:10.1085/jgp.201611724
22. Chapman ER. 2008. How Does Synaptotagmin Trigger Neurotransmitter Release? *Annu Rev Biochem* 77:615–641. doi:10.1146/annurev.biochem.77.062005.101135
23. Chapman ER, Davis AF. 1998. Direct interaction of a Ca²⁺-binding loop of synaptotagmin with lipid bilayers. *J Biol Chem* 273:13995–14001. doi:10.1074/jbc.273.22.13995
24. Chapman ER, Jahn R. 1994. Calcium-dependent interaction of the cytoplasmic region of synaptotagmin with membranes. Autonomous function of a single C2-homologous domain. *J Biol Chem* 269:5735–5741.
25. Chen C, Satterfield R, Young SM, Jonas P. 2017. Triple Function of Synaptotagmin 7 Ensures Efficiency of High-Frequency Transmission at Central GABAergic Synapses. *Cell Rep* 21:2082–2089. doi:10.1016/j.celrep.2017.10.122
26. Chicka MC, Hui E, Liu H, Chapman ER. 2008. Synaptotagmin arrests the SNARE complex before triggering fast, efficient membrane fusion in response to Ca²⁺. *Nat Struct Mol Biol* 15. doi:10.1038/nsmb.1463
27. Cho RW, Buhl LK, Volfson D, Tran A, Li F, Akbergenova Y, Littleton JT. 2015. Phosphorylation of Complexin by PKA Regulates Activity-Dependent Spontaneous Neurotransmitter Release and Structural Synaptic Plasticity. *Neuron* 88:749–761. doi:10.1016/j.neuron.2015.10.011
28. Craxton M. 2010. A manual collection of Syt, Esyt, Rph3a, Rph3al, Doc2, and Dblc2 genes from 46 metazoan genomes - an open access resource for neuroscience and evolutionary biology. *BMC Genomics* 11:1–21. doi:10.1186/1471-2164-11-37
29. Craxton M. 2004. Synaptotagmin gene content of the sequenced genomes. *BMC Genomics* 5:1–14. doi:10.1186/1471-2164-5-43
30. Cummings DD, Wilcox KS, Dichter MA. 1996. Calcium-dependent paired-pulse facilitation of miniature EPSC frequency accompanies depression of EPSCs at hippocampal synapses in culture. *J Neurosci* 16:5312–5323. doi:10.1523/jneurosci.16-17-05312.1996
31. Dai H, Shin O-H, Machius M, Tomchick DR, Südhof TC, Rizo J. 2004. Structural basis for the evolutionary inactivation of Ca²⁺ binding to synaptotagmin 4. *Nat Struct Mol Biol*

- 11:844–849. doi:10.1038/nsmb817
32. Das D, Bao H, Courtney KC, Wu L, Chapman ER. 2020. Resolving kinetic intermediates during the regulated assembly and disassembly of fusion pores. *Nat Commun* 11:1–12. doi:10.1038/s41467-019-14072-7
 33. Davletov BA, Südhof TC. 1993. A single C2 domain from synaptotagmin I is sufficient for high affinity Ca²⁺/phospholipid binding. *J Biol Chem* 268:26386–26390.
 34. De Robertis ED, Bennet HS. 1955. Some features of the submicroscopic morphology of synapses in frog and earthworm. *J Biophys Biochem Cytol* 1:47–58. doi:10.1083/jcb.1.1.47
 35. Dean C, Liu H, Dunning FM, Chang PY, Jackson MB, Chapman ER. 2009. Synaptotagmin-IV modulates synaptic function and long-term potentiation by regulating BDNF release. *Nat Neurosci* 12:767–776. doi:10.1038/nn.2315
 36. del Castillo J, Katz B. 1954. Quantal components of the end-plate potential. *J Physiol* 124:560–573. doi:10.1113/jphysiol.1954.sp005129
 37. Denker A, Rizzoli SO. 2010. Synaptic vesicle pools: An update. *Front Synaptic Neurosci* 2:1–12. doi:10.3389/fnsyn.2010.00135
 38. Desai RC, Vyas B, Earles CA, Littleton JT, Kowalchuck JA, Martin TFJ, Chapman ER. 2000. The C2B domain of synaptotagmin is a Ca²⁺-sensing module essential for exocytosis. *J Cell Biol* 150:1125–1135. doi:10.1083/jcb.150.5.1125
 39. Durán E, Montes MÁ, Jemal I, Satterfield R, Young S, Álvarez de Toledo G. 2018. Synaptotagmin-7 controls the size of the reserve and resting pools of synaptic vesicles in hippocampal neurons. *Cell Calcium* 74:53–60. doi:10.1016/j.ceca.2018.06.004
 40. Fatt P, Katz B. 1952. Spontaneous subthreshold activity at motor nerve endings. *J Physiol* 117:109–128. doi:10.1113/jphysiol.1952.sp004735
 41. Ferguson GD, Wang H, Herschman HR, Storm DR. 2004. Altered hippocampal short-term plasticity and associative memory in synaptotagmin IV (-/-) mice. *Hippocampus* 14:964–974. doi:10.1002/hipo.20013
 42. Fernández-Chacón R, Königstorfer A, Gerber SH, García J, Matos MF, Stevens CF, Brose N, Rizo J, Rosenmund C, Südhof TC. 2001. Synaptotagmin I functions as a calcium regulator of release probability. *Nature* 410:41–49. doi:10.1038/35065004
 43. Fernandez I, Araç D, Ubach J, Gerber SH, Shin OH, Gao Y, Anderson RGW, Südhof TC, Rizo J. 2001. Three-dimensional structure of the synaptotagmin I C2B-domain: Synaptotagmin I as a phospholipid binding machine. *Neuron* 32:1057–1069. doi:10.1016/S0896-6273(01)00548-7
 44. Fioravante D, Regehr WG. 2011. Short-term forms of presynaptic plasticity. *Curr Opin Neurobiol* 21:269–274. doi:10.1016/j.conb.2011.02.003
 45. Fredj N Ben, Burrone J. 2009. A resting pool of vesicles is responsible for spontaneous vesicle fusion at the synapse. *Nat Neurosci* 12:751–758. doi:10.1038/nn.2317
 46. Fukuda M. 2004. RNA interference-mediated silencing of synaptotagmin IX, but not synaptotagmin I, inhibits dense-core vesicle exocytosis in PC12 cells. *Biochem J* 380:875–879. doi:10.1042/BJ20040096
 47. Fukuda M, Kanno E, Satoh M, Saegusa C, Yamamoto A. 2004. Synaptotagmin VII is targeted to dense-core vesicles and regulates their Ca²⁺-dependent exocytosis in PC12 cells. *J Biol Chem* 279:52677–52684. doi:10.1074/jbc.M409241200
 48. Fukuda M, Katayama E, Mikoshiba K. 2002. The calcium-binding loops of the tandem C2 domains of synaptotagmin VII cooperatively mediate calcium-dependent oligomerization. *J Biol Chem* 277:29315–29320. doi:10.1074/jbc.M201697200

49. Fukuda M, Mikoshiba K. 2000. Calcium-Dependent and -Independent Hetero-Oligomerization in the 645:637–645.
50. Gao Z, Reavey-Cantwell J, Young RA, Jegier P, Wolf BA. 2000. Synaptotagmin III/VII isoforms mediate Ca²⁺-induced insulin secretion in pancreatic islet β -cells. *J Biol Chem* 275:36079–36085. doi:10.1074/jbc.M004284200
51. Geppert M, Goda Y, Hammer RE, Li C, Rosahl TW, Stevens CF, Südhof TC. 1994. Synaptotagmin I: A major Ca²⁺ sensor for transmitter release at a central synapse. *Cell* 79:717–727. doi:10.1016/0092-8674(94)90556-8
52. Goda Y, Stevens CF, Goda, Yukiko and Stevens CF. 1994. Two components of transmitter release at a central synapse. *PNAS* 91:12942–12946. doi:10.1073/pnas.91.26.12942
53. Grass I, Thiel S, Höning S, Haucke V. 2004. Recognition of a basic AP-2 binding motif within the C2B domain of synaptotagmin is dependent on multimerization. *J Biol Chem* 279:54872–54880. doi:10.1074/jbc.M409995200
54. Guan Z, Bykhovskaia M, Jorquera RA, Sutton RB, Akbergenova Y, Littleton JT. 2017. A synaptotagmin suppressor screen indicates SNARE binding controls the timing and Ca²⁺ cooperativity of vesicle fusion. *Elife* 6:1–30. doi:10.7554/eLife.28409
55. Gustavsson N, Lao Y, Maximov A, Chuang JC, Kostromina E, Repa JJ, Li C, Radda GK, Südhof TC, Han W. 2008. Impaired insulin secretion and glucose intolerance in synaptotagmin-7 null mutant mice. *Proc Natl Acad Sci U S A* 105:3992–3997. doi:10.1073/pnas.0711700105
56. Harris, K.P., Littleton, J.T., 2015. Transmission, development, and plasticity of synapses. *Genetics* 201, 345–375. doi:10.1534/genetics.115.176529
57. Harris KP, Zhang Y V., Piccioli ZD, Perrimon N, Troy Littleton J. 2016. The postsynaptic t-SNARE syntaxin 4 controls traffic of neuroligin 1 and synaptotagmin 4 to regulate retrograde signaling. *Elife* 5:1–26. doi:10.7554/eLife.13881
58. Hefft S, Jonas P. 2005. Asynchronous GABA release generates long-lasting inhibition at a hippocampal interneuron-principal neuron synapse. *Nat Neurosci* 8:1319–1328. doi:10.1038/nn1542
59. Hennig R, Lømo T. 1985. Firing patterns of motor units in normal rats. *Nature* 314:164–166. doi:10.1038/314164a0
60. Hoang B, Chiba A. 2001. Single-cell analysis of Drosophila larval neuromuscular synapses. *Dev Biol* 229:55–70. doi:10.1006/dbio.2000.9983
61. Hubbard JI. 1963. Repetitive stimulation at the mammalian neuromuscular junction, and the mobilization of transmitter. *J Physiol* 169:641–662. doi:10.1113/jphysiol.1963.sp007286
62. Hudson AW, Birnbaum MJ. 1995. Identification of a nonneuronal isoform of synaptotagmin. *Proc Natl Acad Sci U S A* 92:5895–5899. doi:10.1073/pnas.92.13.5895
63. Hui E, Bai J, Wang P, Sugimori M, Llinas RR, Chapman ER. 2005. Three distinct kinetic groupings of the synaptotagmin family: candidate sensors for rapid and delayed exocytosis. *Proc Natl Acad Sci U S A* 102:5210–4. doi:10.1073/pnas.0500941102
64. Huson V, Regehr WG. 2020. Diverse roles of Synaptotagmin-7 in regulating vesicle fusion. *Curr Opin Neurobiol* 63:42–52. doi:10.1016/j.conb.2020.02.006
65. Iezzi M, Eliasson L, Fukuda M, Wollheim CB. 2005. Adenovirus-mediated silencing of Synaptotagmin 9 inhibits Ca²⁺-dependent insulin secretion in islets. *FEBS Lett* 579:5241–5246. doi:10.1016/j.febslet.2005.08.047
66. Imig C, Min SW, Krinner S, Arancillo M, Rosenmund C, Südhof TC, Rhee JS, Brose N, Cooper BH. 2014. The Morphological and Molecular Nature of Synaptic Vesicle Priming at

- Presynaptic Active Zones. *Neuron* 84:416–431. doi:10.1016/j.neuron.2014.10.009
67. Jackman SL, Regehr WG. 2017. The Mechanisms and Functions of Synaptic Facilitation. *Neuron* 94:447–464. doi:10.1016/j.neuron.2017.02.047
 68. Jackman SL, Turecek J, Belinsky JE, Regehr WG. 2016. The calcium sensor synaptotagmin 7 is required for synaptic facilitation. *Nature* 529:88–91. doi:10.1038/nature16507
 69. Jorquera RA, Huntwork-Rodriguez S, Akbergenova Y, Cho RW, Troy Littleton J. 2012. Complexin controls spontaneous and evoked neurotransmitter release by regulating the timing and properties of synaptotagmin activity. *J Neurosci* 32:18234–18245. doi:10.1523/JNEUROSCI.3212-12.2012
 70. Kaeser PS, Regehr WG. 2017. The readily releasable pool of synaptic vesicles. *Curr Opin Neurobiol* 43:63–70. doi:10.1016/j.conb.2016.12.012
 71. Kaeser PS, Regehr WG. 2014. Molecular Mechanisms for Synchronous, Asynchronous, and Spontaneous Neurotransmitter Release. *Annu Rev Physiol* 76:333–363. doi:10.1146/annurev-physiol-021113-170338
 72. Kamiyama D, Sekine S, Barsi-Rhyne B, Hu J, Chen B, Gilbert LA, Ishikawa H, Leonetti MD, Marshall WF, Weissman JS, Huang B. 2016. Versatile protein tagging in cells with split fluorescent protein. *Nat Commun* 7. doi:10.1038/ncomms11046
 73. Katz B, Miledi R. 1969. Spontaneous and evoked activity of motor nerve endings in calcium Ringer. *J Physiol* 203:689–706. doi:10.1113/jphysiol.1969.sp008887
 74. Katz B, Miledi R. 1967. A study of synaptic transmission in the absence of nerve impulses. *J Physiol* 192:407–436. doi:10.1113/jphysiol.1967.sp008307
 75. Kavalali ET. 2015. The mechanisms and functions of spontaneous neurotransmitter release. *Nat Rev Neurosci* 16:5–16. doi:10.1038/nrn3875
 76. Kennedy D, Takeda K. 1965a. Reflex Control of Abdominal Flexor Muscles in the Crayfish: I. The Twitch System. *J Exp Biol* 43:211–227.
 77. Kennedy D, Takeda K. 1965b. Reflex Control of Abdominal Flexor Muscles in the Crayfish: II. The Tonic System. *J Exp Biol* 43:229–246.
 78. Kittel RJ, Heckmann M. 2016. Synaptic vesicle proteins and active zone plasticity. *Front Synaptic Neurosci* 8:8. doi:10.3389/fnsyn.2016.00008
 79. Körber C, Kuner T. 2016. Molecular machines regulating the release probability of synaptic vesicles at the active zone. *Front Synaptic Neurosci* 8:5. doi:10.3389/fnsyn.2016.00005
 80. Korkut C, Li Y, Koles K, Brewer C, Ashley J, Yoshihara M, Budnik V. 2013. Regulation of Postsynaptic Retrograde Signaling by Presynaptic Exosome Release. *Neuron* 77:1039–1046. doi:10.1016/j.neuron.2013.01.013
 81. Kurdyak P, Atwood HL, Stewart BA, Wu C-F. 1994. Differential physiology and morphology of motor axons to ventral longitudinal muscles in larval *Drosophila*. *J Comp Neurol* 350:463–472. doi:10.1002/cne.903500310
 82. Lee J, Littleton JT. 2015. Transmembrane tethering of synaptotagmin to synaptic vesicles controls multiple modes of neurotransmitter release. *Proc Natl Acad Sci* 112:201420312. doi:10.1073/pnas.1420312112
 83. Li C, Ullrich B, Zhang JZ, Anderson RGW, Brose N, Südhof TC. 1995. Ca²⁺-dependent and -independent activities of neural and non-neural synaptotagmins. *Nature* 375:594–599. doi:10.1038/375594a0
 84. Li YC, Chanaday NL, Xu W, Kavalali ET. 2017. Synaptotagmin-1- and Synaptotagmin-7-Dependent Fusion Mechanisms Target Synaptic Vesicles to Kinetically Distinct Endocytic Pathways. *Neuron* 93:616–631.e3. doi:10.1016/j.neuron.2016.12.010

85. Link E, Edelmann L, Chou JH, Binz T, Yamasaki S, Eisel U, Baumert M, Südhof TC, Niemann H, Jahn R. 1992. Tetanus toxin action: inhibition of neurotransmitter release linked to synaptobrevin proteolysis. *Biochem Biophys Res Commun* 189:1017–23. doi:10.1016/0006-291x(92)92305-h
86. Littleton JT, Stern M, Perin M, Bellen HJ. 1994. Calcium dependence of neurotransmitter release and rate of spontaneous vesicle fusions are altered in *Drosophila* synaptotagmin mutants. *Proc Natl Acad Sci U S A* 91:10888–92.
87. Littleton JT, Stern M, Schulze K, Perin M, Bellen HJ. 1993. Mutational analysis of *Drosophila* synaptotagmin demonstrates its essential role in Ca²⁺-activated neurotransmitter release. *Cell* 74:1125–1134. doi:10.1016/0092-8674(93)90733-7
88. Liu H, Bai H, Hui E, Yang L, Evans CS, Wang Z, Kwon SE, Chapman ER. 2014. Synaptotagmin 7 functions as a Ca²⁺-sensor for synaptic vesicle replenishment. *Elife* 2014:1–18. doi:10.7554/eLife.01524.001
89. Llinás R, Sugimori M, Silver RB. 1992. Microdomains of high calcium concentration in a presynaptic terminal. *Science (80-)* 256:677–679. doi:10.1126/science.1350109
90. Lu T, Trussell LO. 2000. Inhibitory transmission mediated by asynchronous transmitter release. *Neuron* 26:683–694. doi:10.1016/S0896-6273(00)81204-0
91. Luo F, Bacaj T, Südhof TC. 2015. Synaptotagmin-7 Is Essential for Ca²⁺-Triggered Delayed Asynchronous Release But Not for Ca²⁺-Dependent Vesicle Priming in Retinal Ribbon Synapses. *J Neurosci* 35:11024–33. doi:10.1523/JNEUROSCI.0759-15.2015
92. Luo F, Südhof TC. 2017. Synaptotagmin-7-Mediated Asynchronous Release Boosts High-Fidelity Synchronous Transmission at a Central Synapse. *Neuron* 94:826-839.e3. doi:10.1016/j.neuron.2017.04.020
93. Mackler JM, Drummond JA, Loewen CA, Robinson IM, Reist NE. 2002. The C2B Ca²⁺-binding motif of synaptotagmin is required for synaptic transmission in vivo. *Nature* 418:340–344. doi:10.1038/nature00846
94. Mallart A. 1993. Calcium-dependent modulation of the facilitation of transmitter release at neuromuscular junctions of *Drosophila*. *J Physiol - Paris* 87:83–88. doi:10.1016/0928-4257(93)90002-B
95. Marquhze B, Boudier JA, Mizuta M, Inagaki N, Seine S, Seagar M. 1995. Cellular Localization of Synaptotagmin I, II, and III mRNAs in the Central Nervous System and Pituitary and Adrenal Glands of the Rat. *J Neurosci* 15:4906–4917.
96. Martinez I, Chakrabarti S, Hellevik T, Morehead J, Fowler K, Andrews NW. 2000. Synaptotagmin vii regulates Ca²⁺-dependent exocytosis of lysosomes in fibroblasts. *J Cell Biol* 148:1141–1149. doi:10.1083/jcb.148.6.1141
97. Maximov A, Südhof TC. 2005. Autonomous function of synaptotagmin 1 in triggering synchronous release independent of asynchronous release. *Neuron* 48:547–54. doi:10.1016/j.neuron.2005.09.006
98. Menon KP, Carrillo RA, Zinn K. 2013. Development and plasticity of the *Drosophila* larval neuromuscular junction. *Wiley Interdiscip Rev Dev Biol* 2:647–670. doi:10.1002/wdev.108
99. Mittelsteadt T, Seifert G, Álvarez-Barón E, Steinhäuser C, Becker AJ, Schoch S. 2009. Differential mRNA expression patterns of the synaptotagmin gene family in the rodent brain. *J Comp Neurol* 512:514–528. doi:10.1002/cne.21908
100. Monterrat C, Grise F, Benassy MN, Hémar A, Lang J. 2007. The calcium-sensing protein synaptotagmin 7 is expressed on different endosomal compartments in endocrine, neuroendocrine cells or neurons but not on large dense core vesicles. *Histochem Cell Biol*

- 127:625–632. doi:10.1007/s00418-007-0271-0
101. Newman ZL, Hoagland A, Aghi K, Worden K, Levy SL, Ho Son J, Lee LP, Isacoff EY. 2017. Input-Specific Plasticity and Homeostasis at the Drosophila Larval Neuromuscular Junction. *Neuron* 93:1388-1404.e10. doi:10.1016/j.neuron.2017.02.028
102. Nizzardo M, Taiana M, Rizzo F, Aguila Benitez J, Nijssen J, Allodi I, Melzi V, Bresolin N, Comi GP, Hedlund E, Corti S. 2020. Synaptotagmin 13 is neuroprotective across motor neuron diseases. *Acta Neuropathol* 1–17. doi:10.1007/s00401-020-02133-x
103. Palay SL. 1956. Synapses in the central nervous system. *J Biophys Biochem Cytol* 2:193–202. doi:10.1083/jcb.2.4.193
104. Pang ZP, Shin OH, Meyer AC, Rosenmund C, Südhof TC. 2006a. A gain-of-function mutation in synaptotagmin-1 reveals a critical role of Ca²⁺-dependent soluble N-ethylmaleimide-sensitive factor attachment protein receptor complex binding in synaptic exocytosis. *J Neurosci* 26:12556–12565. doi:10.1523/JNEUROSCI.3804-06.2006
105. Pang ZP, Sun J, Rizo J, Maximov A, Südhof TC. 2006b. Genetic analysis of synaptotagmin 2 in spontaneous and Ca²⁺-triggered neurotransmitter release. *EMBO J* 25:2039–2050. doi:10.1038/sj.emboj.7601103
106. Pereda AE. 2014. Electrical synapses and their functional interactions with chemical synapses. *Nat Rev Neurosci* 15:250–263. doi:10.1038/nrn3708
107. Perin M, Brose N, Jahn R, Südhof TC. 1991a. Domain structure of synaptotagmin (p65). *J Biol Chem* 266:623–629.
108. Perin M, Johnston PA, Ozcelik T, Jahn R, Francke U, Südhof TC. 1991b. Structural and functional conservation of synaptotagmin (p65) in Drosophila and humans. *J Biol Chem* 266:615–22.
109. Perin MS, Fried VA, Mignery GA, Jahn R, Südhof TC. 1990. Phospholipid binding by a synaptic vesicle protein homologous to the regulatory region of protein kinase C. *Nature* 345:260–263. doi:10.1038/345260a0
110. Poser Von C, Südhof TC. 2001. Synaptotagmin 13: Structure and expression of a novel synaptotagmin. *Eur J Cell Biol* 80:41–47. doi:10.1078/0171-9335-00133
111. Rahamimoff R, Yaari Y. 1973. Delayed release of transmitter at the frog neuromuscular junction. *J Physiol* 228:241–257. doi:10.1113/jphysiol.1973.sp010084
112. Ramirez DMO, Kavalali ET. 2011. Differential regulation of spontaneous and evoked neurotransmitter release at central synapses. *Curr Opin Neurobiol* 21:275–282. doi:10.1016/j.conb.2011.01.007
113. Rao SK, Huynh C, Proux-Gillardeaux V, Galli T, Andrews NW. 2004. Identification of SNAREs Involved in Synaptotagmin VII-regulated Lysosomal Exocytosis. *J Biol Chem* 279:20471–20479. doi:10.1074/jbc.M400798200
114. Reddy A, Caler E V., Andrews NW. 2001. Plasma Membrane Repair Is Mediated by Ca²⁺-Regulated Exocytosis of Lysosomes. *Cell* 106:157–169. doi:10.1016/S0092-8674(01)00421-4
115. Regehr WG. 2012. Short-term presynaptic plasticity. *Cold Spring Harb Perspect Biol* 4:1–19. doi:10.1101/cshperspect.a005702
116. Rizo J, Rosenmund C. 2008. Synaptic vesicle fusion. *Nat Struct Mol Biol* 15:665–674. doi:10.1038/nsmb.1450
117. Rizo J, Südhof TC. 2002. Snares and munc18 in synaptic vesicle fusion. *Nat Rev Neurosci* 3:641–653. doi:10.1038/nrn898
118. Rizzoli SO. 2014. Synaptic vesicle recycling: Steps and principles. *EMBO J* 33:788–822.

- doi:10.1002/embj.201386357
119. Rizzoli SO, Betz WJ. 2005. Synaptic vesicle pools. *Nat Rev Neurosci* 6:57–69. doi:10.1038/nrn1583
 120. Sabeva N, Cho RW, Vasin A, Gonzalez A, Littleton JT, Bykhovskaia M. 2017. Complexin mutants reveal partial segregation between recycling pathways that drive evoked and spontaneous neurotransmission. *J Neurosci* 37:383–396. doi:10.1523/JNEUROSCI.1854-16.2016
 121. Saheki Y, De Camilli P. 2012. Synaptic vesicle endocytosis. *Cold Spring Harb Perspect Biol* 4. doi:10.1101/cshperspect.a005645
 122. Sara Y, Virmani T, Deák F, Liu X, Kavalali ET. 2005. An isolated pool of vesicles recycles at rest and drives spontaneous neurotransmission. *Neuron* 45:563–573. doi:10.1016/j.neuron.2004.12.056
 123. Saraswati S, Adolfsen B, Littleton JT. 2007. Characterization of the role of the Synaptotagmin family as calcium sensors in facilitation and asynchronous neurotransmitter release. *Proc Natl Acad Sci U S A* 104:14122–14127. doi:10.1073/pnas.0706711104
 124. Schiavo GG, Benfenati F, Poulain B, Rossetto O, De Laureto PP, Dasgupta BR, Montecucco C. 1992. Tetanus and botulinum-B neurotoxins block neurotransmitter release by proteolytic cleavage of synaptobrevin. *Nature* 359:832–835. doi:10.1038/359832a0
 125. Schonh JS, Maximov A, Lao Y, Südhof TC, Sørensen JB. 2008. Synaptotagmin-1 and -7 are functionally overlapping Ca²⁺ sensors for exocytosis in adrenal chromaffin cells. *Proc Natl Acad Sci U S A* 105:3998–4003. doi:10.1073/pnas.0712373105
 126. Schupp M, Malsam J, Rüter M, Scheutrow A, Wierda KDB, Söllner TH, Sørensen JB. 2016. Interactions between SNAP-25 and synaptotagmin-1 are involved in vesicle priming, clamping spontaneous and stimulating evoked neurotransmission. *J Neurosci* 36:11834–11836. doi:10.1523/JNEUROSCI.1011-16.2016
 127. Shao X, Davletov BA, Sutton RB, Südhof TC, Rizo J. 1996. Bipartite Ca²⁺-binding motif in C2 domains of synaptotagmin and protein kinase C. *Science (80-)* 273:248–251. doi:10.1126/science.273.5272.248
 128. Shimojo M, Madara J, Pankow S, Liu X, Yates J, Südhof TC, Maximov A. 2019. Synaptotagmin-11 mediates a vesicle trafficking pathway that is essential for development and synaptic plasticity. *Genes Dev* 33:365–376. doi:10.1101/gad.320077.118
 129. Shin OH, Xu J, Rizo J, Südhof TC. 2009. Differential but convergent functions of Ca²⁺ binding to synaptotagmin-1 C2 domains mediate neurotransmitter release. *Proc Natl Acad Sci U S A* 106:16469–16474. doi:10.1073/pnas.0908798106
 130. Smart TG, Paoletti P. 2012. Synaptic neurotransmitter-gated receptors. *Cold Spring Harb Perspect Biol* 4. doi:10.1101/cshperspect.a009662
 131. Stanley EF. 1993. Single calcium channels and acetylcholine release at a presynaptic nerve terminal. *Neuron* 11:1007–1011. doi:10.1016/0896-6273(93)90214-C
 132. Südhof TC, Rizo J. 2011. Synaptic vesicle exocytosis. *Cold Spring Harb Perspect Biol* 3. doi:10.1101/cshperspect.a005637
 133. Sugita S, Han W, Butz S, Liu X, Fernández-Chacón R, Lao Y, Südhof TC. 2001. Synaptotagmin VII as a Plasma Membrane Ca²⁺ Sensor in Exocytosis. *Neuron* 30:459–473. doi:10.1016/S0896-6273(01)00290-2
 134. Südhof TC. 2012. The Presynaptic Active Zone. *Neuron* 75:11–25. doi:10.1016/j.neuron.2012.06.012
 135. Sutton RB, Davletov BA, Berghuis AM, S TC, Sprang SR, Sutton RB, Davletov BA,

- Berghuis AM, Südhof TC, Sprang SR. 1995. Structure of the first C2 domain of synaptotagmin I: A novel Ca²⁺/phospholipid-binding fold. *Cell* 80:929–938. doi:10.1016/0092-8674(95)90296-1
136. Takamori S, Holt M, Stenius K, Lemke EA, Grønborg M, Riedel D, Urlaub H, Schenck S, Brügger B, Ringler P, Müller SA, Rammner B, Gräter F, Hub JS, De Groot BL, Mieskes G, Moriyama Y, Klingauf J, Grubmüller H, Heuser J, Wieland F, Jahn R. 2006. Molecular Anatomy of a Trafficking Organelle. *Cell* 127:831–846. doi:10.1016/j.cell.2006.10.030
137. Turecek J, Regehr WG. 2019. Neuronal Regulation of Fast Synaptotagmin Isoforms Controls the Relative Contributions of Synchronous and Asynchronous Release. *Neuron* 101:938-949.e4. doi:10.1016/j.neuron.2019.01.013
138. Ubach J, Zhang X, Shao X, Südhof T, Rizo J. 1998. Ca²⁺ binding to synaptotagmin: how many Ca²⁺ ions bind to the tip of a C2 domain? *EMBO J* 17:3921–3930.
139. Van der Kloot W, Molgo J. 1993. Facilitation and delayed release at about 0°C at the frog neuromuscular junction: Effects of calcium chelators, calcium transport inhibitors, and okadaic acid. *J Neurophysiol* 69:717–729. doi:10.1152/jn.1993.69.3.717
140. Voleti R, Tomchick DR, Südhof TC, Rizo J. 2017. Exceptionally tight membrane-binding may explain the key role of the synaptotagmin-7 C2A domain in asynchronous neurotransmitter release. *Proc Natl Acad Sci U S A* 114:E8518–E8527. doi:10.1073/pnas.1710708114
141. Wang C, Wang Y, Hu M, Chai Z, Wu Q, Huang R, Han W, Zhang CX, Zhou Z. 2016. Synaptotagmin-11 inhibits clathrin-mediated and bulk endocytosis. *EMBO Rep* 17:47–63. doi:10.15252/embr.201540689
142. Wang CT, Grishanin R, Earles CA, Chang PY, Martin TFJ, Chapman ER, Jackson MB. 2001. Synaptotagmin modulation of fusion pore kinetics in regulated exocytosis of dense-core vesicles. *Science* 294:1111–1115. doi:10.1126/science.1064002
143. Wang S, Li Y, Ma C. 2016. Synaptotagmin-1 C2B domain interacts simultaneously with SNAREs and membranes to promote membrane fusion. *Elife* 5:e14211. doi:10.7554/eLife.14211
144. Wang Z, Chapman ER. 2010. Rat and Drosophila synaptotagmin 4 have opposite effects during SNARE-catalyzed membrane fusion. *J Biol Chem* 285:30759–30766. doi:10.1074/jbc.M110.137745
145. Weber T, Zemelman B V., McNew JA, Westermann B, Gmachl M, Parlato F, Söllner TH, Rothman JE. 1998. SNAREpins: Minimal machinery for membrane fusion. *Cell* 92:759–772. doi:10.1016/S0092-8674(00)81404-X
146. Wen H, Linhoff MW, McGinley MJ, Li GL, Corson GM, Mandel G, Brehm P. 2010. Distinct roles for two synaptotagmin isoforms in synchronous and asynchronous transmitter release at zebrafish neuromuscular junction. *Proc Natl Acad Sci U S A* 107:13906–13911. doi:10.1073/pnas.1008598107
147. Wu D, Bacaj T, Morishita W, Goswami D, Arendt KL, Xu W, Chen L, Malenka RC, Südhof TC. 2017. Postsynaptic synaptotagmins mediate AMPA receptor exocytosis during LTP. *Nature* 544:316–321. doi:10.1038/nature21720
148. Xiao L, Han Y, Runne H, Murray H, Kochubey O, Luthi-Carter R, Schneggenburger R. 2010. Developmental expression of Synaptotagmin isoforms in single calyx of Held-generating neurons. *Mol Cell Neurosci* 44:374–385. doi:10.1016/j.mcn.2010.05.002
149. Xu J, Mashimo T, Südhof TC. 2007. Synaptotagmin-1, -2, and -9: Ca²⁺ Sensors for Fast Release that Specify Distinct Presynaptic Properties in Subsets of Neurons. *Neuron* 54:567–

581. doi:10.1016/j.neuron.2007.05.004
150. Xu J, Pang ZP, Shin OH, Südhof TC. 2009. Synaptotagmin-1 functions as a Ca²⁺ sensor for spontaneous release. *Nat Neurosci* 12:759–766. doi:10.1038/nn.2320
151. Xue M, Craig TK, Shin O-H, Li L, Brautigam CA, Tomchick DR, Südhof TC, Rosenmund C, Rizo J. 2010. Structural and mutational analysis of functional differentiation between synaptotagmins-1 and -7. *PLoS One* 5:e12544. doi:10.1371/journal.pone.0012544
152. Yao J, Kwon SE, Gaffaney JD, Dunning FM, Chapman ER. 2012. Uncoupling the roles of synaptotagmin I during endo- and exocytosis of synaptic vesicles. *Nat Neurosci* 15:243–249. doi:10.1038/nn.3013
153. Yoshihara M, Guan Z, Littleton JT. 2010. Differential regulation of synchronous versus asynchronous neurotransmitter release by the C2 domains of synaptotagmin I. *Proc Natl Acad Sci U S A* 107:14869–14874. doi:10.1073/pnas.1000606107
154. Yoshihara M, Littleton JT. 2002. Synaptotagmin I Functions as a Calcium Sensor to Synchronize Neurotransmitter Release. *Neuron* 36:897–908. doi:10.1016/S0896-6273(02)01065-6
155. Zhang JZ, Davletov BA, Südhof TC, Anderson RGW. 1994. Synaptotagmin I is a high affinity receptor for clathrin AP-2: Implications for membrane recycling. *Cell*. doi:10.1016/S0092-8674(94)90442-1
156. Zhang X, Rizo J, Südhof TC. 1998. Mechanism of phospholipid binding by the C2A-domain of synaptotagmin I. *Biochemistry* 37:12395–12403. doi:10.1021/bi9807512
157. Zhou Q, Lai Y, Bacaj T, Zhao M, Lyubimov AY, Uervirojnangkoorn M, Zeldin OB, Brewster AS, Sauter NK, Cohen AE, Soltis SM, Alonso-Mori R, Chollet M, Lemke HT, Pfuetzner RA, Choi UB, Weis WI, Diao J, Südhof TC, Brunger AT. 2015. Architecture of the synaptotagmin-SNARE machinery for neuronal exocytosis. *Nature* 525:62–67. doi:10.1038/nature14975
158. Zucker RS, Regehr WG. 2002. Short-Term Synaptic Plasticity. *Annu Rev Physiol* 64:355–405. doi:10.1146/annurev.physiol.64.092501.114547

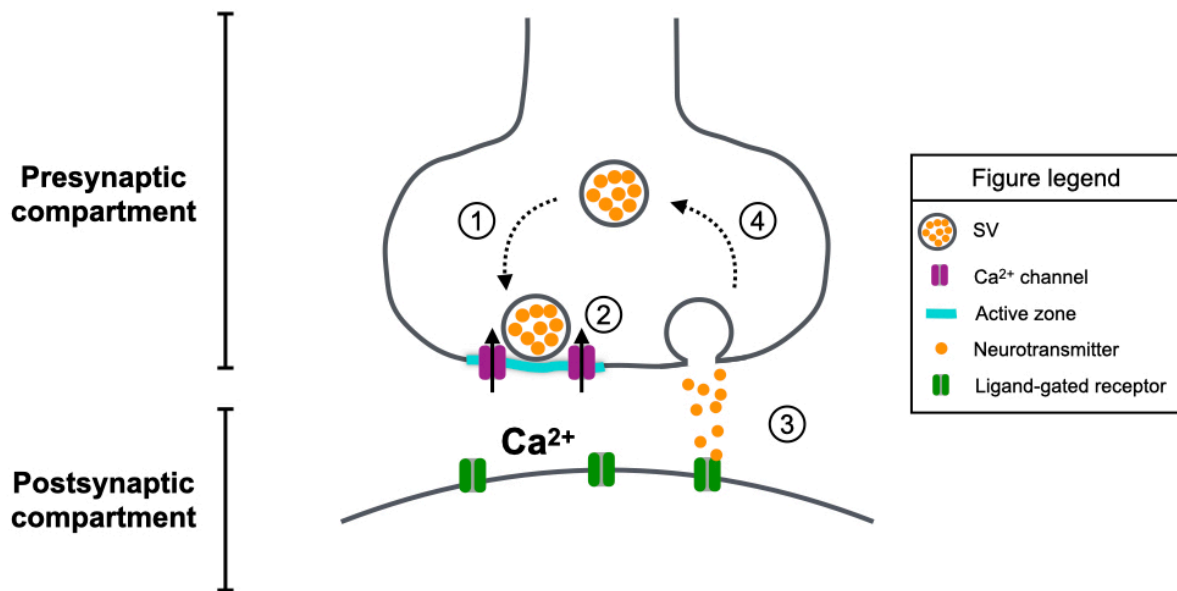


Figure 1. Neurotransmission occurs at synapses. The presynaptic compartment contains neurotransmitter-filled SVs, while the postsynaptic compartment contains ligand-gated receptors that bind to neurotransmitters and regulate the activity of that cell. (1) SVs dock at site called active zones. (2) Action potentials trigger the opening of voltage-gated calcium channels at active zones to allow extracellular calcium into the presynaptic compartment to trigger SV fusion. (3) SVs are retrieved through endocytosis in the peri-active zone. (4) Recycled SVs re-enter the pool and can fuse again during subsequent rounds of stimulation.

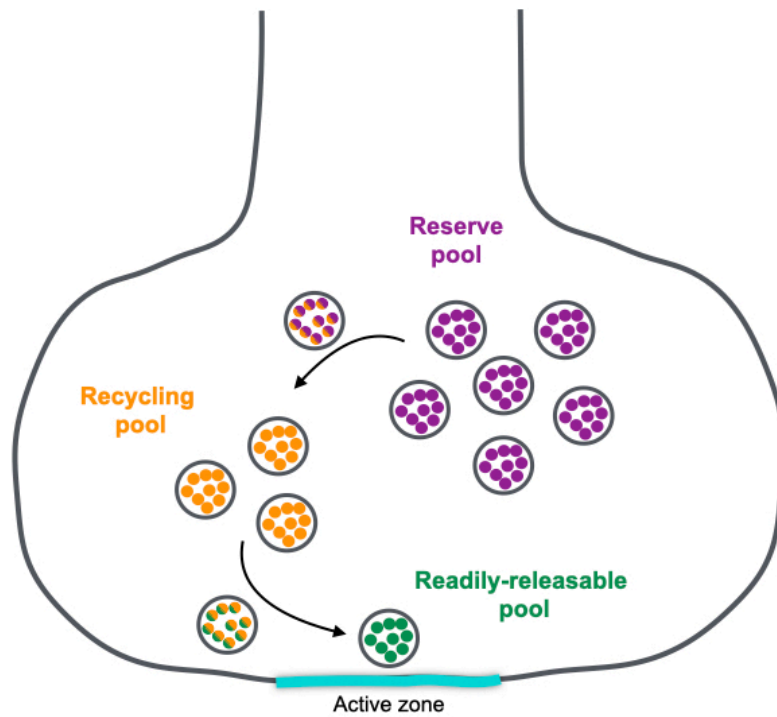


Figure 2. SV pools. SVs are grouped into three functionally distinct pools. The readily releasable pool is recruited to fuse during nerve stimulation (green). The recycling pool replenishes the readily releasable pool (orange). The majority of SVs are in the reserve pool and replenish the recycling pool when it becomes depleted (purple).

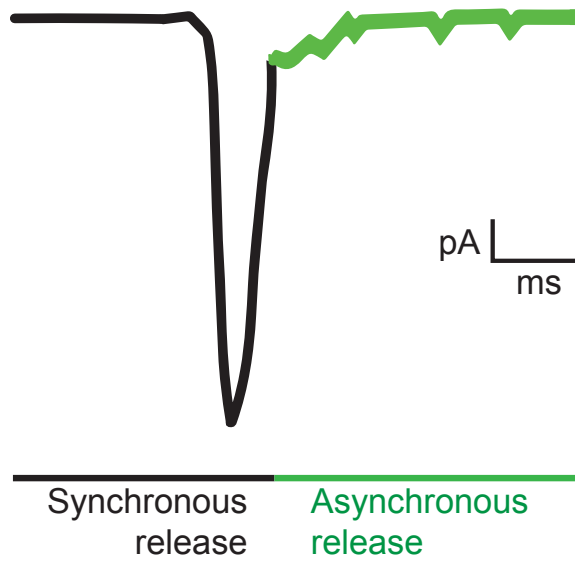


Figure 3. Evoked neurotransmitter. Nerve stimulation triggers neurotransmitter release that can be divided into two kinetic phases called synchronous and asynchronous release.

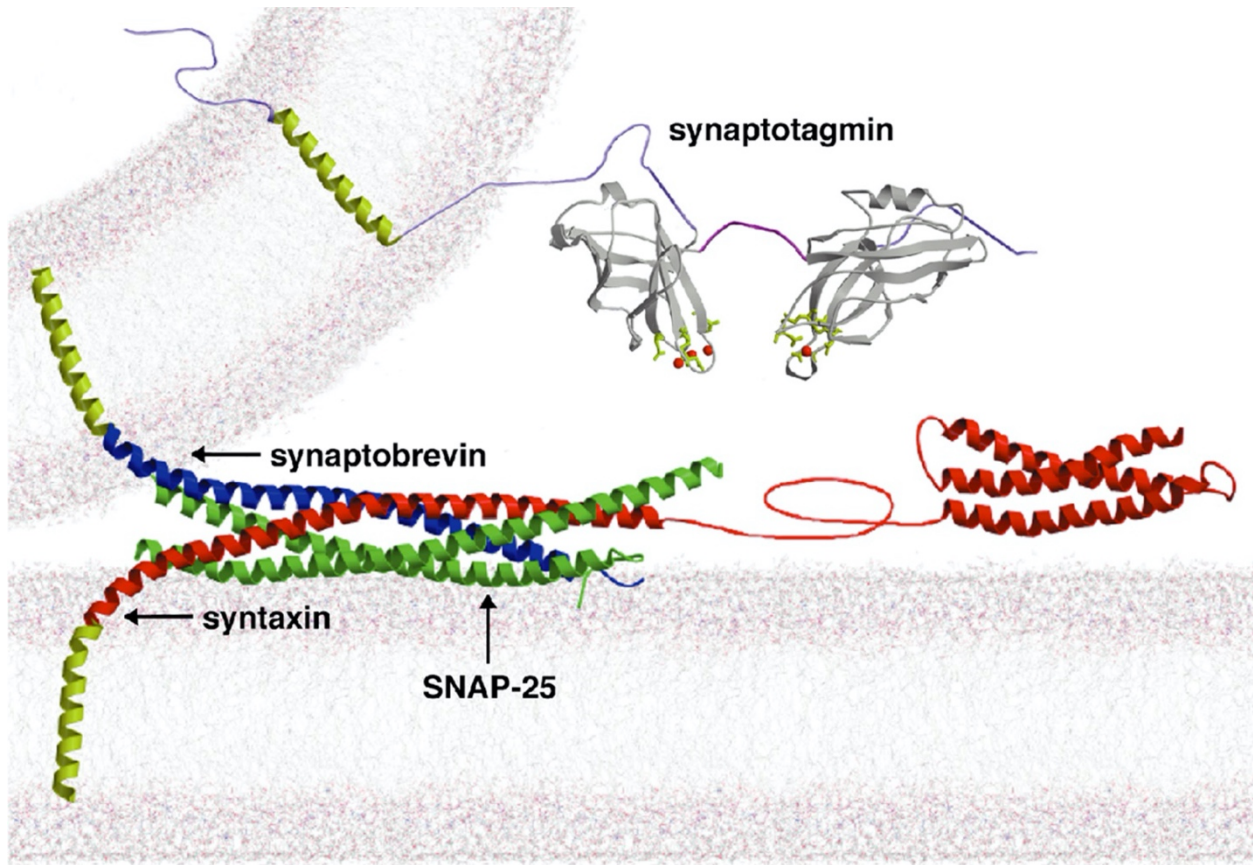


Figure 4. The molecular machine that drives SV fusion. The SNARE complex drives the bilayer fusion of synaptic vesicles and the plasma membrane. Its composed of v-SNARE synaptobrevin (blue) and t-SNAREs syntaxin(red) and SNAP-25(green). The calcium sensor sensor, Synapotagmin(grey), engages the SNARE complex for bilayer fusion during an evoked response. Adapted from (Harris and Littleton, 2015)

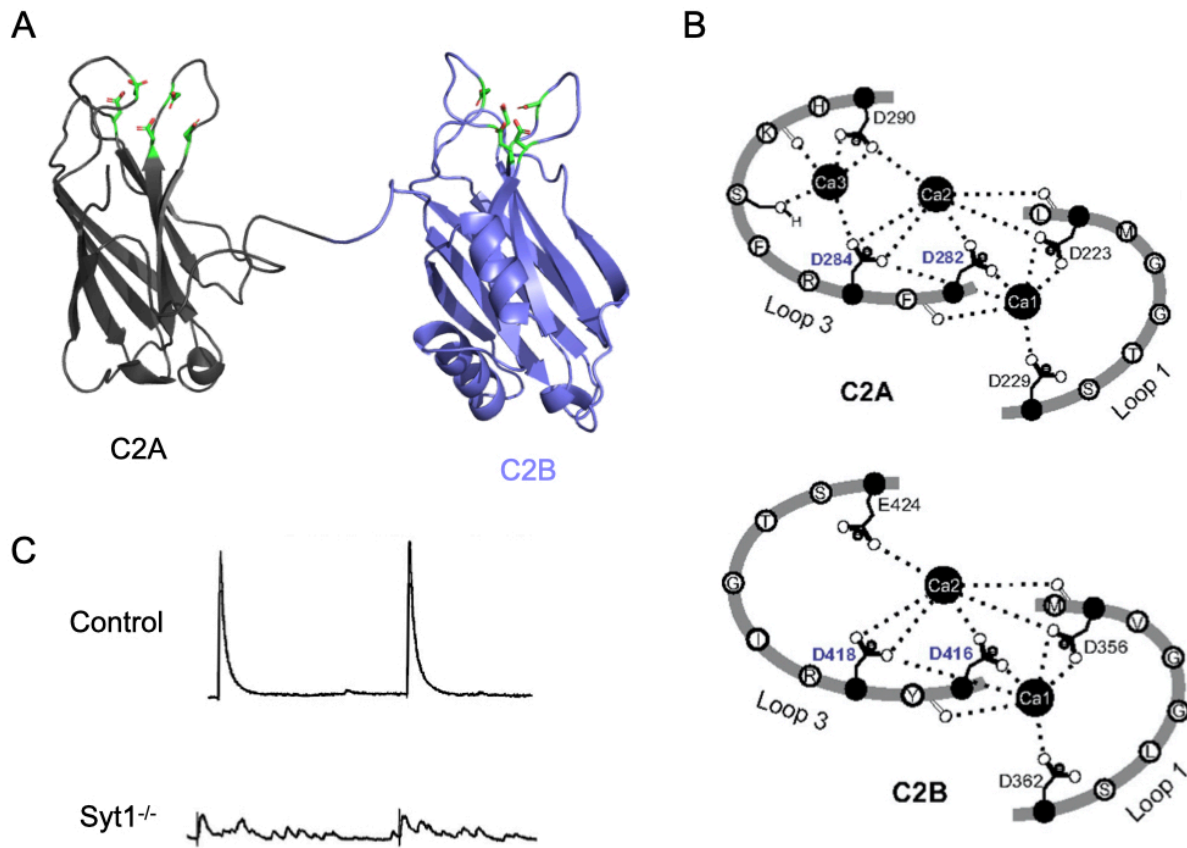


Figure 5. Synaptotagmin 1 is the synchronous release calcium sensor. (A) SYT1 contains a single pass-transmembrane domain (not shown), a variable linker (not shown) and 2 C2 domains, termed C2A (black) and C2B (purple) (Zhuo et al., 2015). (B) In SYT1, each C2 domain contains 3 calcium binding loops that bind 3 calcium ions in C2A and 2 calcium ions in C2B. (C) *Syt1* mutants lack the synchronous component of evoked release while asynchronous release is enhanced.

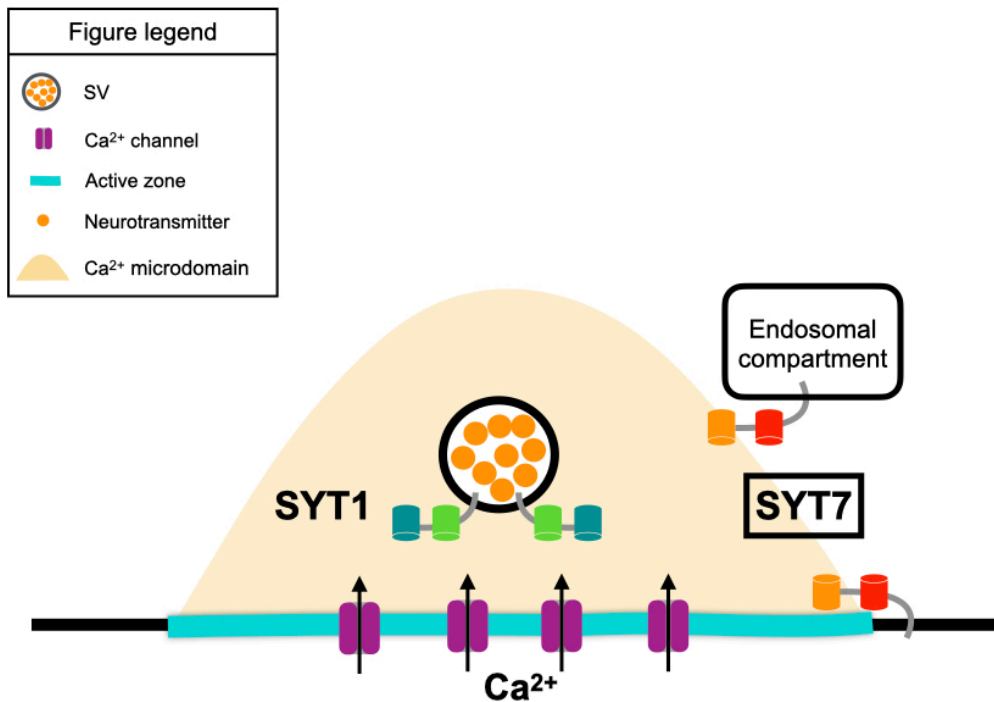


Figure 6. The asynchronous release sensor is loosely coupled to calcium channels. The SV protein, SYT1, is tightly coupled to calcium channels at active zones to regulate synchronous neurotransmitter release. In contrast, SYT7 has been suggested to be uncoupled from calcium channels to regulate asynchronous release. Since SYT7 has high affinity to calcium, it can become activated from the edges of calcium microdomains formed during an evoked response. SYT7 localization at synapses is unclear but some studies suggest it can be at the plasma membrane or an endosomal compartment.

Chapter 2: *Drosophila* Synaptotagmin 7 negatively regulates synaptic vesicle release and replenishment in a dosage-dependent manner

Zhuo Guan*, Mónica C. Quiñones-Frías*, Yulia Akbergenova, J. Troy Littleton

The Picower Institute for Learning and Memory, Department of Biology, Massachusetts
Institute of Technology, Cambridge, MA 02139

The work described was equally contributed by Mónica C. Quiñones-Frías and Zhuo Guan. Generation of genetic tools and imaging experiments were performed by Mónica C. Quiñones-Frías. Voltage clamp experiments were performed by Zhuo Guan. Release probability mapping was performed by Yulia Akbergenova. This work is under review at *Elife*.

Introduction

Neurotransmitter release from presynaptic terminals is the primary mechanism of synaptic communication and is mediated by fusion of synaptic vesicles (SVs) with the plasma membrane at specific sites known as active zones (AZs) (Katz, 1969; Südhof, 2013; Zhai and Bellen, 2004). A highly conserved protein machinery composed of the SNARE complex drives fusion between the SV and AZ lipid bilayers (Littleton et al., 1998; Söllner et al., 1993; Sutton et al., 1998; Tucker et al., 2004). Ca^{2+} influx through voltage-gated Ca^{2+} channels functions as the trigger to activate the fusion process (Borst and Sakmann, 1996; Katz and Miledi, 1970, 1967; Schneggenburger and Rosenmund, 2015; Südhof, 2012). The majority of SVs fuse during a synchronous phase that occurs within a few milliseconds of Ca^{2+} entry (Borst and Sakmann, 1996; Goda and Stevens, 1994; Llinás et al., 1981; Sabatini and Regehr, 1996; Yoshihara and Littleton, 2002). Many synapses also have an asynchronous component that results in SV release over hundreds of milliseconds (Goda and Stevens, 1994; Hefft and Jonas, 2005; Kaeser and Regehr, 2014; Yoshihara and Littleton, 2002). Asynchronous release normally accounts for less than 5% of SV fusion following single action potentials at *Drosophila* neuromuscular junctions (NMJs) (Jorquera et al., 2012). This slower phase of release becomes more prominent during high rates of stimulation (Atluri and Regehr, 1998; Lu and Trussell, 2000; Rozov et al., 2019; Zucker and Regehr, 2002) and mediates all SV fusion at some neuronal connections (Best and Regehr, 2009; Peters et al., 2010). Changes in the kinetics and amount of SV fusion also occur during high frequency stimulation, resulting in facilitation or depression depending on the synapse (Zucker and Regehr, 2002). Defining the molecular machinery and Ca^{2+} sensors that regulate the distinct modes and kinetics of SV release is essential for understanding synaptic transmission.

The Synaptotagmin (SYT) family of Ca^{2+} binding proteins contain key regulators that control the timing of SV release. SYT proteins have a transmembrane domain and two Ca^{2+} binding C2 domains termed C2A and C2B (Adolfson et al., 2004; Adolfson and Littleton, 2001; Perin et al., 1990; Sugita et al., 2002; Ullrich and Südhof, 1995). Mammals have three SYT family members that localize to SVs (SYT1, SYT2 and SYT9), while *Drosophila* contains a single member of the SV subfamily (SYT1) (Littleton et al., 1993a; Pang et al., 2006; Xu et al., 2007). These SYT isoforms bind Ca^{2+} and activate synchronous fusion of SVs via interactions with membranes and the SNARE complex (Chang et al., 2018; Chapman and Jahn, 1994; Fernández-Chacón et al., 2001; Geppert et al., 1994; Guan et al., 2017; Lee et al., 2013; Lee and Littleton, 2015; Littleton et al., 1994, 1993b; Mackler et al., 2002; Nishiki and Augustine, 2004; Tucker et al., 2004; Xu et al., 2007; Yoshihara and Littleton, 2002; Young and Neher, 2009). Beyond SV localized SYTs, SYT7 is the only other family member implicated in Ca^{2+} -dependent SV trafficking, although additional SYT isoforms participate in Ca^{2+} -dependent fusion of other secretory organelles and dense core vesicles (DCVs) (Adolfson et al., 2004; Cao et al., 2011; Dean et al., 2012; Li et al., 1995; Moghadam and Jackson, 2013; Park et al., 2014; Shin et al., 2002; Yoshihara et al., 2005).

Multiple mechanisms have been proposed to mediate the asynchronous component of neurotransmitter release, including distinct Ca^{2+} sensors, heterogeneity in SV protein content, SV distance from Ca^{2+} channels, distinct Ca^{2+} entry pathways, or regulation of Ca^{2+} extrusion and buffering (Chanaday and Kavalali, 2018; Fesce, 1999; Kaeser and Regehr, 2014; Pang and Südhof, 2010; Rozov et al., 2019; Zucker and Regehr, 2002). Although several mechanisms may contribute, the observation that *Syt1* mutants have enhanced asynchronous release indicates another Ca^{2+} sensor(s) activates the remaining slower Ca^{2+} -dependent component of exocytosis

(Huson et al., 2019; Kochubey and Schneggenburger, 2011; Nishiki and Augustine, 2004; Turecek and Regehr, 2019; Yang et al., 2010; Yoshihara et al., 2010; Yoshihara and Littleton, 2002). SYT7 has emerged as a popular candidate for the asynchronous Ca^{2+} sensor (Bacaj et al., 2013; Chen et al., 2017; Maximov et al., 2008; Turecek and Regehr, 2019, 2018; Weber et al., 2014; Wen et al., 2010). SYT7 has also been postulated to function as the Ca^{2+} sensor for short-term synaptic facilitation (Chen et al., 2017; Jackman et al., 2016; Turecek and Regehr, 2018). SYT7 has higher Ca^{2+} sensitivity, tighter membrane binding affinity and longer Ca^{2+} -lipid disassembly kinetics than SYT1 (Hui et al., 2005; Sugita et al., 2002, 2001; Voleti et al., 2017). These properties suggest SYT7 may regulate SV dynamics farther away from the AZ Ca^{2+} nanodomains that are required for SYT1 activation, or during temporal windows following the decay of the initial peak of Ca^{2+} influx. Together, these data have led to a two Ca^{2+} sensor model for evoked SV exocytosis, with SYT1 triggering the rapid synchronous phase of neurotransmitter release and SYT7 mediating asynchronous fusion and facilitation.

Although SYT7 manipulations can alter asynchronous release and facilitation at some synapses, several studies have suggested alternative explanations or identified unrelated defects in SV trafficking (**Figure 1A**). The recent observation that asynchronous release at mammalian synapses is anti-correlated with the levels of the synchronous Ca^{2+} sensors SYT1 and SYT2, but does not correlate with SYT7, prompted re-interpretation of earlier data on the protein's function (Turecek and Regehr, 2019). Besides asynchronous release and facilitation, mammalian SYT7 has been implicated in SV endocytosis, SV replenishment, SV pool mobility, and DCV fusion and replenishment (Bacaj et al., 2015; Dolai et al., 2016; Durán et al., 2018; Fukuda et al., 2004; Gustavsson et al., 2011; Li et al., 2017; Liu et al., 2014; Schonn et al., 2008; Tsuboi and Fukuda,

2007; Virmani et al., 2003; Wu et al., 2015). SYT7 has also been shown to regulate cell migration, lysosomal fusion and membrane repair in non-neuronal cells (Barzilai-Tutsch et al., 2018; Chakrabarti et al., 2003; Colvin et al., 2010; Czibener et al., 2006; Flannery et al., 2010; Jaiswal et al., 2004; Martinez et al., 2000; Reddy et al., 2001; Zhao et al., 2008).

Similar to the uncertainty surrounding SYT7 function, its subcellular localization is also unclear, with different studies localizing the protein to the plasma membrane, DCVs, lysosomes, endosomes or other internal compartments (Adolfson et al., 2004; Czibener et al., 2006; Flannery et al., 2010; Martinez et al., 2000; Mendez et al., 2011; Monterrat et al., 2007; Schonh et al., 2008; Shin et al., 2002; Sugita et al., 2001; Zhao et al., 2008). A key supporting argument for SYT7 as the asynchronous Ca^{2+} sensor is its reported localization to the AZ plasma membrane, positioning it at sites of SV fusion (Sugita et al., 2001). If SYT7 were present on endosomes or other internal membrane compartments, it would be more compatible with a role in SV trafficking rather than the fusion process itself. In summary, conflicting studies have generated confusion over how SYT7 contributes to neurotransmission and if the protein plays distinct roles across different neuronal subpopulations or species.

To examine the function of SYT7 in *Drosophila*, we generated and characterized *Syt7* null mutants. The *Drosophila* NMJ exhibits similar asynchronous release and facilitation properties to those of mammals (Jan and Jan, 1976; Jorquera et al., 2012; Yoshihara and Littleton, 2002), making it a useful system to examine evolutionary conserved functions of SYT7 in neurotransmitter release. We found *Syt7* mutants and *Syt1; Syt7* double mutants display increased evoked neurotransmitter release, indicating SYT7 negatively regulates SV fusion independent of

SYT1. In addition, CRISPR-mediated tagging of the endogenous *Syt7* locus indicates SYT7 localizes to a tubular network inside the presynaptic terminal that resides within the peri-active zone (peri-AZ) region, but is not enriched at sites of SV fusion. These data define a role for SYT7 in restricting SV availability and release, and indicate SYT7 is not a major Ca^{2+} sensor for asynchronous fusion and facilitation in *Drosophila*.

Results

Evolutionary conservation and structural comparison of SYT1 and SYT7

Synaptotagmins form one of the largest protein families involved in membrane tracking, with 17 *Syt* genes encoded in mammals and 7 *Syt* genes found in *Drosophila* (Adolfson and Littleton, 2001; Craxton, 2010; Sugita et al., 2002). Unlike the SV subfamily of SYTs, only a single *Syt7* gene is present in vertebrate and invertebrate genomes, making phenotypic comparisons easier. To examine the evolutionary relationship between SYT1, SYT7 and the more distantly related extended-Synaptotagmin (E-SYT) proteins, a phylogenetic tree was generated using the BLOSUM62 matrix and neighbor joining clustering analysis with protein sequences from placozoa (*Trichoplax adhaerens*), invertebrates (*Caenorhabditis elegans*, *Drosophila melanogaster*, *Ciona intestinalis*) and vertebrates (*Danio rerio*, *Rattus norvegicus*, *Homo sapiens*, **Figure 1B**). Although *Trichoplax* lacks neurons, it is the earliest metazoan that encodes *Syt* genes and contains both a SYT1 and SYT7 homolog (Barber et al., 2009). The phylogenetic tree contains independent clusters that correspond to the SYT1, SYT7 and E-SYT2 protein families. The clustering of SYT1 homologs across evolution correlates with nervous system complexity, with the *Trichoplax* homolog forming the outlier member of the cluster. Within the SYT7 cluster, *C. elegans* SYT7 is the most distantly related member, with the *Trichoplax* homolog residing closer within the cluster. *Drosophila* SYT7 is more distant from the vertebrate subfamily clade than is *Drosophila* SYT1 within its subfamily, suggesting SYT7 sequence conservation is not as closely related to nervous system complexity as SYT1. These observations are consistent with SYT7's broader expression pattern and function within neuronal and non-neuronal cells (MacDougall et al., 2018).

To compare SYT1 and SYT7 proteins, we performed homology modeling between *Drosophila* SYT7 and the published structure of mammalian SYT7 (*R. norvegicus* SYT7; PDB: 6ANK) (Voleti et al., 2017). Key structural features are highly conserved in the homology model, including the eight-stranded β -barrel and the Ca^{2+} binding loops that form the core of C2 domains (**Figure 1C**). In contrast to SYT1, both *Drosophila* and mammalian SYT7 lack the C2B HB helix previously found to have an inhibitory role in SV fusion (Xue et al., 2010). We next performed sequence alignment of SYT proteins from *H. sapiens*, *R. norvegicus* and *D. melanogaster* (**Figure 1 – figure supplement 1**). *Drosophila* SYT7 is 59% identical to human SYT7. Comparing the SYT1 and SYT7 subfamilies, the N-terminus encoding the transmembrane domain and linker region has the greatest variability and shares only 21% identity. Within the C2 domains, there is 100% conservation of the negatively charged Ca^{2+} binding residues in the C2 loops. A polybasic stretch in the C2B domain that mediates Ca^{2+} -independent PI(4,5)P₂-lipid interactions is also conserved. These sequence conservations indicate Ca^{2+} -dependent and Ca^{2+} -independent membrane binding are key properties of both SYT proteins.

Beyond lipid binding, SYT1's interaction with the SNARE complex is essential for its ability to activate SV fusion. Five key C2B residues (S332, R334, E348, Y391, A455) form the primary interaction site that docks SYT1 onto the SNARE complex (Guan et al., 2017; Zhou et al., 2015). Four of the five primary SNARE binding residues are not conserved in *Drosophila* SYT7 (**Figure 1C, Figure 1 – figure supplement 1**). In addition, *Drosophila* and mammalian SYT7 contain specific amino acids substitutions at two of these residues that block SNARE binding and abolish SYT1 function in SV fusion (Guan et al., 2017), including C285 (corresponding to *Syt1* mutant R334C) and K299 (corresponding to *Syt1* mutant E348K). A secondary SNARE complex-binding

interface on SYT1 is mediated by conserved basic residues at the bottom on the C2B β -barrel (R451/R452 in *Drosophila*; R388/R389 in rodents) and is also not conserved in the SYT7 subfamily (Wang et al., 2016; Xue et al., 2010; Zhou et al., 2015). As such, SYT7 is unlikely to engage the SNARE complex via the primary or secondary C2B interface, highlighting a key difference in how the proteins regulate membrane trafficking. Beyond SNARE-binding, 20 nonsynonymous amino acid substitutions are conserved only in the SYT1 or SYT7 subfamilies, suggesting additional interactions have likely diverged during evolution from the common ancestral SYT protein. In summary, SYT1 and SYT7 likely regulate membrane trafficking through distinct mechanisms, consistent with chimeric SYT1/SYT7 rescue experiments in mammals (Xue et al., 2010).

Generation of *Drosophila Syt7* mutations

To assay SYT7 function in *Drosophila*, the CRISPR-Cas9 system was used to generate null mutations in the *Syt7* locus. Using a guide RNA targeted near the *Syt7* start codon, several missense mutations were obtained. To disrupt the coding frame of *Syt7*, a single base pair cytosine deletion mutant (*Syt7^{M1}*) located seven amino acids downstream of the start codon was used for most of the analysis, with an unaffected Cas9 injection line as control (**Figure 1D**). A Minos transposon insertion in the second coding exon of *Syt7* was also identified from the BDGP gene disruption project (Bellen et al., 2004) that generates a premature stop codon before the C2A domain, providing a second independent allele (*Syt7^{M2}*) in a distinct genetic background (**Figure 1D**). To characterize the effects of SYT7 overexpression, a UAS-*Syt7* transgene was crossed with the neuronal *elav^{C155}*-GAL4 driver. Western analysis of adult brain extracts with anti-SYT7 antisera confirmed the absence of SYT7 protein in *Syt7^{M1}* and *Syt7^{M2}* mutants and a 2.5-fold increase in

SYT7 protein levels in *elav^{C155}-GAL4; UAS-Syt7* (**Figure 1E**). Similar to the loss of SYT7 in mice (Maximov et al., 2008), *Drosophila Syt7* null mutants are viable and fertile with no obvious behavioral defects.

Dose-dependent regulation of neurotransmitter release by SYT7

To assay SYT7's role in synaptic transmission, two-electrode voltage clamp (TEVC) recordings were performed at glutamatergic NMJs from 3rd instar larval motor neurons at segment A3 muscle 6 in 2 mM extracellular Ca^{2+} . No significant changes in spontaneous release parameters were identified, as miniature excitatory junctional current (mEJC) amplitude, kinetics and frequency were similar between *Syt7^{M1}* mutants, *Syt7^{M1}* heterozygotes (*Syt7^{M1/+}*) and controls (**Figure 2A-D**). In contrast to spontaneous release, evoked SV fusion (excitatory evoked junctional current (eEJC)) was dramatically enhanced in *Syt7^{M1}* single mutants and elevated to an intermediate level in *Syt7^{M1}* heterozygotes (**Figure 2E, F**; control: 158.33 ± 19.13 nA, n=9; *Syt7^{M1/+}*: $p < 0.05$, 233.08 ± 19.16 nA, n=14; *Syt7^{M1}*: $p < 0.005$, 262.96 ± 13.01 nA, n=10). Although evoked release was increased ~2-fold, there was no change in eEJC kinetics in *Syt7^{M1}* or *Syt7^{M1/+}* (**Figure 2G, H**). In addition, eEJC half-width was unaffected (**Figure 2I**). Loss of SYT7 increased evoked release regardless of whether quantal content was estimated using eEJC amplitude (which primarily measures synchronous release, 98% increase, **Figure 2J**) or eEJC charge (which measures both synchronous and asynchronous release, 128% increase, **Figure 2K**). The enhanced evoked release in *Syt7^{M1}* was observed over a large range of extracellular $[\text{Ca}^{2+}]$ spanning from 0.175 to 2 mM (**Figure 2L**). Although the Ca^{2+} response curve shifted leftward over the entire range in *Syt7^{M1}*, regression analysis revealed no significant difference in the Ca^{2+} cooperativity of release (control: 2.98 ± 0.17 (n=7 larvae); *Syt7^{M1}*: 2.69 ± 0.50 (n=7 larvae), $p=0.53$). We conclude

that loss of SYT7 enhances evoked SV release with no major effect on release kinetics or Ca²⁺ cooperativity at Drosophila NMJs.

The synaptic levels of SYT7 are likely to be rate-limiting for its ability to regulate synaptic transmission since *Syt7^{M1/+}* heterozygotes displayed an intermediate increase in evoked release compared to *Syt7^{M1}* null mutants. To determine if the effects of SYT7 are dosage-sensitive, SYT7 was overexpressed 2.5-fold by driving a UAS-*Syt7* transgene with neuronal *elav^{C155}*-GAL4 (**Figure 1E**). Overexpression of SYT7 had no significant effect on spontaneous mEJC kinetics or amplitude (**Figure 3A, B**), similar to the lack of effect in *Syt7* null mutants. However, SYT7 overexpression resulted in a ~2-fold decrease in mEJC frequency (**Figure 2C**, $p < 0.05$), suggesting elevated levels of SYT7 can reduce spontaneous fusion. Unlike the increased evoked release in *Syt7^{M1}* and *Syt7^{M1/+}* mutants, SYT7 overexpression caused a striking reduction in eEJC amplitude (**Figure 3D, E**) and eEJC charge (**Figure 3F**), with only mild effects on SV release kinetics (**Figure 3G**). To determine if the inhibitory action of SYT7 on SV release is secondary to a presynaptic role, SYT7 was overexpressed postsynaptically using the muscle specific *Mhc*-GAL4 driver. Overexpression of SYT7 in muscles had no effect on eEJC amplitude or kinetics (**Figure 3 – supplemental figure 1A, B**). We conclude that increased presynaptic SYT7 levels reduce both spontaneous and evoked SV release, indicating SYT7 functions as a negative regulator of neurotransmission.

Analysis of synaptic structure, AZ morphology and presynaptic Ca²⁺ influx in *Syt7* mutants

To determine if enhanced SV release in the absence of SYT7 results from an increase in AZ number or SV docking, synaptic morphology and ultrastructure at the NMJ was analyzed in *Syt7^{M1}*

mutants. Motor neurons form en passant synaptic boutons along the axon that contain hundreds of individual AZs marked by a central filamentous T-bar composed of the ELKS/CAST homolog Bruchpilot (BRP) (Ehmann et al., 2014; Wagh et al., 2006). Immunostaining for BRP, the SV-associated protein Complexin (CPX) and a general marker for neuronal membranes (anti-HRP) was performed at muscle 6/7 and muscle 4, the two NMJs analyzed in this study (**Figure 4A-H**). There was no change in the total number of synaptic boutons (**Figure 4C, F**), AZ number defined by BRP puncta (**Figure 4D, G**), or AZ number per muscle surface area (**Figure 4E, H**). To examine the AZ T-bar where SVs cluster, high-resolution structured illumination microscopy (SIM) was performed on larval muscle 4 NMJs following anti-BRP immunostaining. *Syt^{7MI}* mutants displayed the normal BRP ring architecture and showed no major difference in morphology compared to controls (**Figure 4I**). Individual T-bar size and intra-terminal T-bar spacing was quantified in controls and *Syt^{7MI}* mutants on a Zeiss Airyscan confocal. Although BRP ring structure was intact, *Syt^{7MI}* mutants displayed a 25% decrease in the average volume of individual BRP-labeled T-bars (**Figure 4J**), but no change in the spacing of T-bars relative to each other (**Figure 4K**). We conclude that loss of SYT7 does not disrupt overall AZ morphology or AZ number, though *Syt^{7MI}* mutants display a mild decrease in T-bar volume.

To assay if increased release in *Syt^{7MI}* mutants is secondary to elevated presynaptic Ca²⁺ influx, Ca²⁺ dynamics at NMJs were analyzed using Fluo-4 AM at 3rd instar larval Ib motor terminals at segment A3 muscle 6/7 in control and *Syt^{7MI}*. A stimulation paradigm consisting of three epochs of 10 Hz stimulation for 5 seconds separated by a 5 second rest period was performed (**Figure 4L**). Maximum presynaptic Fluo-4 AM fluorescence during the stimulation paradigm was significantly greater in control than in *Syt^{7MI}* (control: $10.7 \times 10^6 \pm 1.25 \times 10^6$, n=11 NMJs from 8

larvae; *Syt7^{MI}*: $6.52 \times 10^6 \pm 0.75 \times 10^6$, n= 9 NMJs from 8 larvae, $p < 0.01$, **Figure 4L, M**). These data indicate SYT7 does not suppress release by acting as a Ca^{2+} buffer or a negative regulator of Ca^{2+} channel function. Although the mechanism by which presynaptic Ca^{2+} influx is reduced in *Syt7* mutants is unknown, these data are consistent with the reduced AZ BRP volume (**Figure 4J**) and may represent a homeostatic response secondary to the enhanced release in *Syt7* mutants.

To determine if enhanced SV docking could increase the number of SVs available for release in *Syt7* mutants, SV distribution was quantified at larval muscle 6/7 NMJs in control and *Syt7^{MI}* using transmission electron microscopy (TEM, **Figure 5A**). No change in overall SV density was observed within *Syt7^{MI}* boutons, indicating SV recycling is largely unperturbed (**Figure 5B**). In contrast to the mild decrease in T-bar area (**Figure 4J**), there was no change in the length of individual AZs defined by the electron dense synaptic cleft (**Figure 5C**, $p = 0.93$; control: 404 ± 34.5 nm, n=21 AZs from 5 larvae; *Syt7^{MI}*: 409 ± 28.9 nm, n=29 AZs from 5 larvae). To examine docking, SVs in contact with the plasma membrane under the T-bar (within 100 nm, **Figure 5D**) or just outside the T-bar (100 to 400 nm, **Figure 5E**) were quantified. No significant change in the number of SVs docked at the AZ plasma membrane was detected (Fig 5D-F), indicating morphological docking defined by EM is not altered in *Syt7^{MI}* mutants. To quantify SV distribution in the cytoplasm around AZs, SV number was binned into four concentric hemi-circles from 100 to 400 nm radius centered on the T-bar. No significant difference in SV distribution was observed in any bin (**Figure 5G, H**), indicating the morphological distribution of SVs around T-bars is intact in the absence of SYT7. We conclude the enhanced release in *Syt7^{MI}* mutants is not due to increased AZ number or docked SVs.

Optical quantal mapping in *Syt7* mutants

Given quantal size (**Figure 2B**), AZ number (**Figure 4D, G**) and SV docking (**Figure 5H**) are unchanged in *Syt7* mutants, increased release probability (P_r) at individual AZs is a candidate mechanism to mediate the elevated quantal content during single stimuli. We previously developed a quantal imaging approach to map AZ P_r at *Drosophila* NMJs by expressing myristoylated GCaMP6s in muscles (Akbergenova et al., 2018; Melom et al., 2013). Using this approach, P_r maps for evoked release were generated for all AZs from Ib boutons at muscle 4 NMJs in control and *Syt7^{MI}* mutants (**Figure 6A**). Similar to controls, AZs formed by single motor neurons in *Syt7^{MI}* displayed heterogeneous P_r (**Figure 6B**). However, P_r distribution was strikingly different between the genotypes, with a greater number of high P_r and fewer low P_r AZs at *Syt7^{MI}* NMJs (**Figure 6C**). *Syt7^{MI}* NMJs also had fewer silent AZs that showed no release (control: 19.9%; *Syt7^{MI}*: 4.6%). Overall, mean P_r was increased 2-fold (**Figure 6D**, $p < 0.01$; control: 0.063 ± 0.002 , $n = 1158$ AZs; *Syt7^{MI}*: 0.12 ± 0.004 , $n = 768$ AZs). In contrast, the maximum AZ P_r in the two genotypes was unchanged (**Figure 6D**, control: 0.61; *Syt7^{MI}*: 0.63), indicating an upper limit on release strength for single AZs that is similar between controls and *Syt7^{MI}*. We conclude that the enhanced release in the absence of SYT7 results from an increase in average P_r across the AZ population.

Loss of SYT7 enhances SV release in *Syt1* null mutants

Drosophila Syt1 null mutants have dramatically reduced synchronous SV fusion and enhanced asynchronous and spontaneous release (Jorquera et al., 2012; Lee et al., 2013; Yoshihara et al., 2010; Yoshihara and Littleton, 2002). We generated *Syt1; Syt7* double mutants to determine if SYT7 mediates the residual asynchronous release present in *Syt1* nulls. A complete loss of

asynchronous release in *Syt1*; *Syt7* double mutants should occur if SYT7 functions as the sole asynchronous Ca^{2+} sensor, while a reduction in release is expected if it is one of several sensors mediating the residual synaptic transmission in *Syt1*. Animals lacking SYT1 were obtained by crossing an intragenic *Syt1* deletion (*Syt1^{NI3}*) with a point mutant containing an early stop codon (*Syt1^{AD4}*), an allelic combination referred to as *Syt1^{Null}*. Loss of SYT1 results in lethality throughout development, although some *Syt1^{Null}* mutants survive to adulthood when cultured under special conditions (Loewen et al., 2001). Surviving *Syt1^{Null}* adults are severely uncoordinated and die within several days. Quantification of survival rates demonstrated 45.3% of *Syt1^{Null}* mutants survived from the 1st instar to the pupal stage, with 44.1% of mutant pupae surviving to adulthood (n=5 groups with >40 starting animals each). In contrast, 5.6% of *Syt1^{Null}*; *Syt7^{M2}* double mutants (referred to as *Double^{Null}*) survived from the 1st instar to the pupal stage, and 6.6% of mutant pupae survived to adulthood (n=6 groups with >80 animals each). Western analysis confirmed loss of both proteins in *Double^{Null}* mutants and demonstrated no change in expression of SYT1 or SYT7 in the absence of the other family member in individual null mutant backgrounds (**Figure 7A**). Although loss of both SYTs caused synergistic defects in survival, residual synaptic transmission must exist given some *Double^{Null}* mutants survive.

To assay synaptic transmission, recordings were performed from 3rd instar larval muscle 6 in 2 mM extracellular Ca^{2+} in *Syt1^{Null}* and *Double^{Null}* mutants. No change in spontaneous mEJC amplitude or kinetics was found between the two genotypes (**Figure 7B**), indicating postsynaptic sensitivity, neurotransmitter loading, and fusion pore dynamics were not disrupted by loss of SYT7. However, a ~2-fold increase in mEJC frequency was observed in the *Double^{Null}* compared to *Syt1^{Null}* (**Figure 7C**, $p < 0.001$; *Syt1^{Null}*: 2.99 ± 0.23 Hz, n=16; *Double^{Null}*: 5.33 ± 0.42 Hz, n=14),

demonstrating loss of both SYTs enhances the already elevated spontaneous release rate found in *Syt1^{Null}* mutants alone. Measurements of evoked release revealed both amplitude and charge transfer were increased ~2-fold in *Double^{Null}* compared to *Syt1^{Null}* mutants (**Figure 7D-F**; eEJC amplitude: $p < 0.001$; *Syt1^{Null}*: 3.18 ± 0.4 nA, $n=15$; *Double^{Null}*: 6.12 ± 0.62 nA, $n=13$; eEJC charge: $p < 0.05$; *Syt1^{Null}*: 33.2 ± 4.4 nA*ms, $n=15$; *Double^{Null}*: 52.6 ± 5.8 nA*ms, $n=13$). In addition, more SVs fused in the first 15 ms following stimulation (**Figure 7G, H**), with less SVs available for release later in the response. *Double^{Null}* mutants also had a reduced rate of evoked failures following nerve stimulation compared to *Syt1^{Null}*, consistent with an increased probability of SV release (**Figure 7I**, $p < 0.01$; *Syt1^{Null}*: $21.1 \pm 3.5\%$ failure rate, $n=17$; *Double^{Null}*: $7.4 \pm 3.4\%$ failure rate, $n=14$). These results indicate SYT7 does not mediate the residual release found in the absence of SYT1. We conclude SYT7 negatively regulates SV release with or without SYT1 present at the synapse.

Short-term facilitation does not require SYT7

Although these results indicate SYT7 is not a key asynchronous Ca^{2+} sensor in *Drosophila*, the protein has also been implicated as the Ca^{2+} sensor for facilitation (Chen et al., 2017; Jackman et al., 2016; Turecek and Regehr, 2018), a short-term form of presynaptic plasticity that results in enhanced SV fusion during closely-spaced stimuli. To examine facilitation, $[\text{Ca}^{2+}]$ was lowered from 2 mM to 0.175 mM or 0.2 mM to identify conditions where the initial P_r was matched between control and *Syt7* mutants. In 0.175 mM Ca^{2+} , controls displayed an 11% failure ratio in response to single action potentials, while *Syt7^{MI}* had no failures (**Figure 8A**). In 0.2 mM Ca^{2+} , neither genotype had failures (**Figure 8A**), although evoked release was increased 3-fold in *Syt7^{MI}* (**Figure 7B, C**, $p < 0.01$, control: 7.73 ± 1.5 nA, $n=9$; *Syt7^{MI}*: 23.72 ± 6.2 nA, $n=9$). In contrast, EJC

amplitude was not statistically different between control in 0.2 mM Ca²⁺ (7.73 ± 1.5 nA, n=9) and *Syt7^{MI}* in 0.175 mM Ca²⁺ (8.70 ± 1.6 nA, n=9). Facilitation was assayed in these conditions where initial P_r was comparable. Control and *Syt7^{MI}* mutants displayed robust facilitation to paired pulses separated by 10 or 50 ms at both Ca²⁺ concentrations (**Figure 8D**). A modest reduction in paired-pulse ratio was observed in *Syt7^{MI}* at 0.175 Ca²⁺ compared to control at 0.2 mM Ca²⁺ (**Figure 8E, F**, p<0.05; 10 ms interval: 31% decrease; 50 ms interval: 22% decrease). These data indicate SYT7 is not the sole effector of facilitation. The mild defect in *Syt7* mutants could be due to a partially redundant role for SYT7 in facilitation or secondary to differences in Ca²⁺ available to activate the true facilitation sensor. Given [Ca²⁺] was lowered in *Syt7^{MI}* to match initial P_r between the genotypes, the latter hypothesis is more likely.

To determine if short-term facilitation could be elicited in the absence of both SYT1 and SYT7, a 10 Hz stimulation train in 2.0 mM Ca²⁺ was given to *Double^{Null}* mutants and eEJC responses were compared to *Syt1^{Null}* mutants alone. Similar to the increased quantal content to single action potentials, *Double^{Null}* mutants displayed larger facilitating responses during the early phase of stimulation (**Figure 8G-I**; cumulative average release for 10 stimuli: *Syt1^{Null}* (n=12): 87 ± 7.0 quanta; *Double^{Null}* (n=13): 109 ± 9.9 quanta; 20 stimuli: *Syt1^{Null}*: 209 ± 13.8 quanta; *Double^{Null}*: 261 ± 22.6 quanta; 50 stimuli: *Syt1^{Null}*: 594 ± 34.5 quanta; *Double^{Null}*: 745 ± 56.2 quanta, p<0.03). These results indicate short-term facilitation can occur in the absence of both SYT1 and SYT7, and is enhanced during the early phases of stimulation, consistent with SYT7 negatively regulating SV fusion with or without SYT1.

***Syt7* mutants have access to a larger pool of fusogenic SVs but maintain a normal rate of SV endocytosis at steady-state**

Enhanced SV release in *Syt7* mutants could reflect increased fusogenicity of the entire SV population or conversion of a non-fusogenic SV pool into one capable of release in the absence of SYT7. To test whether SYT7 normally renders a pool of SVs non-fusogenic, 1000 stimuli at 10 Hz were applied in 2 mM Ca²⁺ at 3rd instar muscle 6 NMJs to deplete the readily releasable pool (RRP) and drive SV cycling to steady-state. The total number of released SVs and the SV recycling rate was then measured. Both control and *Syt7^{MI}* eEJCs depressed during the stimulation train. However, SV release in *Syt7^{MI}* mutants remained elevated over much of the initial stimulation (**Figure 9A**) and the integral of release during the train was greater than controls (**Figure 9B**), indicating *Syt7* nulls have access to more fusogenic SVs. SV release rate in *Syt7^{MI}* eventually reached the same level as control following depletion of the RRP (**Figure 9C**, control quantal content: 131.5 ± 10.7, n=7; *Syt7^{MI}* quantal content: 123.1 ± 10.5, n=8). We conclude that SV endocytosis and recycling rate is SYT7-independent at steady-state, although *Syt7^{MI}* mutants contain a larger RRP available for fusion.

To further examine SV recycling, FM1-43 dye uptake and release assays were performed in control and *Syt7^{MI}* mutants at 3rd instar muscle 6/7 NMJs. At low stimulation rates (0.5 Hz), *Syt7^{MI}* mutants took up significantly more FM1-43 dye than controls (**Figure 9D, F**), consistent with the increased SV release observed by physiology. In contrast, no significant difference in FM1-43 uptake was found following high frequency 10 Hz stimulation for 500 stimuli (**Figure 9E, G**). These data suggest previously exocytosed SVs re-enter the RRP more often in the absence of SYT7 given the normal recycling rate (**Figure 9C**). Consistent with this hypothesis, no change in FM1-

43 release was detected with high $[K^+]$ stimulation following 10 Hz loading (**Figure 9H**). Together with the electrophysiology data, we conclude *Syt7* mutants have a larger RRP, but no changes in SV endocytosis.

***Syt7* mutants have enhanced refilling of the readily-releasable SV pool independent of endocytosis**

To probe how SYT7 regulates SV cycling and the transition between distinct SV pools, eEJC recovery kinetics following high frequency stimulation were characterized. A paradigm consisting of 30 stimuli at 0.5 Hz, 500 stimuli at 10 Hz and a final 50 stimuli at 0.5 Hz was given to *Syt7^{M1}* mutants, *Syt7^{M1/+}* heterozygotes and controls in 2 mM Ca^{2+} (**Figure 10A**). During 0.5 Hz stimulation, *Syt7^{M1}* and *Syt7^{M1/+}* displayed elevated levels of release. Following the onset of high frequency stimulation, *Syt7^{M1}* and *Syt7^{M1/+}* synapses depressed while controls displayed a mild facilitation before quickly transitioning to depression (**Figure 10B**). Remarkably, *Syt7^{M1}* and *Syt7^{M1/+}* displayed an extremely rapid recovery of eEJC amplitude and quantal content during the 2 second interval following termination of the 10 Hz train compared to controls (**Figure 10C**). A similar rapid recovery was observed in *Syt7^{M1}* after 2000 stimuli were given at 10 Hz to fully deplete the RRP and normalize release rates to control levels (**Figure 10 – figure supplement 1A-C**). These observations suggest SYT7 also functions to reduce SV entry into the RRP, while negatively regulating release of newly regenerated SVs. The enhanced refilling of the RRP did not require SYT1 function, as *Double^{Null}* mutants also displayed larger eEJCs than *Syt1^{Null}* alone during the recovery from a 10 Hz stimulation train (**Fig. 8G**).

The partial elevation in RRP refilling rate at *Syt7^{M1/+}* synapses indicates the amount of SYT7 in the presynaptic terminal regulates SV entry into the releasable pool. To determine if RRP refilling is dosage-sensitive, the stimulation paradigm above (0.5 Hz/10 Hz/0.5 Hz) was applied to SYT7 overexpression larvae (*elav^{C155}-GAL4; UAS-Syt7*) in 2 mM Ca²⁺. Presynaptic overexpression of SYT7 had the opposite effect of *Syt7* mutants and *Syt7/+* heterozygotes, not only reducing eEJC amplitude at 0.5 Hz, but greatly limiting the ability of SVs to re-enter the RRP following termination of the 10 Hz stimulation train (**Figure 10 – supplemental figure 2A-C**). We conclude that SYT7 limits release in a dosage-sensitive manner by negatively regulating the number of SVs available for fusion and slowing recovery of the RRP following stimulation.

To determine if increased RRP refilling in *Syt7^{M1}* requires an enhanced rate of SV endocytosis or is mediated through refilling from a pre-existing SV pool, recordings were repeated in the presence of the proton pump inhibitor bafilomycin. Bafilomycin blocks neurotransmitter reloading of newly endocytosed SVs and should eliminate the enhanced refilling of the RRP if recycling is essential. Alternatively, if SVs are recruited more rapidly from pre-existing pools, bafilomycin would not abolish the enhanced recovery. The same 0.5 Hz/10 Hz/0.5 Hz paradigm was applied in three successive epochs in the presence of 4 uM bafilomycin or DMSO (control) in the bath solution. As expected, bafilomycin progressively reduced eEJC amplitude throughout the experiment and eliminated most evoked responses during the 3rd stimulation epoch (**Figure 10D**). *Syt7^{M1}* mutants displayed a similar fold-enhancement in the recovery of the RRP in the presence of bafilomycin, though the absolute numbers of SVs re-entering the pool decreased following the 2nd 10 Hz stimulation as the number of neurotransmitter-containing SVs declined (**Figure 10E, F**). We conclude that the rapid refilling of the RRP can occur from pre-existing SV pools. In

addition to reducing fusogenicity of SVs already docked at the AZ, these data indicate SYT7 regulates transition kinetics between vesicle pools by reducing the number of SVs moving from the reserve pool to the RRP.

SYT7 localizes to an internal membrane network within the peri-AZ that resides in proximity to multiple presynaptic compartments

Defining the subcellular localization of SYT7 could help elucidate how it modulates SV dynamics. SYT7 could be a resident protein of the SV pool it regulates or reside on an alternative compartment that exerts control over a subset of SVs. To examine the subcellular localization of SYT7, an RFP tag was introduced at the 3'-end of the endogenous *Syt7* locus using CRISPR (**Figure 11A**). This approach generated a SYT7^{RFP} C-terminal fusion protein expressed under its endogenous enhancers to avoid any overexpression that might trigger changes in its normal localization. The RFP C-terminal fusion did not abolish SYT7 function, as eEJC amplitude in 2 mM Ca²⁺ was not significantly different between control and SYT7^{RFP} (control: 198.9 ± 8.8 nA, n=14; SYT7^{RFP}, 227 ± 11.3 nA, n=14, p=0.1). A sfGFP version (SYT7^{GFP}) was also generated with CRISPR that showed the same intra-terminal expression pattern as SYT7^{RFP} (**Figure 11 – supplemental figure 1A**). Western analysis with anti-RFP identified a single band at the predicted molecular weight (73kD) of the fusion protein in SYT7^{RFP} animals (**Figure 11B**), indicating a single SYT7 isoform is expressed in *Drosophila*. Immunostaining of 3rd instar larvae with anti-RFP antisera revealed SYT7^{RFP} was enriched in presynaptic terminals and formed an expansive tubular network near the plasma membrane that extended into the center of the bouton (**Figure 11C, D**). Neuronal knockdown of *Syt7* with two independent RNAi lines (*elav^{C155}-GAL4*; UAS-*Syt7* RNAi) dramatically reduced SYT7^{RFP} on Westerns (**Figure 11B**) and eliminated expression

of SYT7^{RFP} at the NMJ (**Figure 11 – supplemental figure 2**), indicating the signal is specific to SYT7 and localizes predominantly to the presynaptic compartment.

To further characterize the subsynaptic localization of SYT7, fluorescently-tagged compartmental markers or compartment-specific antisera were used for labeling in the Syt7^{RFP} background. Images were collected on a Zeiss Airyscan and analyzed in FIJI and Matlab to generate cytofluorogram co-localization plots to calculate the Pearson correlation (r) between SYT7^{RFP} and labeled compartments from individual synaptic boutons at muscle 6/7 NMJs (**Figure 12**, $n=3$ animals each). Co-labeling of the SV proteins nSYB and SYT1 served as a positive control (**Figure 12A**, $r=0.71$). SYT7^{RFP} and the Golgi marker, Golgin84, served as a negative control since Golgi is absent from presynaptic terminals (**Figure 12L**, $r=-0.43$). Co-localization analysis indicates SYT7 resides on a membrane compartment that does not completely overlap with any protein tested (**Figure 12B-L**). The largest overlap was with Dynamin (**Figure 12B**, $r=0.22$), a GTPase involved in endocytosis that localizes to the peri-AZ. The t-SNARE SYX1 also overlapped with a subset of SYT7 immunolabeling near the plasma membrane (**Figure 12C**, $r=0.15$). Although SYT7's pattern of inter-connectivity within the bouton appeared similar to peripheral ER, it did not co-localize with Reticulon-like 1 (RTL1, **Figure 12D**, $r=0.01$), a peripheral ER marker. In addition, SYT7 did not co-localize with SVs ($r=-0.17$), DCVs labeled with ANF-GFP ($r=-0.07$), exosomes ($r=-0.19$), late endosomes ($r=-0.29$), lysosomes ($r=-0.01$) or the plasma membrane (anti-HRP, $r=-0.06$). Neither SYT7^{RFP} (**Figure 12G**, $r=-0.11$) or SYT7^{GFP} (**Figure 11 – supplemental figure 1B**) was enriched at AZs, but instead surrounded BRP as previously described for other peri-AZ proteins. These data are in agreement with anti-SYT7 antibody labeling of sucrose gradient-separated subcellular fractions from wildtype *Drosophila*

head extracts that localized SYT7 to a distinct membrane compartment separate from SVs and the plasma membrane (Adolfson et al., 2004). In conclusion, SYT7 surrounds AZs marked by BRP (**Figure 11 – supplemental figure 1B, Figure 12G**), indicating the protein localizes in part to the previously described peri-AZ domain. Peri-AZs are enriched in proteins regulating SV endocytosis and endosomal trafficking (Coyle et al., 2004; Koh et al., 2004; Marie et al., 2004; Rodal et al., 2008; Sone et al., 2000), indicating SYT7 may modulate SV re-entry into the RRP by interfacing with sorting machinery within this domain.

SYT7 localization was widespread within the peri-AZ region, with SYT7^{RFP} tubules in close proximity to other labeled membrane compartments, including endosomes, lysosomes, and the plasma membrane (**Figure 12 – figure supplement 1**). To determine if the SYT7 compartment required endosomal trafficking for its assembly or maintenance, a panel of dominant-negative, constitutively-active or wildtype endosomal UAS-RAB proteins (Zhang et al., 2007) were expressed with *elav^{C155}*-GAL4 in the SYT7^{RFP} background. Manipulations of RAB5 (early endosomes), RAB7 (late endosomes) or RAB4 and RAB11 (recycling endosomes) did not disrupt the abundance or morphology of the SYT7 tubular network (**Figure 12 – supplemental figure 2**). Similarly, no change in the distribution of several compartment markers were found in *Syt7^{M1}* mutants, including the early endosomal marker RAB5, the late endosomal/peri-AZ marker RAB11 and the peri-AZ protein Nervous Wreck (NWK) (**Figure 12 – supplemental figure 3**). In addition, no defect was observed in trans-synaptic transfer of the exosomal protein SYT4 to the postsynaptic compartment, indicating SYT7 does not regulate exosome trafficking as described for several other peri-AZ proteins (Walsh et al., 2019). Although no sub-compartment overlapped completely with SYT7, the protein is positioned within the peri-AZ to interact with SVs, endosomes and the

recycling machinery to negatively regulate the size of releasable SV pools (**Figure 12 – supplemental figure 4**). We conclude that SYT7 does not localize to SVs and is not enriched at AZs, consistent with SYT7 negatively regulating SV release through an indirect mechanism that does not require its presence at sites of SV fusion.

Discussion

To characterize the location and function of SYT7 in *Drosophila*, we used the CRISPR-Cas9 system to endogenously label the protein and generate null mutations in the *Syt7* locus. Our findings indicate SYT7 acts as a negative regulator of SV release, AZ P_r , RRP size, and RRP refilling. The elevated P_r across the AZ population in *Syt7* mutants provides a robust explanation for why defects in asynchronous release and facilitation are observed in the absence of the protein, as SYT7 levels set the baseline for the amount of evoked release. SYT7's presence on an internal tubular membrane network within the peri-AZ positions the protein to interface with the SV cycle at multiple points to regulate membrane trafficking. In addition, increased SV release in animals lacking both SYT1 and SYT7 indicate the full complement of Ca^{2+} sensors that mediate the distinct phases of SV release remain unknown.

*Syt7 mutants have increased P_r at *Drosophila* NMJs*

Using a combination of synaptic physiology and imaging approaches, our findings indicate SYT7 acts to reduce SV recruitment and release. Minor defects in asynchronous release and facilitation were identified in *Drosophila Syt7* mutants, as observed in mouse and zebrafish models (Bacaj et al., 2013; Chen et al., 2017; Jackman et al., 2016; Turecek and Regehr, 2019, 2018; Weber et al., 2014; Wen et al., 2010). However, we attribute these defects to reduced SV availability as a result of increased P_r in *Syt7* mutants. Indeed, a key feature of facilitation is its critical dependence on initial P_r (Neher and Brose, 2018; Zucker and Regehr, 2002). Low P_r synapses increase SV fusogenicity as Ca^{2+} levels rise during paired-pulses or stimulation trains, resulting in short-term increases in P_r for SVs not recruited during the initial stimuli. In contrast, depression occurs at high P_r synapses due to the rapid depletion of fusion-capable SVs during the

initial response. Prior quantal imaging at *Drosophila* NMJs demonstrated facilitation and depression can occur across different AZs within the same neuron, with high P_r AZs depressing and low P_r AZs facilitating (Peled and Isacoff, 2011). Given the elevated P_r in *Syt7* mutants, the facilitation defects are likely related to differences in initial P_r and depletion of fusion-competent SVs available for release during the 2nd stimuli.

A similar loss of SVs due to elevated P_r in *Syt7* mutants would reduce fusogenic SVs that are available during the delayed phase of the asynchronous response. *Syt1*; *Syt7* double mutants continue to show asynchronous fusion and facilitation, demonstrating there must be other Ca^{2+} sensors that mediate these components of SV release. The predominant localization of endogenous SYT7 to an internal tubular membrane compartment at the peri-AZ also places the majority of the protein away from release sites where it would need to reside to directly activate SV fusion. As such, our data indicate SYT7 regulates SV release through a distinct mechanism from SYT1.

We can also conclude that the remaining components of asynchronous fusion and facilitation must be mediated by an entirely different family of Ca^{2+} -binding proteins than Synaptotagmins (or through Ca^{2+} -lipid interactions). Of the seven *Syt* genes in the *Drosophila* genome, only 3 SYT proteins are expressed at the motor neuron synapses assayed in our study – SYT1, SYT4 and SYT7 (Adolfson et al., 2004). For the remaining SYTs in the genome, SYT- α and SYT- β are expressed in neurosecretory neurons and function in DCV fusion (Adolfson et al., 2004; Park et al., 2014). SYT12 and SYT14 lack Ca^{2+} binding residues in their C2 domains and are not expressed in motor neurons (Adolfson et al., 2004). In addition, SYT4 is found on exosomes and transferred to postsynaptic cells, where it participates in retrograde signaling (Adolfson et al., 2004; Harris et al.,

2016; Korkut et al., 2013; Walsh et al., 2019; Yoshihara et al., 2005). *Syt1*; *Syt4* double mutants display the same SV fusion defects found in *Syt1* mutants alone, indicating SYT4 cannot compensate for SYT1 function in SV release (Barber et al., 2009; Saraswati et al., 2007). As such, SYT1 and SYT7 are the only remaining SYT isoforms that could contribute to SV trafficking within *Drosophila* motor neuron terminals.

A prior study from our lab using a *Syt7* exon-intron hairpin RNAi we generated did not result in an increase in evoked release (Saraswati et al., 2007). Although a reduction in ectopic expression of SYT7 in muscles could be seen with *Mhc*-GAL4 driving the UAS-*Syt7* RNAi, our anti-SYT7 antisera does not recognize the endogenous protein in neurons using immunocytochemistry, preventing a determination of presynaptic SYT7 levels following neuronal RNAi. To further examine this issue, we performed western analysis with this RNAi and compared it those used in the current study. Our results confirmed that the RNAi line failed to reduce endogenous GFP-tagged SYT7 (data not shown), although the two commercial RNAi lines we used here were highly effective (**Figure 11B**). Based on these data, we conclude that the previous *Syt7* UAS-RNAi line was ineffective in knocking down endogenous SYT7. Given the *Syt7^{M1}* and *Syt7^{M2}* alleles result in early stop codons and lack SYT7 expression by Western analysis and display elevated levels of fusion, our data indicate SYT7 normally acts to suppress SV release as demonstrated by electrophysiology and optical *P_r* imaging. SYT7 overexpression reduces SV release even more, further confirming that the levels of SYT7 set the baseline amount of SV fusion at *Drosophila* NMJ synapses.

SYT7 regulates the recruitment and fusion of SVs in a dose-dependent manner

Although our data indicate SYT7 is not the primary asynchronous or facilitation Ca^{2+} sensor in *Drosophila*, we found it inhibits SV release in a dosage-sensitive manner. The reduction in SV release is not due to changes in the Ca^{2+} cooperativity of fusion or enhanced presynaptic Ca^{2+} entry, ruling out the possibility that SYT7 normally acts as a local Ca^{2+} buffer or an inhibitor of presynaptic voltage-gated Ca^{2+} channels. The reduction in release is also not due to altered endocytosis, as *Syt7* mutants have a normal steady-state rate of SV cycling following depletion of the RRP. Instead, SYT7 regulates SV fusogenicity at a stage between SV endocytosis and fusion. Given the rapid enhanced refilling of the RRP observed in *Syt7* mutants, and the suppression of RRP refilling following SYT7 overexpression, our data indicate SYT7 regulates releasable SVs in part through changes in SV mobilization to the RRP. Ca^{2+} is well known to control the replenishment rate of releasable SVs, with Calmodulin-UNC13 identified as one of several molecular pathways that accelerate RRP refilling in a Ca^{2+} -dependent manner (Dittman et al., 2000; Dittman and Regehr, 1998; Junge et al., 2004; Lipstein et al., 2013; Ritzau-Jost et al., 2018). Our findings indicate SYT7 acts in an opposite fashion and slows RRP refilling, providing a Ca^{2+} -dependent counter-balance for SV recruitment into the RRP. Although such an effect has not been described for mammalian SYT7, defects in RRP replenishment have been observed when both SYT1 and SYT7 are deleted or following high frequency stimulation trains (Bacaj et al., 2015; Durán et al., 2018; Liu et al., 2014).

SYT7's role in restricting SV fusion and RRP size also affects spontaneous release. Although *Syt7* mutants alone do not show elevated mini frequency, *Double^{Null}* mutants have a 2-fold increase in spontaneous release. Similar increases in spontaneous release were observed at mammalian

synapses lacking both SYT7 and SYT1 (or SYT2), with the effect being attributed to a dual role in clamping fusion in the absence of Ca^{2+} (Luo and Südhof, 2017; Turecek and Regehr, 2019). Our results indicate the elevation in spontaneous release at *Drosophila* synapses is a result of an increase in releasable SVs rather than a clamping function for SYT7. Following overexpression of SYT7, there is a reduction in the number of fusogenic SVs available for both evoked and spontaneous release. The dosage-sensitivity of the various phenotypes indicate SYT7 abundance is a critical node in controlling SV release rate. Indeed, mammalian SYT7 levels are post-transcriptionally modulated by γ -secretase proteolytic activity and APP, linking it to SV trafficking defects in Alzheimer's disease (Barthet et al., 2018).

How does SYT7 negatively regulate recruitment and fusion of SVs?

The precise mechanism by which SYT7 reduces release and slows refilling of the RRP is uncertain given it is not enriched at sites of SV fusion. Although we cannot rule out the possibility that a small fraction of the protein is found at AZs, SYT7 is predominantly localized to an internal membrane compartment at the peri-AZ where SV endocytosis and endosomal sorting occurs (Coyle et al., 2004; Koh et al., 2004; Marie et al., 2004; Rodal et al., 2008; Sone et al., 2000). SYT7 membrane tubules are in close proximity and could potentially interact with peri-AZs proteins, endosomes, lysosomes and the plasma membrane. Given its primary biochemical activity is to bind membranes in a Ca^{2+} -dependent manner, SYT7 could mediate cargo or lipid movement across multiple compartments within peri-AZs. In addition, it is possible SYT7 tubules could form part of the poorly defined SV recycling endosome compartment. However, we observed no change in SV density or SV localization around AZs, making it unlikely SYT7 would be essential for endosomal trafficking of SVs. The best characterized regulator of the SV endosome compartment

in *Drosophila* is the RAB35 GAP Skywalker (SKY) (Uytterhoeven et al., 2011). Although *Sky* mutations display some similarities to *Syt7*, including increased neurotransmitter release and larger RRP size, *Syt7* lacks most of the well-described *Sky* phenotypes such as behavioral paralysis, FM1-43 uptake into discrete punctated compartments, cisternal accumulation within terminals and reduced SV density. In addition, we found no co-localization between SKY-GFP and SYT7^{RFP} within presynaptic terminals.

By blocking SV refilling with bafilomycin, our findings indicate the fast recovery of the RRP can occur via enhanced recruitment from the reserve pool and does not require changes in endocytosis rate. The phosphoprotein Synapsin has been found to maintain the reserve SV pool by tethering vesicles to actin filaments at rest (Akbergenova and Bykhovskaia, 2007; Bykhovskaia, 2011; Hilfiker et al., 1999; Milovanovic and De Camilli, 2017; Shupliakov et al., 2011). Synapsin interacts with the peri-AZ protein Dap160/Intersectin to form a protein network within the peri-AZ that regulates clustering and release of SVs (Gerth et al., 2017; Marie et al., 2004; Winther et al., 2015). Synapsin-mediated phase separation is also implicated in clustering SVs near release sites (Milovanovic et al., 2018; Milovanovic and De Camilli, 2017). SYT7 could similarly maintain a subset of SVs in a non-releasable pool and provide a dual mechanism for modulating SV mobilization. Phosphorylation of Synapsin and Ca²⁺ activation of SYT7 would allow multiple activity-dependent signals to regulate SV entry into the RRP. As such, SYT7 could play a key role in organizing membrane trafficking and protein interactions within the peri-AZ network by adding a Ca²⁺-dependent regulator of SV recruitment and fusogenicity.

Additional support for a role for SYT7 in regulating SV availability through differential SV sorting comes from recent studies on the SNARE complex binding protein CPX. Analysis of *Drosophila Cpx* mutants, which have a dramatic increase in minis (Buhl et al., 2013; Huntwork and Littleton, 2007; Jorquera et al., 2012), revealed a segregation of recycling pathways for SVs undergoing spontaneous versus evoked fusion (Sabeva et al., 2017). Under conditions where intracellular Ca^{2+} is low and SYT7 is not activated, spontaneously-released SVs do not transit to the reserve pool and rapidly return to the AZ for re-release. In contrast, SVs released during high frequency evoked stimulation when Ca^{2+} is elevated and SYT7 is engaged, re-enter the RRP at a much slower rate. This mechanism slows re-entry of SVs back into the releasable pool when stimulation rates are high and large numbers of SV proteins are deposited onto the plasma membrane at the same time, allowing time for endosomal sorting that might be required in these conditions. In contrast, SVs released during spontaneous fusion or at low stimulation rates would likely have less need for endosomal re-sorting. Given SYT7 restricts SV transit into the RRP, it provides an activity-regulated Ca^{2+} -triggered switch for redirecting and retaining SVs in a non-fusogenic pool that could facilitate sorting mechanisms.

Beyond SV fusion, presynaptic membrane trafficking is required for multiple signaling pathways important for developmental maturation of NMJs (Harris and Littleton, 2015; McCabe et al., 2003; Packard et al., 2002; Piccioli and Littleton, 2014; Rodal et al., 2011). In addition, alterations in neuronal activity or SV endocytosis can result in synaptic undergrowth or overgrowth (Akbergenova et al., 2018; Budnik et al., 1990; Dickman et al., 2006; Guan et al., 2005; Koh et al., 2004). We did not find any defect in synaptic bouton or AZ number, indicating SYT7 does not participate in membrane trafficking pathways that regulate synaptic growth and maturation.

However, a decrease in T-bar area and presynaptic Ca^{2+} influx in *Syt7* mutants was found. Although it is unclear how these phenotypes arise, they may represent a form of homeostatic plasticity downstream of elevated synaptic transmission (Frank et al., 2020). There is also ample evidence that SV distance to Ca^{2+} channels plays a key role in defining the kinetics of SV release and the size of the RRP (Böhme et al., 2016; Chen et al., 2015; Neher, 2015; Neher and Brose, 2018; Wadel et al., 2007), suggesting a change in such coupling in *Syt7* mutants might contribute to elevations in P_r and RRP refilling. Further studies will be required to precisely define how SYT7 controls the baseline level of SV release at synapses.

Materials and Methods

Drosophila stocks

Drosophila melanogaster were cultured on standard medium at 22-25°C. Genotypes used in the study include: *elav^{C155}*-GAL4 (Bloomington Drosophila Stock Center (BDSC)#8765), UAS-ANF-Emerald (BDSC#7001), SYT4^{GFP-2M} (Harris et al., 2016), *Syt1^{AD4}* (DiAntonio and Schwarz, 1994), *Syt1^{N13}* (Littleton et al., 1993b), UAS-*Syt7* (Saraswati et al., 2007), *Mhc*-GAL4 (BDSC#55132), UAS-*Syt7* RNAi#1 (Vienna#24989) and UAS-*Syt7* RNAi#2 (BDSC#27279). Lines used for testing co-localization with SYT7^{RFP} or mis-localization in *Syt7^{M1}* include: endogenous nSYB^{GFP} (this study), UAS-NHE-GFP (this study), UAS-ANF-Emerald (BDSC#7001), SYT4^{GFP-2M} (Harris et al., 2016), UAS-RTNL1-GFP (BDSC#77908), RAB5-YFP (BDSC#62543) and RAB11-YFP (BDSC#62549). Lines used for assaying SYT7^{RFP} localization after overexpressing RABs: UAS-RAB4-YFP (BDSC#9767), UAS-RAB4(Q67L)-YFP (BDSC#9770), UAS-RAB5-YFP (BDSC#24616), UAS-RAB5(S43N)-YFP (BDSC#9772), UAS-RAB5(T22N)-YFP (BDSC#9778), UAS-RAB7-YFP (BDSC#23641), UAS-RAB7(Q67L)-YFP (BDSC#9779), UAS-RAB11-YFP (BDSC#50782) and UAS-RAB11(S25N)-YFP (BDSC#9792) (Zhang et al., 2007).

*Genome engineering of *Syt7^{M1}* mutant and SYT7^{RFP} knock-in*

Guide RNAs were selected using the CRISPR Optimal Target Finder resource (Gratz et al., 2014) and cloned into the plasmid pCFD4-U6:1_U6:3tandemgRNAs (Addgene #49411) (Port et al., 2014). To generate *Syt7^{M1}*, guide RNA containing pCFD4 plasmid was injected into *vasa*-Cas9 embryos (BDSC #56552) by Best Gene Inc (Chino Hills, CA, USA). *Syt7^{M1}* and an unaffected injection line (control) were brought into the *white* background and the *vasa*-Cas9 chromosome

was removed. To generate SYT7^{RFP}, a donor plasmid that flanked RFP and a DsRed cassette was generated from the pScarless plasmid (courtesy of Kate O'Connor-Giles) with 1 Kb homology arms from the 3' end of the *Syt7* gene. The left homology arm was generated by PCR and the right homology arm was synthesized by Epoch Life Science (Sugarland, TX, USA). The donor plasmid and guide RNA containing pCFD4 plasmid was co-injected into Act5C-Cas9, Lig4 (BDSC #58492) by Best Gene Inc. *Syt7^{MI}* and SYT7^{RFP} transformants were confirmed by DNA sequencing.

Sequence alignment, phylogenetic tree construction and molecular modeling

NCBI BLAST was used to identify homologs of SYT1, SYT7 and ESYT-2 in the genomes of *C. elegans*, *C. intestinalis*, *D. rerio*, *M. musculus*, *H. sapiens*, *R. norvegicus* and *T. adherens*. Jalview was used to align SYT1 and SYT7 protein sequences from *D. melanogaster*, *M. Musculus* and *H. sapiens* with the T-coffee multiple sequence alignment algorithm. Jalview and Matlab were used to generate a phylogenetic tree using BLOSUM62 matrix and neighbor joining clustering. The SWISS model server (<https://swissmodel.expasy.org>) was used for homology modeling of Drosophila SYT7 from *R. norvegicus* SYT7 (PDB: 6ANK) (Waterhouse et al., 2018). The PyMOL Molecular Graphics System (Version 2.0 Schrödinger, LLC) was used to visualize SYT1 and SYT7 protein structures.

Sequences used for sequence alignment and phylogenetic tree		
Protein	Species	NCBI Accession number
ESYT2	<i>C. elegans</i>	NP_741181.1
	<i>C. intestinalis</i>	XP_018671537.1
	<i>D. melanogaster</i>	NP_733011.2
	<i>D. rerio</i>	XP_005171456.1
	<i>H. sapiens</i>	XP_024302614.1
	<i>R. norvegicus</i>	NP_001258098.1
	<i>T. adhaerens</i>	EDV19885.1
SYT1	<i>C. elegans</i>	NP_495394.3
	<i>C. intestinalis</i>	NP_001107602.1
	<i>D. melanogaster</i>	NP_523460.2
	<i>D. rerio</i>	NP_001314758.1
	<i>H. sapiens</i>	NP_001129277.1
	<i>R. norvegicus</i>	NP_001028852.2
	<i>T. adhaerens</i>	XP_002117742.1
SYT7	<i>C. elegans</i>	NP_001254022.1
	<i>C. intestinalis</i>	XP_026696415.1
	<i>D. melanogaster</i>	NP_726560.5
	<i>D. rerio</i>	XP_021326273.1
	<i>H. sapiens</i>	NP_004191.2
	<i>R. norvegicus</i>	NP_067691.1
	<i>T. adhaerens</i>	XP_002117784.1

Western analysis and immunocytochemistry

Western blotting of adult head lysates (1 head/lane) was performed using standard laboratory procedures with anti-SYT7 (1:500) (Adolfson et al., 2004), anti-SYX1 (8C3, 1:1000, Developmental Studies Hybridoma Bank (DSHB, Iowa City, IA) and anti-RFP (600-401-379; Rockland, 1:5000). Visualization and quantification were performed with a LI-COR Odyssey Imaging System (LI-COR Biosciences, Lincoln, MA, USA). Secondary antibodies for Westerns included Alexa Fluor 680-conjugated goat anti-rabbit IgG (1:5000, Invitrogen; A21109) and IR Dye 800-conjugated goat anti-mouse IgG (1:5000, LICOR; 926-32211).

Immunostaining for AZ and bouton counting was performed on wandering stage 3rd instar larvae dissected in Ca^{2+} -free HL3.1 and fixed for 17 min in Ca^{2+} -free HL3.1 containing 4% PFA. Larvae were blocked and permeabilized for 1 hr in PBS containing 0.1% Triton X-100, 2.5% NGS, 2.5% BSA and 0.1% sodium azide. Larvae were incubated overnight with primary antibody at 4°C and 2 hrs in secondary antibody at room temperature. Samples were mounted on slides with Vectashield (Vector Laboratories, Burlingame, CA). Immunostaining for SYT7^{RFP} and STY7^{GFP} co-localization analysis was similar, except larvae were blocked and permeabilized overnight in PBS containing 0.25% Saponin, 2.5% normal goat serum (NGS), 2.5% bovine serum albumin (BSA) and 0.1% sodium azide. Fixed larvae were incubated with primary antibody at 4°C for 24 hrs and with secondary antibodies for 1.5 hrs at room temperature. Fixed larvae were mounted in ProLong® Diamond Antifade Mountant (#P36970; Thermo Fisher Scientific, Waltham, MA, USA).

Antibodies used for immunolabeling were: mouse anti-BRP at 1:500 (Nc82; DSHB), mouse anti-DYN at 1:1000 (Clone 41, Dynamin (RUO); BD Transduction Laboratories, San Jose, CA, USA), mouse anti-Golgin84 at 1:50 (Golgin84 12-1; DSHB), mouse anti-RAB7 at 1:10 (Rab7; DSHB), mouse anti-RFP at 1:1000 (200-301-379; Rockland, Limerick, PA, USA) mouse anti-SYX1 at 1:100 (8C3; DSHB), rabbit anti-CPX at 1:5000 (Huntwork and Littleton, 2007), rabbit anti-NWK at 1:1000 (gift from Avital Rodal), rabbit anti-SYT1 1:500, mouse anti-GFP at 1:1000 (#A-11120; Thermo Fisher Scientific, Waltham, MA, USA), rabbit anti-GFP at 1:1000 (#G10362; Thermo Fisher Scientific, Waltham, MA, USA), mouse anti-RFP at 1:1000 (200-301-379; Rockland), rabbit anti-RFP at 1:1000 (600-401-379; Rockland) and DyLight 649 conjugated anti-HRP at 1:1000 (#123-605-021; Jackson Immuno Research, West Grove, PA, USA). Secondary antibodies used for AZ and bouton counting were used at 1:1000: goat anti-rabbit Alexa Fluor 488-conjugated antibody (A-11008; ThermoFisher) and goat anti-mouse Alexa Fluor 546-conjugated antibody (A-11030; ThermoFisher). Secondary antibodies used for co-localization were used at 1:1000: goat anti-mouse Alexa Fluor Plus 555 (A32727; ThermoFisher), goat anti-mouse Alexa Fluor Plus 488 (A32723; ThermoFisher), goat anti-rabbit Alexa Fluor Plus 555 (A32732; ThermoFisher) and goat anti-rabbit Alexa Fluor Plus 488 (A32731; ThermoFisher).

Immunoreactive proteins were imaged on either a Zeiss Pascal Confocal (Carl Zeiss Microscopy, Jena, GERMANY) using a 40x or 63X NA 1.3 Plan Neofluar oil immersion objective or a ZEISS LSM 800 microscope with Airyscan using a 63X oil immersion objective. For AZ volume and AZ proximity measurements, samples were imaged on a Zeiss Airyscan microscope and BRP labeling was analyzed in Volocity 6.3.1 software (Quorum Technologies Inc., Puslinch, Ontario, CAN). AZs clusters larger than $0.2 \mu\text{m}^3$ were rarely found, but could not be resolved into

single objects by the software. To ensure such clusters did not affect AZ size analysis, all AZs larger than $0.2 \mu\text{m}^3$ were excluded from the analysis.

Electrophysiology

Postsynaptic currents from the indicated genotypes were recorded from 3rd instar muscle fiber 6 at segment A3 using two-electrode voltage clamp with a -80 mV holding potential in HL3.1 saline solution (in mM, 70 NaCl, 5 KCl, 10 NaHCO₃, 4 MgCl₂, 5 trehalose, 115 sucrose, 5 HEPES, pH 7.2) as previously described (Jorquera et al., 2012). Final [Ca²⁺] was adjusted to the level indicated in the text. The Ca²⁺ cooperativity of release was determined from the slopes of a linear fit of a double logarithmic plot of evoked responses in the linear range (0.175 to 0.4 mM Ca²⁺). Inward currents recorded during TEVC are labeled as positive values in the figures for simplicity. For experiments using bafilomycin, 4 μM bafilomycin (LC Laboratories, Woburn, MA, USA) was dissolved in dimethyl sulphoxide (DMSO, Sigma, St. Louis, MO, USA) in HL3.1 and bath applied to dissected larvae. DMSO containing HL3.1 was used for control. Data acquisition and analysis was performed using Axoscope 9.0 and Clampfit 9.0 software (Molecular Devices, Sunnyvale, CA, USA). mEJCs were analyzed with Mini Analysis software 6.0.3 (Synaptosoft, Decatur, GA, USA). Motor nerves innervating the musculature were severed and placed into a suction electrode. Action potential stimulation was applied at the indicated frequencies using a programmable stimulator (Master8, AMPI; Jerusalem, Israel).

Fluo-4 AM imaging

Fluo-4 AM (F14201; ThermoFisher) loading was performed as previously described (Dawson-Scully et al., 2000). During incubation, neuronal membranes were labeled with DyLight 649

conjugated anti-HRP at 1:1000 (#123-605-021; Jackson Immuno Research, West Grove, PA, USA). NMJs of Ib motoneurons at muscle 6/7 were identified and motor nerves were stimulated in HL3 saline with 20 mM MgCl₂ and 1.1 mM Ca²⁺ for 5 seconds at 10 Hz for 3 epochs, each with a 5 second rest period between stimulation. Imaging of Fluo-4 AM fluorescent signal was performed on a Zeiss Axio Imager 2 equipped with a spinning-disk confocal head (CSU-X1; Yokagawa, JAPAN) and ImagEM X2 EM-CCD camera (Hamamatsu, Hamamatsu City JAPAN). 5 μm stacks from synaptic boutons were imaged at a frame rate of 1.25 Hz and mean Fluo-4 AM fluorescent intensity was determined during the stimulation protocol for each trial.

Optical quantal imaging and P_r mapping

P_r mapping was performed on a Zeiss Axio Imager 2 equipped with a spinning-disk confocal head (CSU-X1; Yokagawa, JAPAN) and ImagEM X2 EM-CCD camera (Hamamatsu, Hamamatsu City JAPAN) as previously described (Akbergenova et al., 2018). Myristoylated-GCaMP6s was expressed in larval muscles with 44H10-LexAp65 (provided by Gerald Rubin). Individual PSDs were visualized by expression of GluRIIA-RFP under its endogenous promoter (provided by Stephan Sigrist). An Olympus LUMFL N 60X objective with a 1.10 NA was used to acquire GCaMP6s imaging data at 8 Hz. 3rd instar larvae were dissected in Ca²⁺-free HL3 containing 20 mM MgCl₂. After dissection, preparations were maintained in HL3 with 20 mM MgCl₂ and 1.0 mM Ca²⁺ for 5 minutes. A dual channel multiplane stack was imaged at the beginning of each experiment to identify GluRIIA-positive PSDs. Single focal plane videos were then recorded while motor nerves were stimulated with a suction electrode at 1 Hz. GluRIIA-RFP PSD position was re-imaged every 25 seconds during experiments. The dual channel stack was merged with single plane images using the max intensity projection algorithm from Volocity 6.3.1 software. The

position of all GluRIIA-RFP PSDs was then spliced with the myr-GCaMP6s stimulation video. GluRIIA positive PSDs were detected automatically using the spot finding function of Volocity and equal size ROIs were assigned to the PSD population. In cases where the software failed to label visible GluRIIA-RFP PSDs, ROIs were added manually. GCaMP6s peak flashes were then detected and assigned to ROIs based on centroid proximity. The time and location of Ca^{2+} events were imported into Excel or Matlab for further analysis. Observed GCaMP events per ROI were divided by stimulation number to calculate *AZ Pr*.

FM1-43 uptake and release assays

3rd instar wandering larvae were dissected in Ca^{2+} -free HL3.1 and axons were severed from the CNS. Axon bundles were stimulated with a suction electrode in 1.5 mM CaCl_2 HL3.1 solution containing 2 μM of the lipophilic dye FM 1-43FX (F35355; Thermo Fisher Scientific, Waltham, MA, USA). Dye loading was performed at 10 Hz for 50 seconds (500 events) or at 0.5 Hz for 300 seconds (150 events), 600 seconds (300 events) and 900 seconds (600 events) as indicated. After stimulation, samples were washed for 2 min in Ca^{2+} free HL3.1 containing 100 μM Advacep-7 (Sigma; A3723) to help remove non-internalized FM 1-43 dye. Image stacks from muscle 6/7 at segment A3 were obtained using a spinning disk confocal microscope. FM1-43 unloading was done with a high K^+ (90 mM) HL3.1 solution for 1 min, followed by washing in a Ca^{2+} free HL3.1 solution for 1 min. An image stack at segment A3 muscle 6-7 was obtained on a Zeiss Axio Imager 2 equipped with a spinning-disk confocal head with a 63X water immersion objective. Mean FM1-43 intensity at the NMJ was quantified using the Volocity 3D Image Analysis software (Quorum Technologies Inc., Puslinch, Ontario, CAN).

Electron microscopy

Syt1^{MI} and control 3rd instar larvae were dissected in Ca²⁺-free HL3.1 solution and fixed in 1% glutaraldehyde, 4% formaldehyde, and 0.1 M sodium cacodylate for 10 min at room temperature as previously described (Akbergenova and Bykhovskaia, 2009). Fresh fixative was added and samples were microwaved in a BioWave Pro Pelco (Ted Pella, Inc., Redding, CA, USA) with the following protocol: (1) 100W 1 min, (2) 1 min off, (3) 100W 1 min, (4) 300W 20 secs, (5) 20 secs off, (6) 300W 20 secs. Steps 4- 6 were repeated twice more. Samples were then incubated for 30 min at room temperature with fixative. After washing in 0.1 M sodium cacodylate and 0.1 M sucrose, samples were stained for 30 min in 1% osmium tetroxide and 1.5% potassium ferrocyanide in 0.1 M sodium cacodylate solution. After washing with 0.1 M sodium cacodylate, samples were stained for 30 mins in 2% uranyl acetate and dehydrated through a graded series of ethanol and acetone, before embedding in epoxy resin (Embed 812; Electron Microscopy Sciences). Thin sections (50–60 nm) were collected on Formvar/carbon-coated copper slot grids and contrasted with lead citrate. Sections were imaged at 49,000× magnification at 80 kV with a Tecnai G2 electron microscope (FEI, Hillsboro, OR, USA) equipped with a charge-coupled device camera (Advanced Microscopy Techniques, Woburn, MA, USA). Type Ib boutons at muscle 6/7 were analyzed. All data analysis was done blinded.

For SV counting, T-bars at Ib boutons were identified and a FIJI macro was used to draw four concentric circles with 100 nm, 200 nm, 300 nm or 400 nm radius. The concentric circles were drawn with the T-bar at the center. To quantify vesicle density, FIJI was used to measure the area of the bouton and quantify the total number of vesicles within it. Final analysis was performed in Matlab and Excel.

Co-localization analysis and 3D reconstruction

The JaCOP FIJI algorithm (Bolte and Cordelières, 2006) was used to obtain cytofluorogram plots of bouton image stacks that were probed for RFP and a 2nd labeled compartment in SYT7^{RFP} 3rd instar larvae. Automatic thresholding was used to identify pixels above background for both channels. To obtain an average Pearson correlation, cytofluorograms from boutons obtained from 3 animals were analyzed in Matlab. All data analysis was done blinded. 3D reconstruction was performed using the 3D Viewer plugin in FIJI (Schmid et al., 2010). The bouton stack was displayed as a surface and labeled with SYT7^{RFP} in magenta and HRP in black.

Statistical analysis

Statistical analysis and graphing was performed with either Origin Software (OriginLab Corporation, Northampton, MA, USA) or GraphPad Prism (San Diego, CA, USA). Statistical significance was determined using specific tests as indicated in the text. Appropriate sample size was determined using GraphPad Statmate. Asterisks denote p-values of: *, $P \leq 0.05$; **, $P \leq 0.01$; and ***, $P \leq 0.001$. All histograms and measurements are shown as mean \pm SEM.

Acknowledgements

This work was supported by NIH grant NS40296 to J.T.L. M.C.Q-F. was supported in part by NIH pre-doctoral training grant T32GM007287. We thank the Bloomington Drosophila Stock Center (NIH P40OD018537), Kate O’Conner-Giles, Hugo Bellen, Gerry Rubin and Stephan Sigrist for Drosophila stocks, Kate O’Conner-Giles (Brown University) for help with CRISPR, Avi Rodal (Brandeis University) and Noreen Reist (Colorado State University) for providing antisera, Jan Melom (MIT) for generating the UAS-NHE-GFP transgenic line, Dina Volfson (MIT) for

assistance with *Drosophila* stock generation, and members of the Littleton lab for helpful discussions and comments on the manuscript.

Competing Interests

The authors declare no competing interests.

References

1. Adolfsen, B., Littleton, J.T., 2001. Genetic and molecular analysis of the synaptotagmin family. *Cell Mol. Life Sci.* 58, 393–402. doi:10.1007/PL00000865
2. Adolfsen, B., Saraswati, S., Yoshihara, M., Littleton, J.T., 2004. Synaptotagmins are trafficked to distinct subcellular domains including the postsynaptic compartment. *J. Cell Biol.* 166, 249–260. doi:10.1083/jcb.200312054
3. Akbergenova, Y., Bykhovskaia, M., 2007. Synapsin maintains the reserve vesicle pool and spatial segregation of the recycling pool in *Drosophila* presynaptic boutons. *Brain Res.* 1178, 52–64. doi:10.1016/j.brainres.2007.08.042
4. Akbergenova, Y., Bykhovskaia, M., 2009. Stimulation-induced formation of the reserve pool of vesicles in *Drosophila* motor boutons. *J. Neurophysiol.* 101, 2423–2433. doi:10.1152/jn.91122.2008
5. Akbergenova, Y., Cunningham, K.L., Zhang, Y.V., Weiss, S., Littleton, J.T., 2018. Characterization of developmental and molecular factors underlying release heterogeneity at *Drosophila* synapses. *Elife* 7. doi:10.7554/eLife.38268
6. Atluri, P.P., Regehr, W.G., 1998. Delayed release of neurotransmitter from cerebellar granule cells. *J. Neurosci.* 18, 8214–8227.
7. Bacaj, T., Wu, D., Burré, J., Malenka, R.C., Liu, X., Südhof, T.C., 2015. Synaptotagmin-1 and -7 Are Redundantly Essential for Maintaining the Capacity of the Readily-Releasable Pool of Synaptic Vesicles. *PLoS Biol.* 13, e1002267. doi:10.1371/journal.pbio.1002267
8. Bacaj, T., Wu, D., Yang, X., Morishita, W., Zhou, P., Xu, W., Malenka, R.C., Südhof, T.C., 2013. Synaptotagmin-1 and synaptotagmin-7 trigger synchronous and asynchronous phases of neurotransmitter release. *Neuron* 80, 947–959. doi:10.1016/j.neuron.2013.10.026
9. Barber, C.F., Jorquera, R.A., Melom, J.E., Littleton, J.T., 2009. Postsynaptic regulation of synaptic plasticity by synaptotagmin 4 requires both C2 domains. *J. Cell Biol.* 187, 295–310. doi:10.1083/jcb.200903098
10. Barthet, G., Jordà-Siquier, T., Rumi-Masante, J., Bernadou, F., Müller, U., Mülle, C., 2018. Presenilin-mediated cleavage of APP regulates synaptotagmin-7 and presynaptic plasticity. *Nat. Commun.* 9, 4780. doi:10.1038/s41467-018-06813-x
11. Barzilai-Tutsch, H., Dewulf, M., Lamaze, C., Butler Browne, G., Pines, M., Halevy, O., 2018. A promotive effect for halofuginone on membrane repair and synaptotagmin-7 levels in muscle cells of dysferlin-null mice. *Hum. Mol. Genet.* 27, 2817–2829. doi:10.1093/hmg/ddy185
12. Bellen, H.J., Levis, R.W., Liao, G., He, Y., Carlson, J.W., Tsang, G., Evans-Holm, M., Hiesinger, P.R., Schulze, K.L., Rubin, G.M., Hoskins, R.A., Spradling, A.C., 2004. The BDGP gene disruption project: single transposon insertions associated with 40% of *Drosophila* genes. *Genetics* 167, 761–781. doi:10.1534/genetics.104.026427
13. Best, A.R., Regehr, W.G., 2009. Inhibitory regulation of electrically coupled neurons in the inferior olive is mediated by asynchronous release of GABA. *Neuron* 62, 555–565. doi:10.1016/j.neuron.2009.04.018
14. Böhme, M.A., Beis, C., Reddy-Alla, S., Reynolds, E., Mampell, M.M., Grasskamp, A.T., Lützkendorf, J., Bergeron, D.D., Driller, J.H., Babikir, H., Göttfert, F., Robinson, I.M., O’Kane, C.J., Hell, S.W., Wahl, M.C., Stelzl, U., Loll, B., Walter, A.M., Sigrist, S.J., 2016. Active zone scaffolds differentially accumulate Unc13 isoforms to tune Ca²⁺ channel-vesicle coupling. *Nat. Neurosci.* 19, 1311–1320. doi:10.1038/nn.4364

15. Bolte, S., Cordelières, F.P., 2006. A guided tour into subcellular colocalization analysis in light microscopy. *J. Microsc.* 224, 213–232. doi:10.1111/j.1365-2818.2006.01706.x
16. Borst, J.G., Sakmann, B., 1996. Calcium influx and transmitter release in a fast CNS synapse. *Nature* 383, 431–434. doi:10.1038/383431a0
17. Budnik, V., Zhong, Y., Wu, C.F., 1990. Morphological plasticity of motor axons in *Drosophila* mutants with altered excitability. *J. Neurosci.* 10, 3754–3768.
18. Buhl, L.K., Jorquera, R.A., Akbergenova, Y., Huntwork-Rodriguez, S., Volfson, D., Littleton, J.T., 2013. Differential regulation of evoked and spontaneous neurotransmitter release by C-terminal modifications of complexin. *Mol. Cell. Neurosci.* 52, 161–172. doi:10.1016/j.mcn.2012.11.009
19. Bykhovskaia, M., 2011. Synapsin regulation of vesicle organization and functional pools. *Semin. Cell Dev. Biol.* 22, 387–392. doi:10.1016/j.semcdb.2011.07.003
20. Cao, P., Maximov, A., Südhof, T.C., 2011. Activity-dependent IGF-1 exocytosis is controlled by the Ca(2+)-sensor synaptotagmin-10. *Cell* 145, 300–311. doi:10.1016/j.cell.2011.03.034
21. Chakrabarti, S., Kobayashi, K.S., Flavell, R.A., Marks, C.B., Miyake, K., Liston, D.R., Fowler, K.T., Gorelick, F.S., Andrews, N.W., 2003. Impaired membrane resealing and autoimmune myositis in synaptotagmin VII-deficient mice. *J. Cell Biol.* 162, 543–549. doi:10.1083/jcb.200305131
22. Chanaday, N.L., Kavalali, E.T., 2018. Presynaptic origins of distinct modes of neurotransmitter release. *Curr. Opin. Neurobiol.* 51, 119–126. doi:10.1016/j.conb.2018.03.005
23. Chang, S., Trimbuch, T., Rosenmund, C., 2018. Synaptotagmin-1 drives synchronous Ca²⁺-triggered fusion by C2B-domain-mediated synaptic-vesicle-membrane attachment. *Nat. Neurosci.* 21, 33–40. doi:10.1038/s41593-017-0037-5
24. Chapman, E.R., Jahn, R., 1994. Calcium-dependent interaction of the cytoplasmic region of synaptotagmin with membranes. Autonomous function of a single C2-homologous domain. *J. Biol. Chem.* 269, 5735–5741.
25. Chen, C., Satterfield, R., Young, S.M., Jonas, P., 2017. Triple Function of Synaptotagmin 7 Ensures Efficiency of High-Frequency Transmission at Central GABAergic Synapses. *Cell Rep.* 21, 2082–2089. doi:10.1016/j.celrep.2017.10.122
26. Chen, Z., Das, B., Nakamura, Y., DiGregorio, D.A., Young, S.M., 2015. Ca²⁺ channel to synaptic vesicle distance accounts for the readily releasable pool kinetics at a functionally mature auditory synapse. *J. Neurosci.* 35, 2083–2100. doi:10.1523/JNEUROSCI.2753-14.2015
27. Colvin, R.A., Means, T.K., Diefenbach, T.J., Moita, L.F., Friday, R.P., Sever, S., Campanella, G.S.V., Abraszinski, T., Manice, L.A., Moita, C., Andrews, N.W., Wu, D., Hacohen, N., Luster, A.D., 2010. Synaptotagmin-mediated vesicle fusion regulates cell migration. *Nat. Immunol.* 11, 495–502. doi:10.1038/ni.1878
28. Coyle, I.P., Koh, Y.-H., Lee, W.-C.M., Slind, J., Fergestad, T., Littleton, J.T., Ganetzky, B., 2004. Nervous wreck, an SH3 adaptor protein that interacts with Wsp, regulates synaptic growth in *Drosophila*. *Neuron* 41, 521–534.
29. Craxton, M., 2010. A manual collection of Syt, Esyt, Rph3a, Rph3al, Doc2, and Dblc2 genes from 46 metazoan genomes--an open access resource for neuroscience and evolutionary biology. *BMC Genomics* 11, 37. doi:10.1186/1471-2164-11-37
30. Czubener, C., Sherer, N.M., Becker, S.M., Pypaert, M., Hui, E., Chapman, E.R., Mothes, W.,

- Andrews, N.W., 2006. Ca²⁺ and synaptotagmin VII-dependent delivery of lysosomal membrane to nascent phagosomes. *J. Cell Biol.* 174, 997–1007. doi:10.1083/jcb.200605004
31. Dawson-Scully, K., Bronk, P., Atwood, H.L., Zinsmaier, K.E., 2000. Cysteine-string protein increases the calcium sensitivity of neurotransmitter exocytosis in *Drosophila*. *J. Neurosci.* 20, 6039–6047.
 32. Dean, C., Dunning, F.M., Liu, H., Bomba-Warczak, E., Martens, H., Bharat, V., Ahmed, S., Chapman, E.R., 2012. Axonal and dendritic synaptotagmin isoforms revealed by a pHluorin-syt functional screen. *Mol. Biol. Cell* 23, 1715–1727. doi:10.1091/mbc.E11-08-0707.
 33. DiAntonio, A., Schwarz, T.L., 1994. The effect on synaptic physiology of synaptotagmin mutations in *Drosophila*. *Neuron* 12, 909–920. doi:10.1016/0896-6273(94)90342-5.
 34. Dickman, D.K., Lu, Z., Meinertzhagen, I.A., Schwarz, T.L., 2006. Altered synaptic development and active zone spacing in endocytosis mutants. *Curr. Biol.* 16, 591–598.
 35. Dittman, J.S., Kreitzer, A.C., Regehr, W.G., 2000. Interplay between facilitation, depression, and residual calcium at three presynaptic terminals. *J. Neurosci.* 20, 1374–1385.
 36. Dittman, J.S., Regehr, W.G., 1998. Calcium dependence and recovery kinetics of presynaptic depression at the climbing fiber to Purkinje cell synapse. *J. Neurosci.* 18, 6147–6162.
 37. Dolai, S., Xie, L., Zhu, D., Liang, T., Qin, T., Xie, H., Kang, Y., Chapman, E.R., Gaisano, H.Y., 2016. Synaptotagmin-7 Functions to Replenish Insulin Granules for Exocytosis in Human Islet β -Cells. *Diabetes* 65, 1962–1976. doi:10.2337/db15-1436.
 38. Durán, E., Montes, M.Á., Jemal, I., Satterfield, R., Young, S., Álvarez de Toledo, G., 2018. Synaptotagmin-7 controls the size of the reserve and resting pools of synaptic vesicles in hippocampal neurons. *Cell Calcium* 74, 53–60. doi:10.1016/j.ceca.2018.06.004
 39. Ehmann, N., van de Linde, S., Alon, A., Ljaschenko, D., Keung, X.Z., Holm, T., Rings, A., DiAntonio, A., Hallermann, S., Ashery, U., Heckmann, M., Sauer, M., Kittel, R.J., 2014. Quantitative super-resolution imaging of Bruchpilot distinguishes active zone states. *Nat. Commun.* 5, 4650. doi:10.1038/ncomms5650
 40. Fernández-Chacón, R., Königstorfer, A., Gerber, S.H., García, J., Matos, M.F., Stevens, C.F., Brose, N., Rizo, J., Rosenmund, C., Südhof, T.C., 2001. Synaptotagmin I functions as a calcium regulator of release probability. *Nature* 410, 41–49. doi:10.1038/35065004
 41. Fesce, R., 1999. The kinetics of nerve-evoked quantal secretion. *Philos. Trans. R. Soc. Lond. B, Biol. Sci.* 354, 319–329. doi:10.1098/rstb.1999.0383
 42. Flannery, A.R., Czibener, C., Andrews, N.W., 2010. Palmitoylation-dependent association with CD63 targets the Ca²⁺ sensor synaptotagmin VII to lysosomes. *J. Cell Biol.* 191, 599–613. doi:10.1083/jcb.201003021
 43. Frank, C.A., James, T.D., Müller, M., 2020. Homeostatic control of *Drosophila* neuromuscular junction function. *Synapse* 74, e22133. doi:10.1002/syn.22133
 44. Fukuda, M., Kanno, E., Satoh, M., Saegusa, C., Yamamoto, A., 2004. Synaptotagmin VII is targeted to dense-core vesicles and regulates their Ca²⁺-dependent exocytosis in PC12 cells. *J. Biol. Chem.* 279, 52677–52684. doi:10.1074/jbc.M409241200
 45. Geppert, M., Goda, Y., Hammer, R.E., Li, C., Rosahl, T.W., Stevens, C.F., Südhof, T.C., 1994. Synaptotagmin I: a major Ca²⁺ sensor for transmitter release at a central synapse. *Cell* 79, 717–727. doi:10.1016/0092-8674(94)90556-8
 46. Gerth, F., Jäpel, M., Pechstein, A., Kochlamazashvili, G., Lehmann, M., Puchkov, D., Onofri, F., Benfenati, F., Nikonenko, A.G., Fredrich, K., Shupliakov, O., Maritzen, T., Freund, C., Haucke, V., 2017. Intersectin associates with synapsin and regulates its nanoscale localization and function. *Proc. Natl. Acad. Sci. USA* 114, 12057–12062.

- doi:10.1073/pnas.1715341114
47. Goda, Y., Stevens, C.F., 1994. Two components of transmitter release at a central synapse. *Proc. Natl. Acad. Sci. USA* 91, 12942–12946. doi:10.1073/pnas.91.26.12942
 48. Gratz, S.J., Ukken, F.P., Rubinstein, C.D., Thiede, G., Donohue, L.K., Cummings, A.M., O'Connor-Giles, K.M., 2014. Highly specific and efficient CRISPR/Cas9-catalyzed homology-directed repair in *Drosophila*. *Genetics* 196, 961–971. doi:10.1534/genetics.113.160713
 49. Guan, Z., Bykhovskaia, M., Jorquera, R.A., Sutton, R.B., Akbergenova, Y., Littleton, J.T., 2017. A synaptotagmin suppressor screen indicates SNARE binding controls the timing and Ca²⁺ cooperativity of vesicle fusion. *Elife* 6. doi:10.7554/eLife.28409
 50. Guan, Z., Saraswati, S., Adolfsen, B., Littleton, J.T., 2005. Genome-wide transcriptional changes associated with enhanced activity in the *Drosophila* nervous system. *Neuron* 48, 91–107. doi:10.1016/j.neuron.2005.08.036
 51. Gustavsson, N., Wang, Y., Kang, Y., Seah, T., Chua, S., Radda, G.K., Han, W., 2011. Synaptotagmin-7 as a positive regulator of glucose-induced glucagon-like peptide-1 secretion in mice. *Diabetologia* 54, 1824–1830. doi:10.1007/s00125-011-2119-3
 52. Harris, K.P., Littleton, J.T., 2015. Transmission, development, and plasticity of synapses. *Genetics* 201, 345–375. doi:10.1534/genetics.115.176529
 53. Harris, K.P., Zhang, Y.V., Piccioli, Z.D., Perrimon, N., Littleton, J.T., 2016. The postsynaptic t-SNARE Syntaxin 4 controls traffic of Neuroligin 1 and Synaptotagmin 4 to regulate retrograde signaling. *Elife* 5. doi:10.7554/eLife.13881
 54. Hefft, S., Jonas, P., 2005. Asynchronous GABA release generates long-lasting inhibition at a hippocampal interneuron-principal neuron synapse. *Nat. Neurosci.* 8, 1319–1328. doi:10.1038/nn1542
 55. Hilfiker, S., Pieribone, V.A., Czernik, A.J., Kao, H.T., Augustine, G.J., Greengard, P., 1999. Synapsins as regulators of neurotransmitter release. *Philos. Trans. R. Soc. Lond. B, Biol. Sci.* 354, 269–279. doi:10.1098/rstb.1999.0378
 56. Hui, E., Bai, J., Wang, P., Sugimori, M., Llinas, R.R., Chapman, E.R., 2005. Three distinct kinetic groupings of the synaptotagmin family: candidate sensors for rapid and delayed exocytosis. *Proc. Natl. Acad. Sci. USA* 102, 5210–5214. doi:10.1073/pnas.0500941102
 57. Huntwork, S., Littleton, J.T., 2007. A complexin fusion clamp regulates spontaneous neurotransmitter release and synaptic growth. *Nat. Neurosci.* 10, 1235–1237. doi:10.1038/nn1980
 58. Huson, V., van Boven, M.A., Stuefer, A., Verhage, M., Cornelisse, L.N., 2019. Synaptotagmin-1 enables frequency coding by suppressing asynchronous release in a temperature dependent manner. *Sci. Rep.* 9, 11341. doi:10.1038/s41598-019-47487-9
 59. Jackman, S.L., Turecek, J., Belinsky, J.E., Regehr, W.G., 2016. The calcium sensor synaptotagmin 7 is required for synaptic facilitation. *Nature* 529, 88–91. doi:10.1038/nature16507
 60. Jaiswal, J.K., Chakrabarti, S., Andrews, N.W., Simon, S.M., 2004. Synaptotagmin VII restricts fusion pore expansion during lysosomal exocytosis. *PLoS Biol.* 2, E233. doi:10.1371/journal.pbio.0020233
 61. Jan, L.Y., Jan, Y.N., 1976. Properties of the larval neuromuscular junction in *Drosophila melanogaster*. *J. Physiol. (Lond.)* 262, 189–214. doi:10.1113/jphysiol.1976.sp011592
 62. Jorquera, R.A., Huntwork-Rodriguez, S., Akbergenova, Y., Cho, R.W., Littleton, J.T., 2012. Complexin controls spontaneous and evoked neurotransmitter release by regulating the

- timing and properties of synaptotagmin activity. *J. Neurosci.* 32, 18234–18245. doi:10.1523/JNEUROSCI.3212-12.2012
63. Junge, H.J., Rhee, J.-S., Jahn, O., Varoqueaux, F., Spiess, J., Waxham, M.N., Rosenmund, C., Brose, N., 2004. Calmodulin and Munc13 form a Ca²⁺ sensor/effector complex that controls short-term synaptic plasticity. *Cell* 118, 389–401. doi:10.1016/j.cell.2004.06.029
 64. Kaeser, P.S., Regehr, W.G., 2014. Molecular mechanisms for synchronous, asynchronous, and spontaneous neurotransmitter release. *Annu. Rev. Physiol.* 76, 333–363. doi:10.1146/annurev-physiol-021113-170338
 65. Katz, B., Miledi, R., 1967. The timing of calcium action during neuromuscular transmission. *J. Physiol. (Lond.)* 189, 535–544. doi:10.1113/jphysiol.1967.sp008183
 66. Katz, B., Miledi, R., 1970. Further study of the role of calcium in synaptic transmission. *J. Physiol. (Lond.)* 207, 789–801. doi:10.1113/jphysiol.1970.sp009095
 67. Katz, B.S., 1969. *The Release of Neural Transmitter Substances (Sherrington Lecture): Bernard S. Katz: 9780853230601: Amazon.com: Books.* Liverpool University Press.
 68. Kochubey, O., Schneggenburger, R., 2011. Synaptotagmin increases the dynamic range of synapses by driving Ca²⁺-evoked release and by clamping a near-linear remaining Ca²⁺ sensor. *Neuron* 69, 736–748. doi:10.1016/j.neuron.2011.01.013
 69. Koh, T.-W., Verstreken, P., Bellen, H.J., 2004. Dap160/intersectin acts as a stabilizing scaffold required for synaptic development and vesicle endocytosis. *Neuron* 43, 193–205. doi:10.1016/j.neuron.2004.06.029
 70. Korkut, C., Li, Y., Koles, K., Brewer, C., Ashley, J., Yoshihara, M., Budnik, V., 2013. Regulation of postsynaptic retrograde signaling by presynaptic exosome release. *Neuron* 77, 1039–1046. doi:10.1016/j.neuron.2013.01.013
 71. Lee, J., Guan, Z., Akbergenova, Y., Littleton, J.T., 2013. Genetic analysis of synaptotagmin C2 domain specificity in regulating spontaneous and evoked neurotransmitter release. *J. Neurosci.* 33, 187–200. doi:10.1523/JNEUROSCI.3214-12.2013
 72. Lee, J., Littleton, J.T., 2015. Transmembrane tethering of synaptotagmin to synaptic vesicles controls multiple modes of neurotransmitter release. *Proc. Natl. Acad. Sci. USA* 112, 3793–3798. doi:10.1073/pnas.1420312112
 73. Li, C., Ullrich, B., Zhang, J.Z., Anderson, R.G., Brose, N., Südhof, T.C., 1995. Ca(2+)-dependent and -independent activities of neural and non-neural synaptotagmins. *Nature* 375, 594–599. doi:10.1038/375594a0
 74. Li, Y.C., Chanaday, N.L., Xu, W., Kavalali, E.T., 2017. Synaptotagmin-1- and Synaptotagmin-7-Dependent Fusion Mechanisms Target Synaptic Vesicles to Kinetically Distinct Endocytic Pathways. *Neuron* 93, 616–631.e3. doi:10.1016/j.neuron.2016.12.010
 75. Lipstein, N., Sakaba, T., Cooper, B.H., Lin, K.-H., Strenzke, N., Ashery, U., Rhee, J.-S., Taschenberger, H., Neher, E., Brose, N., 2013. Dynamic control of synaptic vesicle replenishment and short-term plasticity by Ca(2+)-calmodulin-Munc13-1 signaling. *Neuron* 79, 82–96. doi:10.1016/j.neuron.2013.05.011
 76. Littleton, J.T., Bellen, H.J., Perin, M.S., 1993a. Expression of synaptotagmin in *Drosophila* reveals transport and localization of synaptic vesicles to the synapse. *Development* 118, 1077–1088.
 77. Littleton, J.T., Chapman, E.R., Kreber, R., Garment, M.B., Carlson, S.D., Ganetzky, B., 1998. Temperature-sensitive paralytic mutations demonstrate that synaptic exocytosis requires SNARE complex assembly and disassembly. *Neuron* 21, 401–413.
 78. Littleton, J.T., Stern, M., Perin, M., Bellen, H.J., 1994. Calcium dependence of

- neurotransmitter release and rate of spontaneous vesicle fusions are altered in *Drosophila* synaptotagmin mutants. *Proc. Natl. Acad. Sci. USA* 91, 10888–10892.
79. Littleton, J.T., Stern, M., Schulze, K., Perin, M., Bellen, H.J., 1993b. Mutational analysis of *Drosophila* synaptotagmin demonstrates its essential role in Ca²⁺-activated neurotransmitter release. *Cell* 74, 1125–1134. doi:10.1016/0092-8674(93)90733-7
 80. Liu, H., Bai, H., Hui, E., Yang, L., Evans, C.S., Wang, Z., Kwon, S.E., Chapman, E.R., 2014. Synaptotagmin 7 functions as a Ca²⁺-sensor for synaptic vesicle replenishment. *Elife* 3, e01524. doi:10.7554/eLife.01524
 81. Llinás, R., Steinberg, I.Z., Walton, K., 1981. Relationship between presynaptic calcium current and postsynaptic potential in squid giant synapse. *Biophys. J.* 33, 323–351. doi:10.1016/S0006-3495(81)84899-0
 82. Loewen, C.A., Mackler, J.M., Reist, N.E., 2001. *Drosophila* synaptotagmin I null mutants survive to early adulthood. *Genesis* 31, 30–36. doi:10.1002/gene.10002
 83. Lu, T., Trussell, L.O., 2000. Inhibitory transmission mediated by asynchronous transmitter release. *Neuron* 26, 683–694. doi:10.1016/s0896-6273(00)81204-0
 84. Luo, F., Südhof, T.C., 2017. Synaptotagmin-7-Mediated Asynchronous Release Boosts High-Fidelity Synchronous Transmission at a Central Synapse. *Neuron* 94, 826–839.e3. doi:10.1016/j.neuron.2017.04.020
 85. MacDougall, D.D., Lin, Z., Chon, N.L., Jackman, S.L., Lin, H., Knight, J.D., Anantharam, A., 2018. The high-affinity calcium sensor synaptotagmin-7 serves multiple roles in regulated exocytosis. *J. Gen. Physiol.* 150, 783–807. doi:10.1085/jgp.201711944
 86. Mackler, J.M., Drummond, J.A., Loewen, C.A., Robinson, I.M., Reist, N.E., 2002. The C(2)B Ca²⁺-binding motif of synaptotagmin is required for synaptic transmission in vivo. *Nature* 418, 340–344. doi:10.1038/nature00846
 87. Marie, B., Sweeney, S.T., Poskanzer, K.E., Roos, J., Kelly, R.B., Davis, G.W., 2004. Dap160/intersectin scaffolds the periactional zone to achieve high-fidelity endocytosis and normal synaptic growth. *Neuron* 43, 207–219. doi:10.1016/j.neuron.2004.07.001
 88. Martinez, I., Chakrabarti, S., Hellevik, T., Morehead, J., Fowler, K., Andrews, N.W., 2000. Synaptotagmin VII regulates Ca²⁺-dependent exocytosis of lysosomes in fibroblasts. *J. Cell Biol.* 148, 1141–1149. doi:10.1083/jcb.148.6.1141
 89. Maximov, A., Lao, Y., Li, H., Chen, X., Rizo, J., Sørensen, J.B., Südhof, T.C., 2008. Genetic analysis of synaptotagmin-7 function in synaptic vesicle exocytosis. *Proc. Natl. Acad. Sci. USA* 105, 3986–3991. doi:10.1073/pnas.0712372105
 90. McCabe, B.D., Marqués, G., Haghghi, A.P., Fetter, R.D., Crotty, M.L., Haerry, T.E., Goodman, C.S., O’Connor, M.B., 2003. The BMP homolog Gbb provides a retrograde signal that regulates synaptic growth at the *Drosophila* neuromuscular junction. *Neuron* 39, 241–254. doi:10.1016/s0896-6273(03)00426-4
 91. Melom, J.E., Akbergenova, Y., Gavornik, J.P., Littleton, J.T., 2013. Spontaneous and evoked release are independently regulated at individual active zones. *J. Neurosci.* 33, 17253–17263. doi:10.1523/JNEUROSCI.3334-13.2013
 92. Mendez, J.A., Bourque, M.-J., Fasano, C., Kortleven, C., Trudeau, L.-E., 2011. Somatodendritic dopamine release requires synaptotagmin 4 and 7 and the participation of voltage-gated calcium channels. *J. Biol. Chem.* 286, 23928–23937. doi:10.1074/jbc.M111.218032
 93. Milovanovic, D., De Camilli, P., 2017. Synaptic vesicle clusters at synapses: A distinct liquid phase? *Neuron* 93, 995–1002. doi:10.1016/j.neuron.2017.02.013

94. Milovanovic, D., Wu, Y., Bian, X., De Camilli, P., 2018. A liquid phase of synapsin and lipid vesicles. *Science* 361, 604–607. doi:10.1126/science.aat5671
95. Moghadam, P.K., Jackson, M.B., 2013. The functional significance of synaptotagmin diversity in neuroendocrine secretion. *Front. Endocrinol. (Lausanne)* 4, 124. doi:10.3389/fendo.2013.00124
96. Monterrat, C., Grise, F., Benassy, M.N., Hémar, A., Lang, J., 2007. The calcium-sensing protein synaptotagmin 7 is expressed on different endosomal compartments in endocrine, neuroendocrine cells or neurons but not on large dense core vesicles. *Histochem. Cell Biol.* 127, 625–632. doi:10.1007/s00418-007-0271-0
97. Neher, E., 2015. Merits and limitations of vesicle pool models in view of heterogeneous populations of synaptic vesicles. *Neuron* 87, 1131–1142. doi:10.1016/j.neuron.2015.08.038
98. Neher, E., Brose, N., 2018. Dynamically Primed Synaptic Vesicle States: Key to Understand Synaptic Short-Term Plasticity. *Neuron* 100, 1283–1291. doi:10.1016/j.neuron.2018.11.024
99. Nishiki, T., Augustine, G.J., 2004. Synaptotagmin I synchronizes transmitter release in mouse hippocampal neurons. *J. Neurosci.* 24, 6127–6132. doi:10.1523/JNEUROSCI.1563-04.2004
100. Packard, M., Koo, E.S., Gorczyca, M., Sharpe, J., Cumberledge, S., Budnik, V., 2002. The *Drosophila* Wnt, wingless, provides an essential signal for pre- and postsynaptic differentiation. *Cell* 111, 319–330. doi:10.1016/s0092-8674(02)01047-4
101. Pang, Z.P., Melicoff, E., Padgett, D., Liu, Y., Teich, A.F., Dickey, B.F., Lin, W., Adachi, R., Südhof, T.C., 2006. Synaptotagmin-2 is essential for survival and contributes to Ca²⁺ triggering of neurotransmitter release in central and neuromuscular synapses. *J. Neurosci.* 26, 13493–13504. doi:10.1523/JNEUROSCI.3519-06.2006
102. Pang, Z.P., Südhof, T.C., 2010. Cell biology of Ca²⁺-triggered exocytosis. *Curr. Opin. Cell Biol.* 22, 496–505. doi:10.1016/j.ceb.2010.05.001
103. Park, D., Li, P., Dani, A., Taghert, P.H., 2014. Peptidergic cell-specific synaptotagmins in *Drosophila*: localization to dense-core granules and regulation by the bHLH protein DIMMED. *J. Neurosci.* 34, 13195–13207. doi:10.1523/JNEUROSCI.2075-14.2014
104. Peled, E.S., Isacoff, E.Y., 2011. Optical quantal analysis of synaptic transmission in wild-type and rab3-mutant *Drosophila* motor axons. *Nat. Neurosci.* 14, 519–526. doi:10.1038/nn.2767
105. Perin, M.S., Fried, V.A., Mignery, G.A., Jahn, R., Südhof, T.C., 1990. Phospholipid binding by a synaptic vesicle protein homologous to the regulatory region of protein kinase C. *Nature* 345, 260–263. doi:10.1038/345260a0
106. Peters, J.H., McDougall, S.J., Fawley, J.A., Smith, S.M., Andresen, M.C., 2010. Primary afferent activation of thermosensitive TRPV1 triggers asynchronous glutamate release at central neurons. *Neuron* 65, 657–669. doi:10.1016/j.neuron.2010.02.017
107. Piccioli, Z.D., Littleton, J.T., 2014. Retrograde BMP signaling modulates rapid activity-dependent synaptic growth via presynaptic LIM kinase regulation of cofilin. *J. Neurosci.* 34, 4371–4381. doi:10.1523/JNEUROSCI.4943-13.2014
108. Port, F., Chen, H.-M., Lee, T., Bullock, S.L., 2014. Optimized CRISPR/Cas tools for efficient germline and somatic genome engineering in *Drosophila*. *Proc. Natl. Acad. Sci. USA* 111, E2967-76. doi:10.1073/pnas.1405500111
109. Reddy, A., Caler, E.V., Andrews, N.W., 2001. Plasma membrane repair is mediated by Ca²⁺-regulated exocytosis of lysosomes. *Cell* 106, 157–169. doi:10.1016/s0092-8674(01)00421-4

110. Ritzau-Jost, A., Jablonski, L., Viotti, J., Lipstein, N., Eilers, J., Hallermann, S., 2018. Apparent calcium dependence of vesicle recruitment. *J. Physiol. (Lond.)* 596, 4693–4707. doi:10.1113/JP275911
111. Rodal, A.A., Blunk, A.D., Akbergenova, Y., Jorquera, R.A., Buhl, L.K., Littleton, J.T., 2011. A presynaptic endosomal trafficking pathway controls synaptic growth signaling. *J. Cell Biol.* 193, 201–217. doi:10.1083/jcb.201009052
112. Rodal, A.A., Motola-Barnes, R.N., Littleton, J.T., 2008. Nervous wreck and Cdc42 cooperate to regulate endocytic actin assembly during synaptic growth. *J. Neurosci.* 28, 8316–8325. doi:10.1523/JNEUROSCI.2304-08.2008
113. Rozov, A., Bolshakov, A.P., Valiullina-Rakhmatullina, F., 2019. The Ever-Growing Puzzle of Asynchronous Release. *Front. Cell Neurosci.* 13, 28. doi:10.3389/fncel.2019.00028
114. Sabatini, B.L., Regehr, W.G., 1996. Timing of neurotransmission at fast synapses in the mammalian brain. *Nature* 384, 170–172. doi:10.1038/384170a0
115. Sabeva, N., Cho, R.W., Vasin, A., Gonzalez, A., Littleton, J.T., Bykhovskaia, M., 2017. Complexin Mutants Reveal Partial Segregation between Recycling Pathways That Drive Evoked and Spontaneous Neurotransmission. *J. Neurosci.* 37, 383–396. doi:10.1523/JNEUROSCI.1854-16.2016
116. Saraswati, S., Adolfsen, B., Littleton, J.T., 2007. Characterization of the role of the Synaptotagmin family as calcium sensors in facilitation and asynchronous neurotransmitter release. *Proc. Natl. Acad. Sci. USA* 104, 14122–14127. doi:10.1073/pnas.0706711104
117. Schmid, B., Schindelin, J., Cardona, A., Longair, M., Heisenberg, M., 2010. A high-level 3D visualization API for Java and ImageJ. *BMC Bioinformatics* 11, 274. doi:10.1186/1471-2105-11-274
118. Schneggenburger, R., Rosenmund, C., 2015. Molecular mechanisms governing Ca(2+) regulation of evoked and spontaneous release. *Nat. Neurosci.* 18, 935–941. doi:10.1038/nn.4044
119. Schonn, J.-S., Maximov, A., Lao, Y., Südhof, T.C., Sørensen, J.B., 2008. Synaptotagmin-1 and -7 are functionally overlapping Ca²⁺ sensors for exocytosis in adrenal chromaffin cells. *Proc. Natl. Acad. Sci. USA* 105, 3998–4003. doi:10.1073/pnas.0712373105
120. Shin, O.-H., Rizo, J., Südhof, T.C., 2002. Synaptotagmin function in dense core vesicle exocytosis studied in cracked PC12 cells. *Nat. Neurosci.* 5, 649–656. doi:10.1038/nn869
121. Shupliakov, O., Haucke, V., Pechstein, A., 2011. How synapsin I may cluster synaptic vesicles. *Semin. Cell Dev. Biol.* 22, 393–399. doi:10.1016/j.semcdb.2011.07.006
122. Söllner, T., Whiteheart, S.W., Brunner, M., Erdjument-Bromage, H., Geromanos, S., Tempst, P., Rothman, J.E., 1993. SNAP receptors implicated in vesicle targeting and fusion. *Nature* 362, 318–324. doi:10.1038/362318a0
123. Sone, M., Suzuki, E., Hoshino, M., Hou, D., Kuromi, H., Fukata, M., Kuroda, S., Kaibuchi, K., Nabeshima, Y., Hama, C., 2000. Synaptic development is controlled in the periaxonal zones of Drosophila synapses. *Development* 127, 4157–4168.
124. Südhof, T.C., 2012. Calcium control of neurotransmitter release. *Cold Spring Harb. Perspect. Biol.* 4, a011353. doi:10.1101/cshperspect.a011353
125. Südhof, T.C., 2013. Neurotransmitter release: the last millisecond in the life of a synaptic vesicle. *Neuron* 80, 675–690. doi:10.1016/j.neuron.2013.10.022
126. Sugita, S., Han, W., Butz, S., Liu, X., Fernández-Chacón, R., Lao, Y., Südhof, T.C., 2001. Synaptotagmin VII as a plasma membrane Ca(2+) sensor in exocytosis. *Neuron* 30, 459–473. doi:10.1016/s0896-6273(01)00290-2

127. Sugita, S., Shin, O.-H., Han, W., Lao, Y., Südhof, T.C., 2002. Synaptotagmins form a hierarchy of exocytotic Ca(2+) sensors with distinct Ca(2+) affinities. *EMBO J.* 21, 270–280. doi:10.1093/emboj/21.3.270
128. Sutton, R.B., Fasshauer, D., Jahn, R., Brunger, A.T., 1998. Crystal structure of a SNARE complex involved in synaptic exocytosis at 2.4 Å resolution. *Nature* 395, 347–353. doi:10.1038/26412
129. Tsuboi, T., Fukuda, M., 2007. Synaptotagmin VII modulates the kinetics of dense-core vesicle exocytosis in PC12 cells. *Genes Cells* 12, 511–519. doi:10.1111/j.1365-2443.2007.01070.x
130. Tucker, W.C., Weber, T., Chapman, E.R., 2004. Reconstitution of Ca²⁺-regulated membrane fusion by synaptotagmin and SNAREs. *Science* 304, 435–438. doi:10.1126/science.1097196
131. Turecek, J., Regehr, W.G., 2018. Synaptotagmin 7 mediates both facilitation and asynchronous release at granule cell synapses. *J. Neurosci.* 38, 3240–3251. doi:10.1523/JNEUROSCI.3207-17.2018
132. Turecek, J., Regehr, W.G., 2019. Neuronal regulation of fast synaptotagmin isoforms controls the relative contributions of synchronous and asynchronous release. *Neuron* 101, 938–949.e4. doi:10.1016/j.neuron.2019.01.013
133. Ullrich, B., Südhof, T.C., 1995. Differential distributions of novel synaptotagmins: comparison to synapsins. *Neuropharmacology* 34, 1371–1377. doi:10.1016/0028-3908(95)00132-P
134. Uytterhoeven, V., Kuenen, S., Kasprovicz, J., Miskiewicz, K., Verstreken, P., 2011. Loss of skywalker reveals synaptic endosomes as sorting stations for synaptic vesicle proteins. *Cell* 145, 117–132. doi:10.1016/j.cell.2011.02.039
135. Virmani, T., Han, W., Liu, X., Südhof, T.C., Kavalali, E.T., 2003. Synaptotagmin 7 splice variants differentially regulate synaptic vesicle recycling. *EMBO J.* 22, 5347–5357. doi:10.1093/emboj/cdg514
136. Voleti, R., Tomchick, D.R., Südhof, T.C., Rizo, J., 2017. Exceptionally tight membrane-binding may explain the key role of the synaptotagmin-7 C2A domain in asynchronous neurotransmitter release. *Proc. Natl. Acad. Sci. USA* 114, E8518–E8527. doi:10.1073/pnas.1710708114
137. Wadel, K., Neher, E., Sakaba, T., 2007. The coupling between synaptic vesicles and Ca²⁺ channels determines fast neurotransmitter release. *Neuron* 53, 563–575. doi:10.1016/j.neuron.2007.01.021
138. Wagh, D.A., Rasse, T.M., Asan, E., Hofbauer, A., Schwenkert, I., Dürrbeck, H., Buchner, S., Dabauvalle, M.-C., Schmidt, M., Qin, G., Wichmann, C., Kittel, R., Sigris, S.J., Buchner, E., 2006. Bruchpilot, a protein with homology to ELKS/CAST, is required for structural integrity and function of synaptic active zones in *Drosophila*. *Neuron* 49, 833–844. doi:10.1016/j.neuron.2006.02.008
139. Walsh, R.B., Becalska, A.N., Zunitch, M.J., Wang, S., Isaac, B., Yeh, A., Koles, K., Rodal, A.A., 2019. Opposing functions for retromer and Rab11 in extracellular vesicle cargo traffic at synapses. *BioRxiv*. doi:10.1101/645713
140. Wang, S., Li, Y., Ma, C., 2016. Synaptotagmin-1 C2B domain interacts simultaneously with SNAREs and membranes to promote membrane fusion. *Elife* 5. doi:10.7554/eLife.14211
141. Waterhouse, A., Bertoni, M., Bienert, S., Studer, G., Tauriello, G., Gumienny, R., Heer,

- F.T., de Beer, T.A.P., Rempfer, C., Bordoli, L., Lepore, R., Schwede, T., 2018. SWISS-MODEL: homology modelling of protein structures and complexes. *Nucleic Acids Res.* 46, W296–W303. doi:10.1093/nar/gky427
142. Weber, J.P., Toft-Bertelsen, T.L., Mohrmann, R., Delgado-Martinez, I., Sørensen, J.B., 2014. Synaptotagmin-7 is an asynchronous calcium sensor for synaptic transmission in neurons expressing SNAP-23. *PLoS One* 9, e114033. doi:10.1371/journal.pone.0114033
143. Wen, H., Linhoff, M.W., McGinley, M.J., Li, G.-L., Corson, G.M., Mandel, G., Brehm, P., 2010. Distinct roles for two synaptotagmin isoforms in synchronous and asynchronous transmitter release at zebrafish neuromuscular junction. *Proc. Natl. Acad. Sci. USA* 107, 13906–13911. doi:10.1073/pnas.1008598107
144. Winther, Å.M.E., Vorontsova, O., Rees, K.A., Näreoja, T., Sopova, E., Jiao, W., Shupliakov, O., 2015. An Endocytic Scaffolding Protein together with Synapsin Regulates Synaptic Vesicle Clustering in the Drosophila Neuromuscular Junction. *J. Neurosci.* 35, 14756–14770. doi:10.1523/JNEUROSCI.1675-15.2015
145. Wu, B., Wei, S., Petersen, N., Ali, Y., Wang, X., Bacaj, T., Rorsman, P., Hong, W., Südhof, T.C., Han, W., 2015. Synaptotagmin-7 phosphorylation mediates GLP-1-dependent potentiation of insulin secretion from β -cells. *Proc. Natl. Acad. Sci. USA* 112, 9996–10001. doi:10.1073/pnas.1513004112
146. Xu, J., Mashimo, T., Südhof, T.C., 2007. Synaptotagmin-1, -2, and -9: Ca²⁺ sensors for fast release that specify distinct presynaptic properties in subsets of neurons. *Neuron* 54, 567–581. doi:10.1016/j.neuron.2007.05.004
147. Xue, M., Craig, T.K., Shin, O.-H., Li, L., Brautigam, C.A., Tomchick, D.R., Südhof, T.C., Rosenmund, C., Rizo, J., 2010. Structural and mutational analysis of functional differentiation between synaptotagmins-1 and -7. *PLoS One* 5. doi:10.1371/journal.pone.0012544
148. Yang, X., Kaeser-Woo, Y.J., Pang, Z.P., Xu, W., Südhof, T.C., 2010. Complexin clamps asynchronous release by blocking a secondary Ca²⁺ sensor via its accessory α helix. *Neuron* 68, 907–920. doi:10.1016/j.neuron.2010.11.001
149. Yoshihara, M., Adolfsen, B., Galle, K.T., Littleton, J.T., 2005. Retrograde signaling by Syt 4 induces presynaptic release and synapse-specific growth. *Science* 310, 858–863. doi:10.1126/science.1117541
150. Yoshihara, M., Guan, Z., Littleton, J.T., 2010. Differential regulation of synchronous versus asynchronous neurotransmitter release by the C2 domains of synaptotagmin 1. *Proc. Natl. Acad. Sci. USA* 107, 14869–14874. doi:10.1073/pnas.1000606107
151. Yoshihara, M., Littleton, J.T., 2002. Synaptotagmin I functions as a calcium sensor to synchronize neurotransmitter release. *Neuron* 36, 897–908.
152. Young, S.M., Neher, E., 2009. Synaptotagmin has an essential function in synaptic vesicle positioning for synchronous release in addition to its role as a calcium sensor. *Neuron* 63, 482–496. doi:10.1016/j.neuron.2009.07.028
153. Zhai, R.G., Bellen, H.J., 2004. The architecture of the active zone in the presynaptic nerve terminal. *Physiology (Bethesda)* 19, 262–270. doi:10.1152/physiol.00014.2004
154. Zhang, J., Schulze, K.L., Hiesinger, P.R., Suyama, K., Wang, S., Fish, M., Acar, M., Hoskins, R.A., Bellen, H.J., Scott, M.P., 2007. Thirty-one flavors of Drosophila rab proteins. *Genetics* 176, 1307–1322. doi:10.1534/genetics.106.066761
155. Zhao, H., Ito, Y., Chappel, J., Andrews, N.W., Teitelbaum, S.L., Ross, F.P., 2008. Synaptotagmin VII regulates bone remodeling by modulating osteoclast and osteoblast

- secretion. *Dev. Cell* 14, 914–925. doi:10.1016/j.devcel.2008.03.022
156. Zhou, Q., Lai, Y., Bacaj, T., Zhao, M., Lyubimov, A.Y., Uervirojnangkoorn, M., Zeldin, O.B., Brewster, A.S., Sauter, N.K., Cohen, A.E., Soltis, S.M., Alonso-Mori, R., Chollet, M., Lemke, H.T., Pfuetzner, R.A., Choi, U.B., Weis, W.I., Diao, J., Südhof, T.C., Brunger, A.T., 2015. Architecture of the synaptotagmin-SNARE machinery for neuronal exocytosis. *Nature* 525, 62–67. doi:10.1038/nature14975
157. Zucker, R.S., Regehr, W.G., 2002. Short-term synaptic plasticity. *Annu. Rev. Physiol.* 64, 355–405. doi:10.1146/annurev.physiol.64.092501.114547

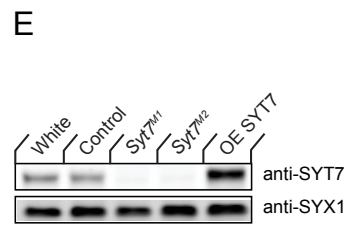
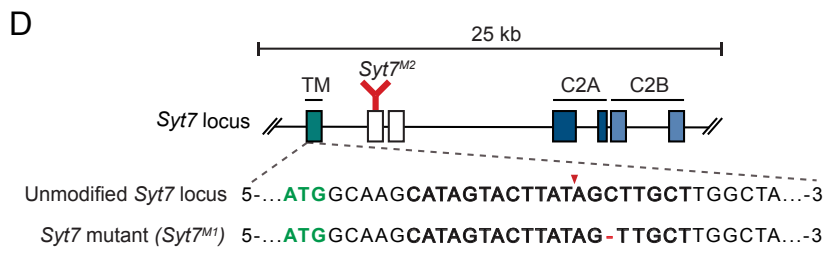
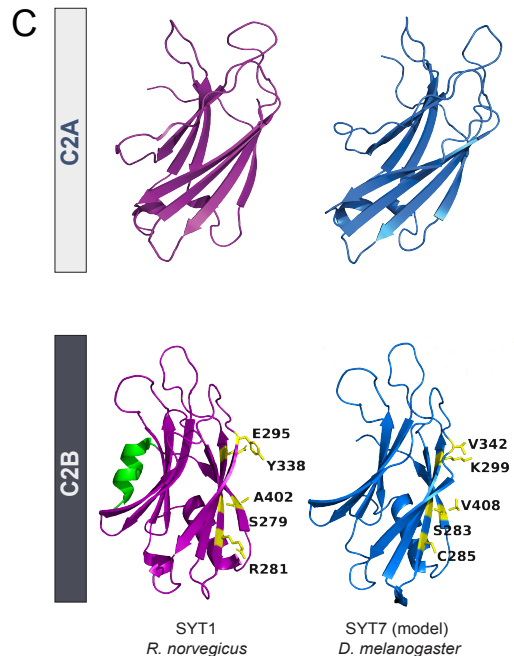
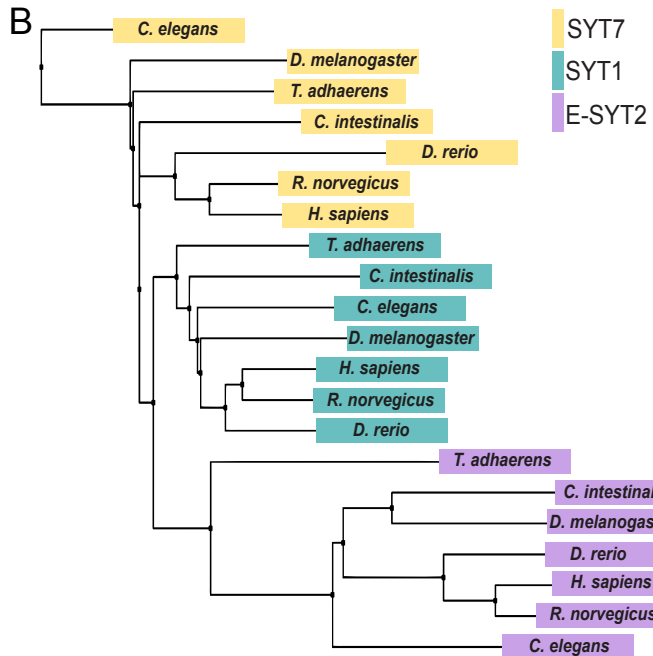
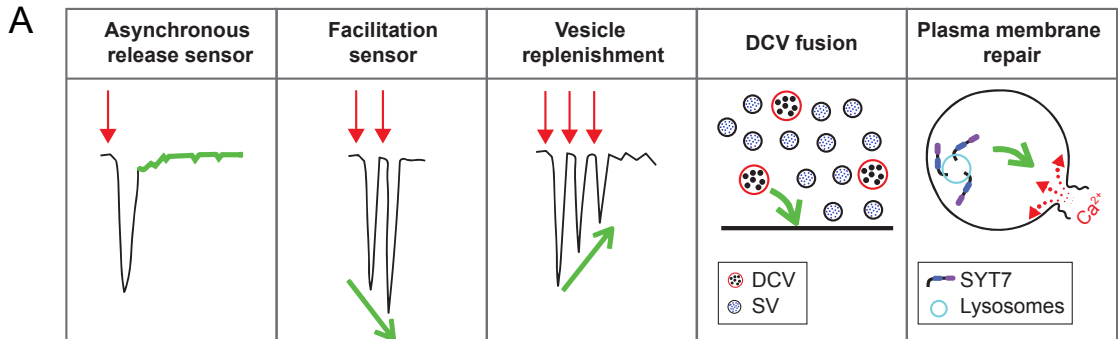


Figure 1. SYT1 and SYT7 comparison and generation of *Syt7* mutants. (A) Proposed roles for SYT7 in Ca²⁺-regulated membrane trafficking. (B) Phylogenetic tree of SYT1, SYT7 and E-SYT2 from the indicated species generated using the BLOSUM62 matrix with neighbor joining clustering. (C) Comparison of the structure of the C2A and C2B domains of *R. norvegicus* SYT1 (magenta) with a homology model of *D. melanogaster* SYT7 (blue). The C2B residues that form the SYT1-SNARE complex primary binding site are highlighted in yellow, with the counterpart changes noted in SYT7. The C2B HB helix in SYT1 is highlighted in green and missing from SYT7. (D) Diagram of the *Syt7* genomic locus on chromosome 4 with coding exons indicated with boxes. Exon 1 (teal) encodes the intravesicular and transmembrane (TM) domains; exons 2 and 3 (white) encode the linker region; exons 4 and 5 encode the C2A domain (dark blue); and exons 6 and 7 encode the C2B domain (light blue). The location of the *Syt7*^{M2} Minos transposon insertion in exon 2 is indicated in red. Sequence of the *Syt7*^{M1} CRISPR mutant versus control is shown below with the start codon in green. The guide RNA sequence used to target *Syt7* is bolded, with the cleavage site noted by the red arrowhead and the deleted cytosine with a red dash. (E) Western of SYT7 protein levels in head extracts of *white*, CRISPR control, *Syt7*^{M1}, *Syt7*^{M2} and *elav*^{C155}-GAL4; UAS-*Syt7* (OE SYT7) with anti-SYT7 antisera (top panel). Syntaxin 1 (SYX1) antisera was used as a loading control (bottom panel). SYT7 is overexpressed 2.48 ± 0.4-fold compared to controls (p<0.05, Mann-Whitney unpaired t-test, n=4).

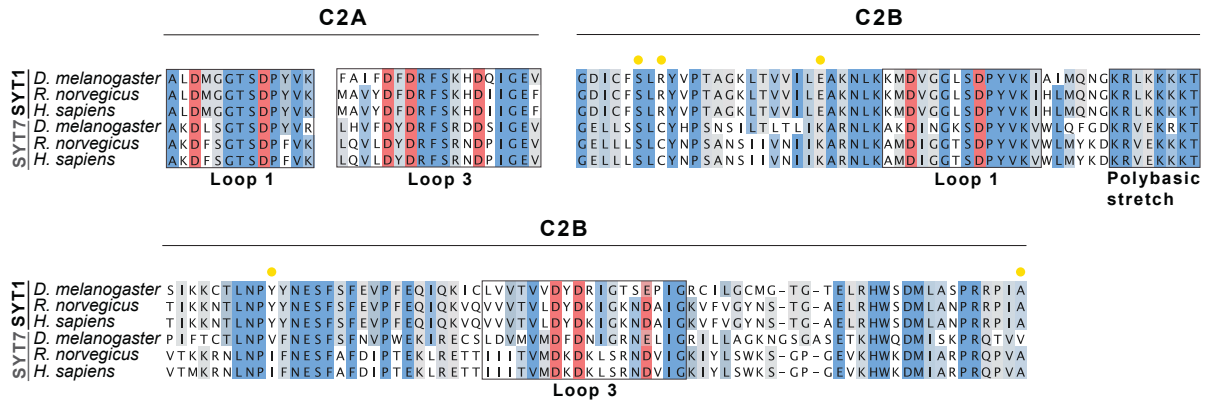


Figure 1 – figure supplement 1. SYT1 and SYT7 sequence comparisons. Annotated sequence alignment of the C2A Ca²⁺ binding loops and the C2B domain of SYT1 and SYT7 from the indicated species. Conserved residues are shaded dark blue, with conservative amino acid substitutions in light blue. Grey shading denotes subfamily-specific residue conservation in only SYT1 or SYT7. C2A and C2B Ca²⁺ binding residues are shaded red. Yellow circles denote residues that form the primary SYT1-SNARE complex binding interface. Four of the five residues are not conserved in *Drosophila* SYT7, with two containing identical substitutions previously found to abolish SYT1 function (R334H and E348K).

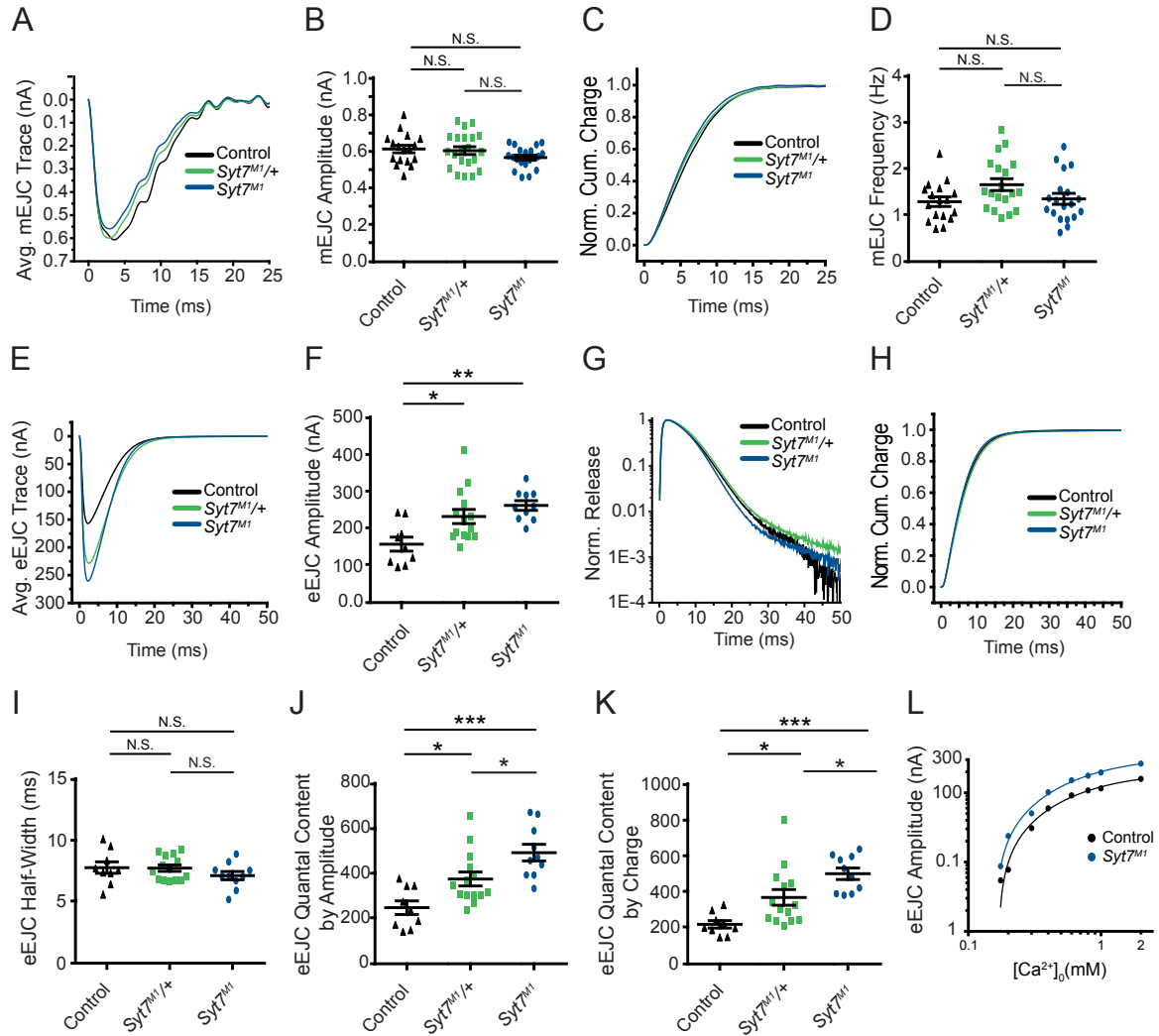


Figure 2. *Syt7* mutants and *Syt7/+* heterozygotes display enhanced neurotransmitter release. (A) Average mEJC traces in control (black), *Syt7^{M1/+}* (green) and *Syt7^{M1}* mutants (blue). (B) Quantification of mean mEJC amplitude for the indicated genotypes (control: 0.62 ± 0.020 nA, n=17; *Syt7^{M1/+}*: 0.61 ± 0.021 nA, n=21; *Syt7^{M1}*: 0.57 ± 0.013 nA, n=20). (C) Normalized cumulative mEJC charge for each genotype. (D) Quantification of mean mEJC frequency for the indicated genotypes (control: 1.30 ± 0.10 Hz, n=17; *Syt7^{M1/+}*: 1.66 ± 0.13 Hz, n=19; *Syt7^{M1}*: 1.36 ± 0.12 Hz, n=19). (E) Average eEJC traces in control (black), *Syt7^{M1/+}* (green) and *Syt7^{M1}* (blue). (F) Quantification of mean eEJC amplitude for the indicated genotypes. (G) Average normalized responses for each genotype plotted on a semi-logarithmic graph to display release components. (H) Cumulative release normalized to the maximum response in 2 mM Ca^{2+} for each genotype. (I) Quantification of mean eEJC half-width in the indicated genotypes (control: 7.81 ± 0.47 ms, n=9; *Syt7^{M1/+}*: 7.77 ± 0.26 ms, n=14; *Syt7^{M1}*: 7.15 ± 0.34 ms, n=10). (J) Quantification of evoked quantal content with mEJC amplitude for the indicated genotypes (control: 250.1 ± 30.58 SVs, n=9; *Syt7^{M1/+}*: 377.9 ± 31.13 , n=14; *Syt7^{M1}*: 495.3 ± 36.75 , n=10). (K) Quantification of evoked quantal content with mEJC charge for the indicated genotypes (control: 221.3 ± 20.54 SVs, n=9; *Syt7^{M1/+}*: 371.6 ± 43.56 , n=14; *Syt7^{M1}*: 503.6 ± 31.99 , n=10). (L) Log-log plot for eEJC amplitudes recorded in 0.175, 0.2, 0.3, 0.4, 0.6, 0.8, 1, and 2 mM extracellular $[Ca^{2+}]$ from control (black) and *Syt7^{M1}* mutants (blue), with a Hill fit for each genotype noted. Recordings were performed from 3rd instar segment A3 muscle 6. Extracellular $[Ca^{2+}]$ in E-K was 2 mM. Statistical significance was determined using one-way ANOVA (nonparametric) with post hoc Tukey's multiple comparisons test. N.S. = no significant change. Error bars represent SEM.

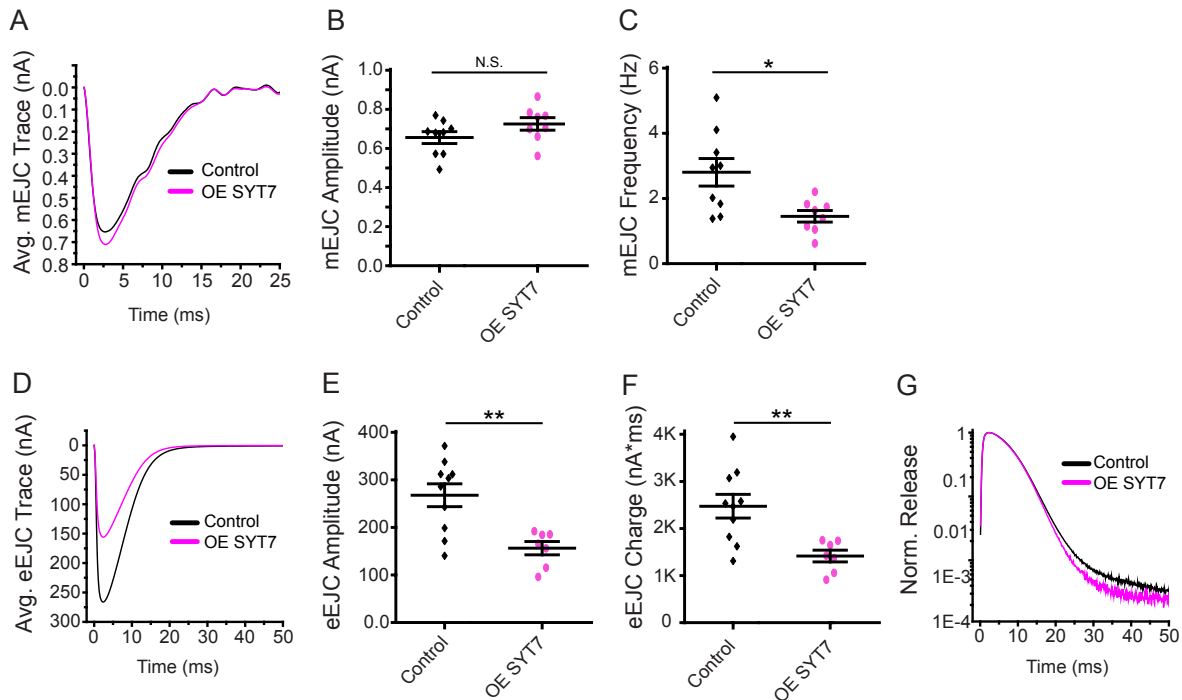


Figure 3. Neuronal overexpression of SYT7 reduces spontaneous and evoked SV release. (A) Average mEJC traces in control (black) and *elav^{C155}-GAL4; UAS-Syt7* (OE SYT7, magenta). **(B)** Quantification of mean mEJC amplitudes in the indicated genotypes (control: 0.66 ± 0.03 nA, n=9; OE SYT7: 0.73 ± 0.03 nA, n=8). **(C)** Quantification of mean mEJC frequency in the indicated genotypes (control: 2.81 ± 0.42 Hz, n=9; OE SYT7: 1.45 ± 0.18 Hz, n=8). **(D)** Average eEJC traces in control (black) and *elav^{C155}-GAL4; UAS-Syt7* (OE SYT7, magenta). **(E)** Quantification of mean eEJC amplitudes in the indicated genotypes (control: 256.24 ± 22.38 nA, n=10; OE SYT7: 166.66 ± 10.74 nA, n=7). **(F)** Quantification of mean eEJC charge in the indicated genotypes (control: $2.5 \times 10^3 \pm 0.25 \times 10^3$ nA*ms, n=10; OE SYT7: $1.4 \times 10^3 \pm 0.12 \times 10^3$ nA*ms, n=7). **(G)** Average normalized responses for each genotype plotted on a semi-logarithmic graph to display release components. Recordings were performed from 3rd instar segment A3 muscle 6 in 2 mM Ca²⁺. Statistical significance was determined with a Mann-Whitney unpaired t-test.

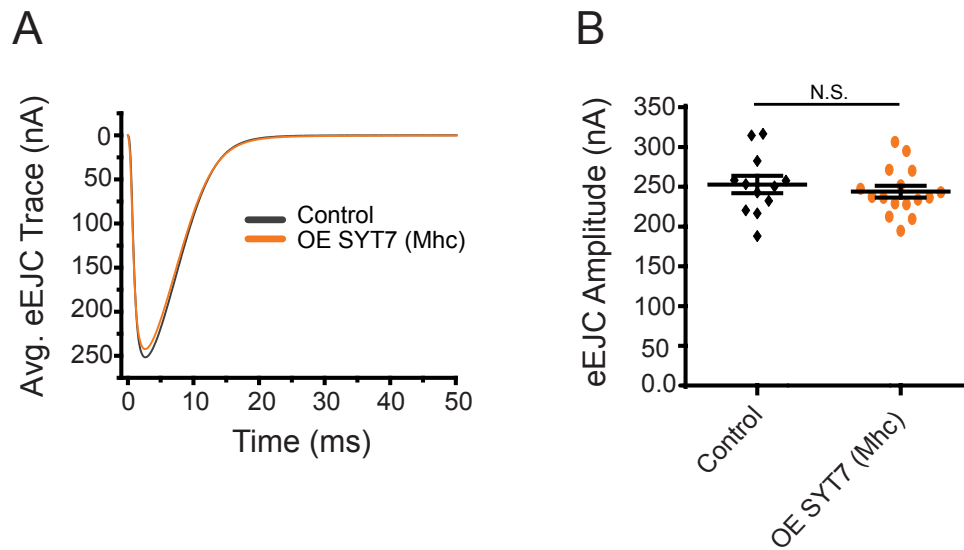


Figure 3 – figure supplement 1. Overexpression of SYT7 in postsynaptic muscles does not disrupt synaptic transmission. (A) Average eEJC traces in control (black) and *Mhc*-GAL4; UAS-*Syt7* (OE SYT7, orange). **(B)** Quantification of mean eEJC amplitudes in the indicated genotypes (control: 252.82 ± 10.98 nA, n=12; *Mhc*-GAL4; UAS-*Syt7*: 243.91 ± 7.46 nA, n=16). Recordings were performed from 3rd instar segment A3 muscle 6 in 2 mM Ca²⁺. Statistical significance was determined with the Mann-Whitney unpaired test.

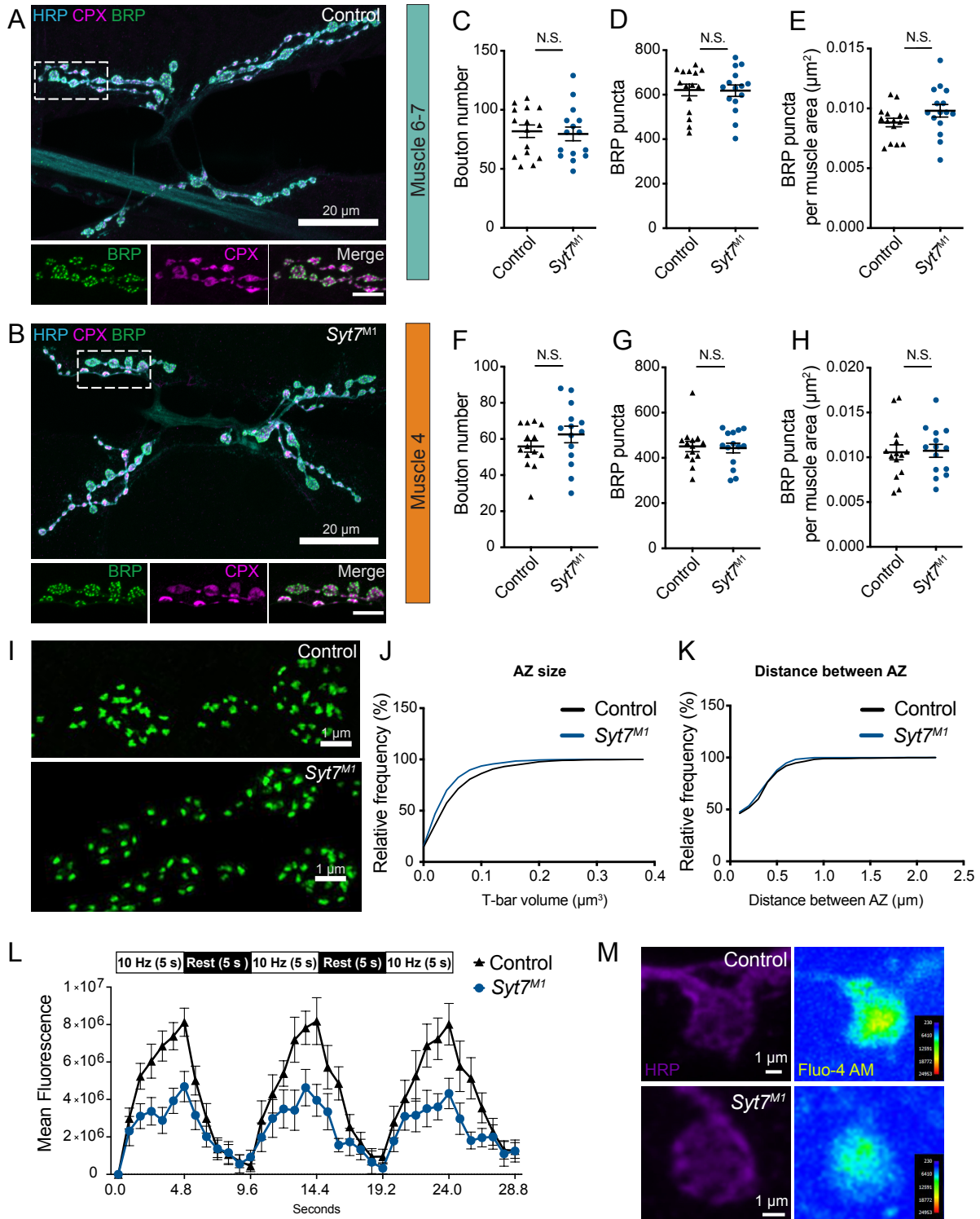


Figure 4. Analysis of synaptic morphology in *Syt7* mutants. (A, B) Immunocytochemistry of 3rd instar muscle 6/7 NMJs with anti-HRP (blue), anti-CPX (magenta) and anti-BRP (green) in control and *Syt7^{MI}*. The boxed region is magnified below with channels showing BRP, CPX and the merge. Scale bar = 20 μm for large panels and 2 μm for boxed regions. Synaptic morphology was quantified for 3rd instar muscle 6/7 (C-E) and muscle 4 (F-H) in controls and *Syt7^{MI}* mutants. No significant differences were detected in synaptic bouton number (C, F; muscle 6/7: $p = 0.78$; control: 81.87 ± 5.301 , $n=15$; *Syt7^{MI}*: 79.60 ± 5.824 , $n=15$; muscle 4: $p = 0.24$; control: 55.86 ± 3.141 , $n=14$; *Syt7^{MI}*: 62.50 ± 4.575 , $n=14$), BRP puncta (D, G, muscle 6/7: $p = 0.94$; control: 621.1 ± 26.28 , $n=15$; *Syt7^{MI}*: 618.1 ± 25.73 , $n=15$; muscle 4: $p = 0.83$; control: 450.5 ± 23.25 , $n=14$; *Syt7^{MI}*: 443.5 ± 21.47 , $n=14$) or BRP puncta per muscle surface area (E, H, muscle 6/7: $p = 0.13$; control: 0.0088 ± 0.0004 , $n=15$; *Syt7^{MI}*: 0.0098 ± 0.0005 , $n=15$; muscle 4: $p = 0.88$; control: 0.0105 ± 0.0008 , $n=14$; *Syt7^{MI}*: 0.0107 ± 0.0007 , $n=14$). (I) Anti-BRP staining at 3rd instar muscle 4 in control and *Syt7^{MI}* imaged with SIM microscopy. Scale bar = 1 μm . (J) Relative cumulative frequency of AZ T-bar volume defined with anti-BRP staining at 3rd instar muscle 6/7 NMJs ($p = 0.026$; control: $0.055 \pm 0.004 \mu\text{m}^2$, $n = 19$ NMJs from 5 larvae; *Syt7^{MI}*: $0.044 \pm 0.003 \mu\text{m}^2$, $n=15$ NMJs from 4 larvae). (K) Relative cumulative frequency of T-bar spacing defined by distance between nearest BRP puncta at 3rd instar muscle 6/7 NMJs ($p = 0.48$; control: $0.28 \pm 0.016 \mu\text{m}$, $n=20$ NMJs from 5 larvae; *Syt7^{MI}*: $0.27 \pm 0.014 \mu\text{m}$, $n=15$ NMJs from 4 larvae). Statistical significance was determined with Student's t-test. (L) Mean fluorescence intensity of Fluo-4 AM in control (black) and *Syt7^{MI}* mutants (blue) during the indicated stimulation protocol. (M) Representative images of synaptic boutons stained with anti-HRP (left), with Fluo-4 AM maximum fluorescence intensity during stimulation shown on the right for control (above) and *Syt7^{MI}* (below). Scale bar = 1 μm .

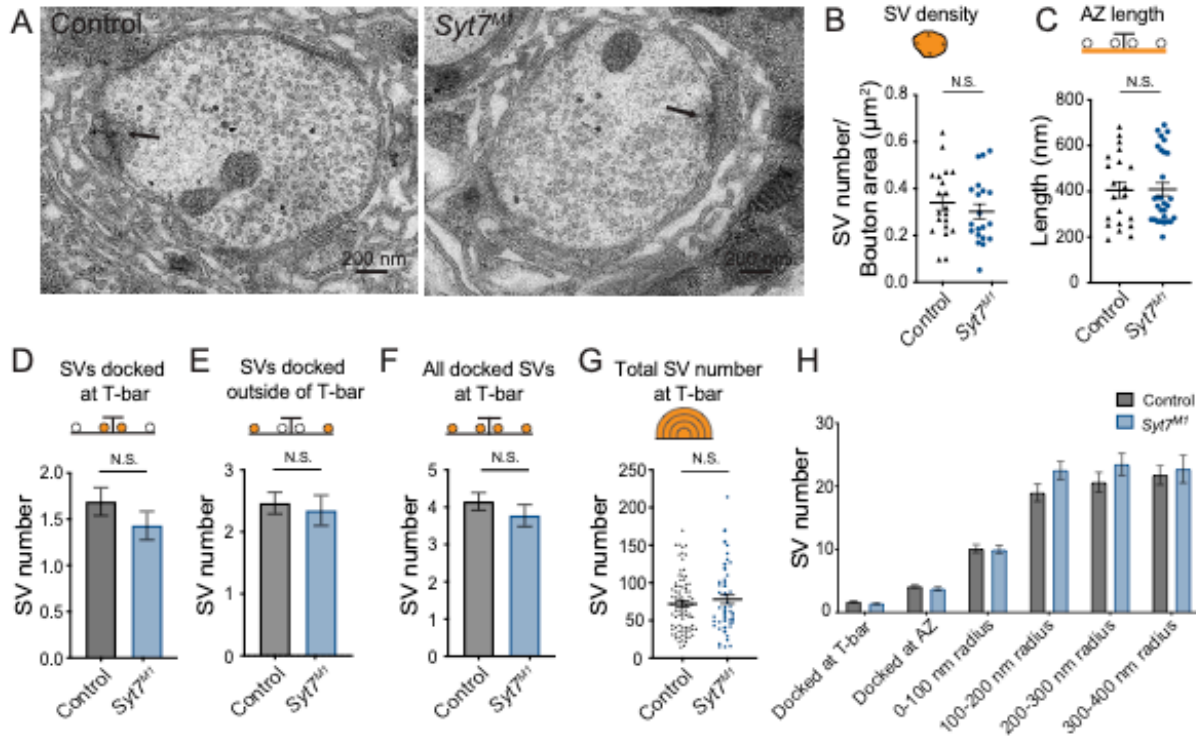


Figure 5. Ultrastructural analysis of SV distribution in *Syt7* mutants. (A) Representative EM micrographs of muscle 6/7 synaptic boutons in control and *Syt7^{MI}* 3rd instar larvae. An AZ with its associated electron dense T-bar is denoted with an arrowhead in each micrograph. (B) Quantification of SV density ($p = 0.41$; control = 0.34 ± 0.033 SVs/ μm^2 , $n = 20$; *Syt7^{MI}* = 0.30 ± 0.031 SVs/ μm^2 , $n = 20$). (C) Quantification of AZ length defined by the electron dense synaptic cleft ($p=0.93$; control: 404 ± 34.5 nm, $n=21$ AZs from 5 larvae; *Syt7^{MI}*: 409 ± 28.9 nm, $n=29$ AZs from 5 larvae). (D) Quantification of SVs docked within 100 nm of the T-bar ($p = 0.41$; control = 1.69 ± 0.15 SVs $n = 84$; *Syt7^{MI}* = 1.43 ± 0.15 SVs, $n = 58$). (E) Quantification of SVs docked within 100 - 400 nm of the T-bar ($p = 0.68$; control = 2.46 ± 0.17 SVs $n = 84$; *Syt7^{MI}* = 2.35 ± 0.25 SVs, $n = 58$). (F) Quantification of all docked SVs at 0-400 nm from the T-bar ($p = 0.31$; control = 4.16 ± 0.23 SVs $n = 84$; *Syt7^{MI}* = 3.78 ± 0.29 SVs, $n = 58$). (G) Quantification of all SVs within a 400 nm radius from the T-bar ($p = 0.38$; control = 71.98 ± 4.05 SVs $n = 84$; *Syt7^{MI}* = 78.12 ± 5.89 SVs, $n = 58$). (H) Quantification of SV distribution at AZs in control and *Syt7^{MI}* mutants. Statistical significance was determined with Student's t-test.

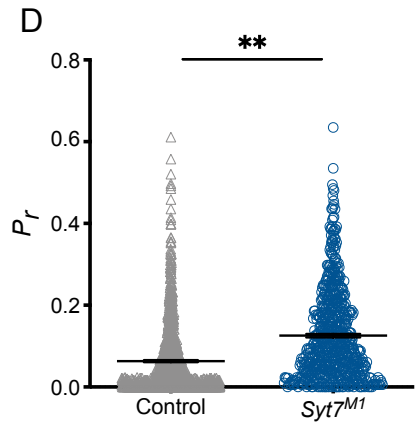
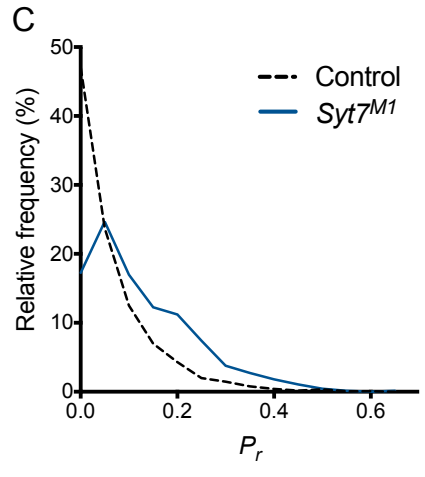
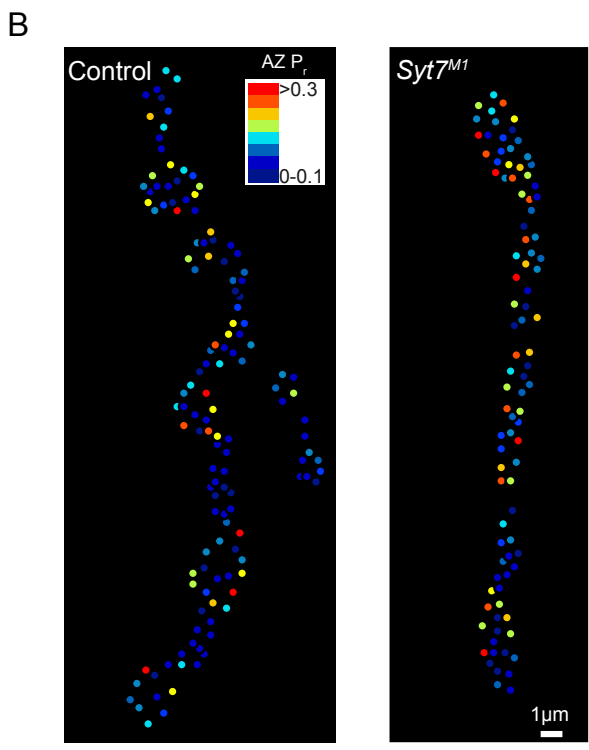
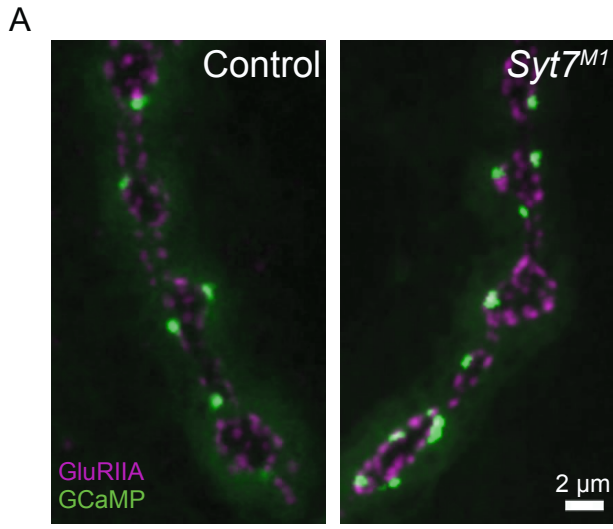


Figure 6. Quantal imaging reveals elevated release probability across the AZ population in *Syt7* mutants. (A) Representative images of GluRIIA positive PSDs (red) and postsynaptic myr-GCaMP6 flashes (green) in response to evoked stimulation in control and *Syt7^{M1}* mutants. (B) P_r heatmaps for muscle 4 NMJs generated following 0.3 Hz stimulation for 5 minutes in control and *Syt7^{M1}* mutants. The P_r color map is displayed in the upper right. (C) Frequency distribution of AZ P_r after a 0.3 Hz 5-minute stimulation for control (black dashed line) and *Syt7^{M1}* (blue line). (D) Quantification of mean AZ P_r for the two genotypes ($p \leq 0.01$, Student's t-test; control: 0.063 ± 0.002 , $n=1158$; *Syt7^{M2}*: 0.12 ± 0.004 , $n=768$).

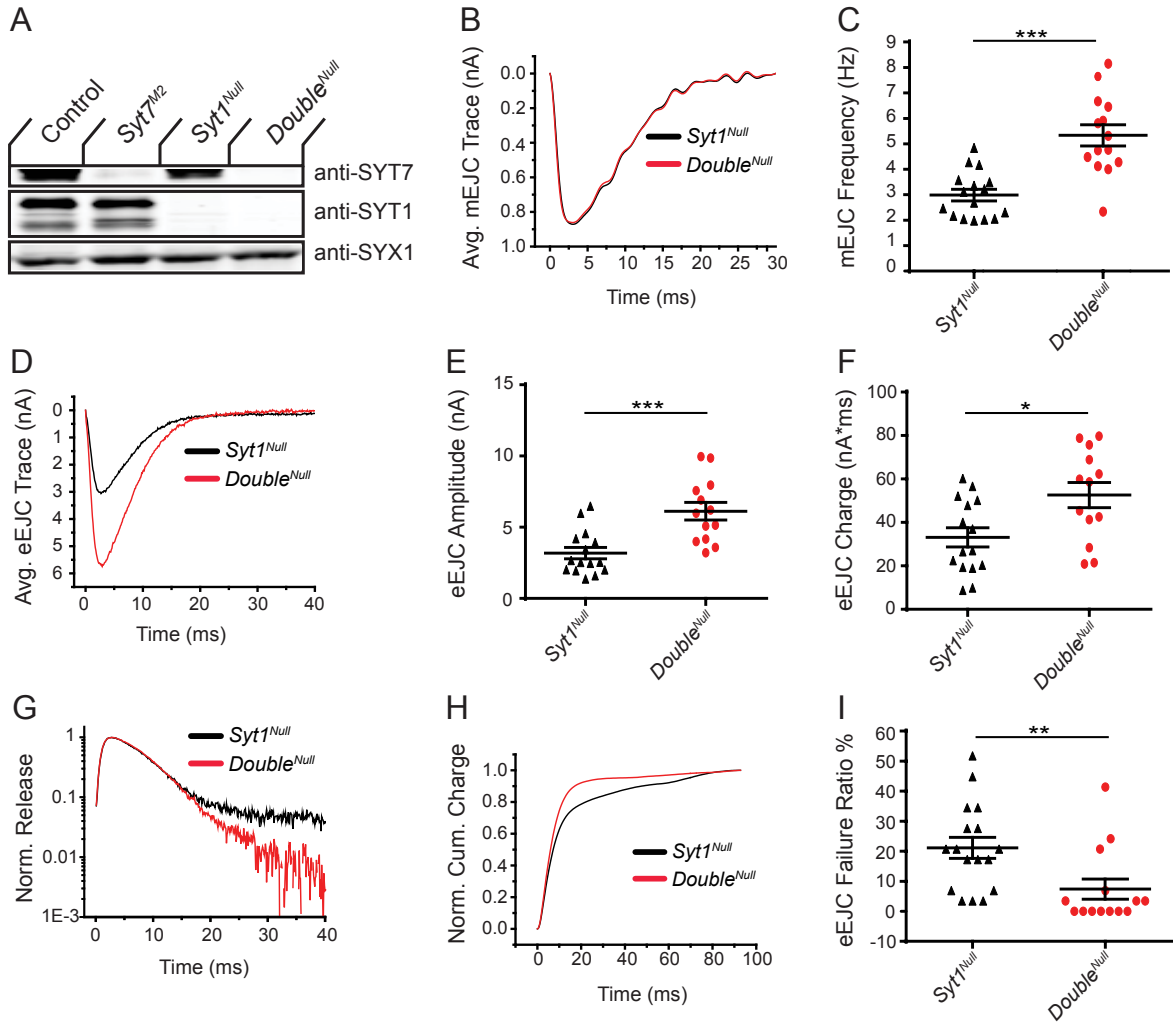


Figure 7. Loss of SYT7 enhances the residual release observed in *Syt1* null mutants. (A) Western of head extracts from control, *Syt7^{M2}*, *Syt1^{Null}* and *Syt1^{null}; Syt7^{M2} (Double^{Null})* probed with anti-SYT7, anti-SYT1 and anti-SYX1 (loading control). SYT1 migrates as a doublet at 55 and 70 kD (Littleton et al., 1993a). (B) Average mEJC traces in *Syt1^{Null}* (black trace) and *Double^{Null}* (red trace) mutants obtained by summing all mEPSC events under the first peak distribution. (C) Quantification of mean mEJC frequency for the indicated genotypes. (D) Average eEJC traces in *Syt1^{Null}* (black trace) and *Double^{Null}* (red trace). (E) Quantification of mean eEJC amplitude for the indicated genotypes. (F) Quantification of mean eEJC charge for the indicated genotypes obtained by measuring total release over time. (G) Average normalized responses for each genotype plotted on a semi-logarithmic graph to display release components. (H) Cumulative release normalized to the maximum response in 2 mM Ca²⁺ for each genotype. Each trace was adjusted to a double exponential fit. (I) Quantification of eEJC failure ratio (%) in the indicated genotypes. Recordings were performed from 3rd instar segment A3 muscle 6 in 2 mM extracellular Ca²⁺. Statistical significance was determined with the Mann-Whitney unpaired t-test.

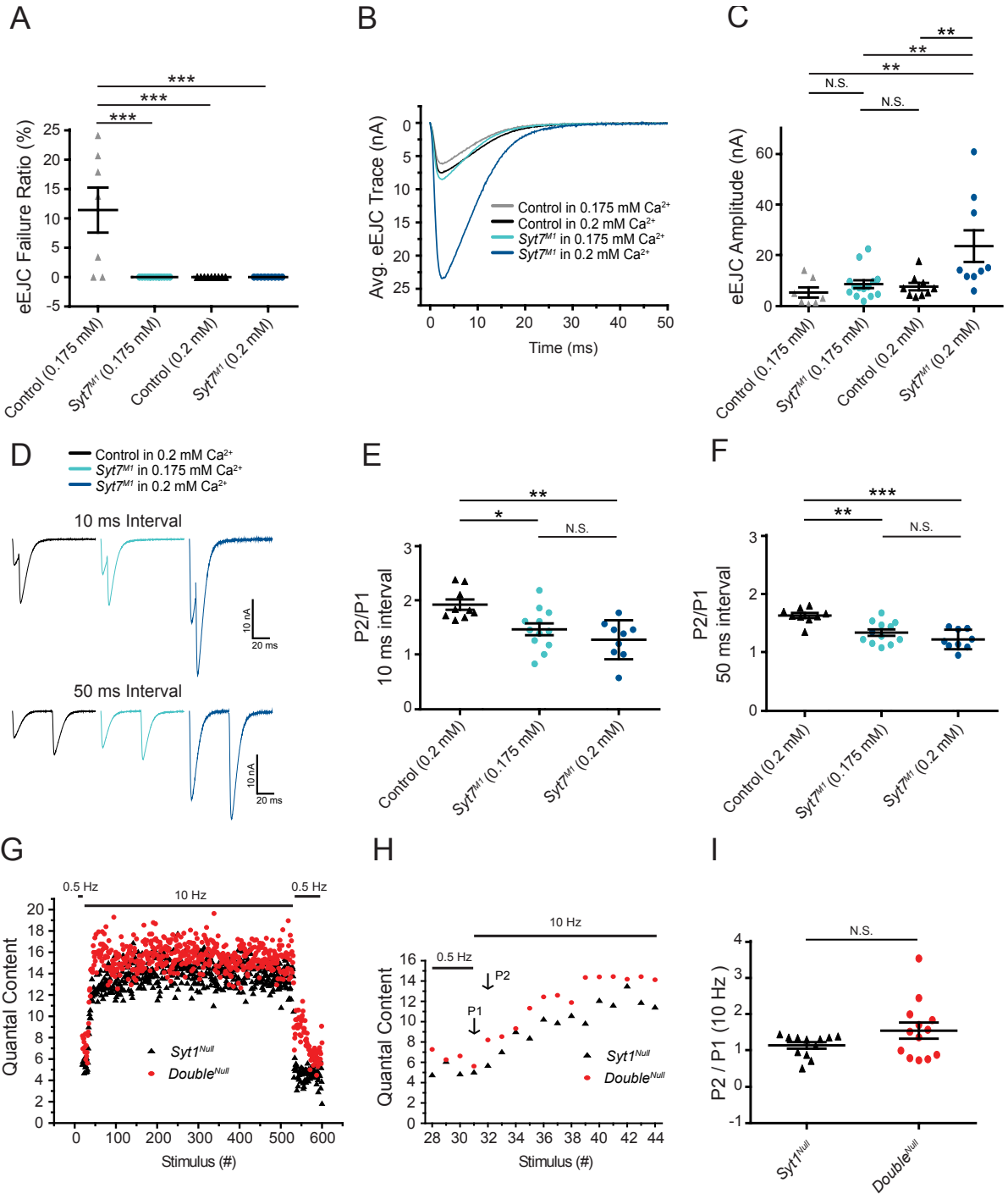


Figure 8. Short-term synaptic facilitation can occur without SYT7 or SYT1. (A) Quantification of eEJC failure ratio (%) in the indicated genotypes. (B) Average eEJC traces recorded in 0.175 mM Ca²⁺ (control, grey; *Syt7^{M1}*, light blue) or 0.2 mM Ca²⁺ (control, black; *Syt7^{M1}*, dark blue). (C) Quantification of mean eEJC amplitude for the indicated genotypes (0.175 mM Ca²⁺: control, 5.42 ± 2.0 nA, n=7; *Syt7^{M1}*, 8.70 ± 1.6 nA, n=14; 0.2 mM Ca²⁺: control, 7.73 ± 1.5 nA, n=9; *Syt7^{M1}*, 23.72 ± 6.2 nA, n=9). (D) Representative eEJC traces to 10 ms or 50 ms paired-pulse stimuli recorded in 0.2 mM Ca²⁺ (control, black; *Syt7^{M1}*, dark blue) or 0.175 mM Ca²⁺ (*Syt7^{M1}*, light blue). (E) Quantification of facilitation (P2/P1) at 10 ms interval for the indicated genotypes (0.2 mM Ca²⁺: 1.93 ± 0.095, n=9; *Syt7^{M1}*, 1.28 ± 0.12, n=9; 0.175 mM Ca²⁺: *Syt7^{M1}*, 1.47 ± 0.11, n=12). (F) Quantification of facilitation (P2/P1) at 50 ms interval for the indicated genotypes (0.2 mM Ca²⁺: control, 1.64 ± 0.043, n=9; *Syt7^{M1}*, 1.23 ± 0.056, n=9; 0.175 mM Ca²⁺: *Syt7^{M1}*, 1.34 ± 0.054, n=12). Statistical significance was determined using one-way ANOVA (nonparametric) with post hoc Tukey's multiple comparisons test for panels A-F. (G) Average eEJC quantal content determined from mEJC charge in 2 mM Ca²⁺ during a 10 Hz stimulation paradigm (30 stimuli at 0.5 Hz, 500 stimuli at 10 Hz, and return to 0.5 Hz) in *Syt1^{Null}* (black) and *Double^{Null}* (red). (H) Average quantal content for the last four responses of 0.5 Hz stimulation and the first 14 responses during 10 Hz stimulation in *Syt1^{Null}* (black) and *Double^{Null}* (red). P1 denotes the 1st response and P2 the 2nd response to 10 Hz stimulation. (I) Quantification of P2/P1 ratio in *Syt1^{Null}* (black, 1.15 ± 0.089, n=12) and *Double^{Null}* (red, 1.55 ± 0.22, n=13) at onset of 10 Hz stimulation. Statistical significance was determined with a Mann-Whitney unpaired t-test for panels H and I.

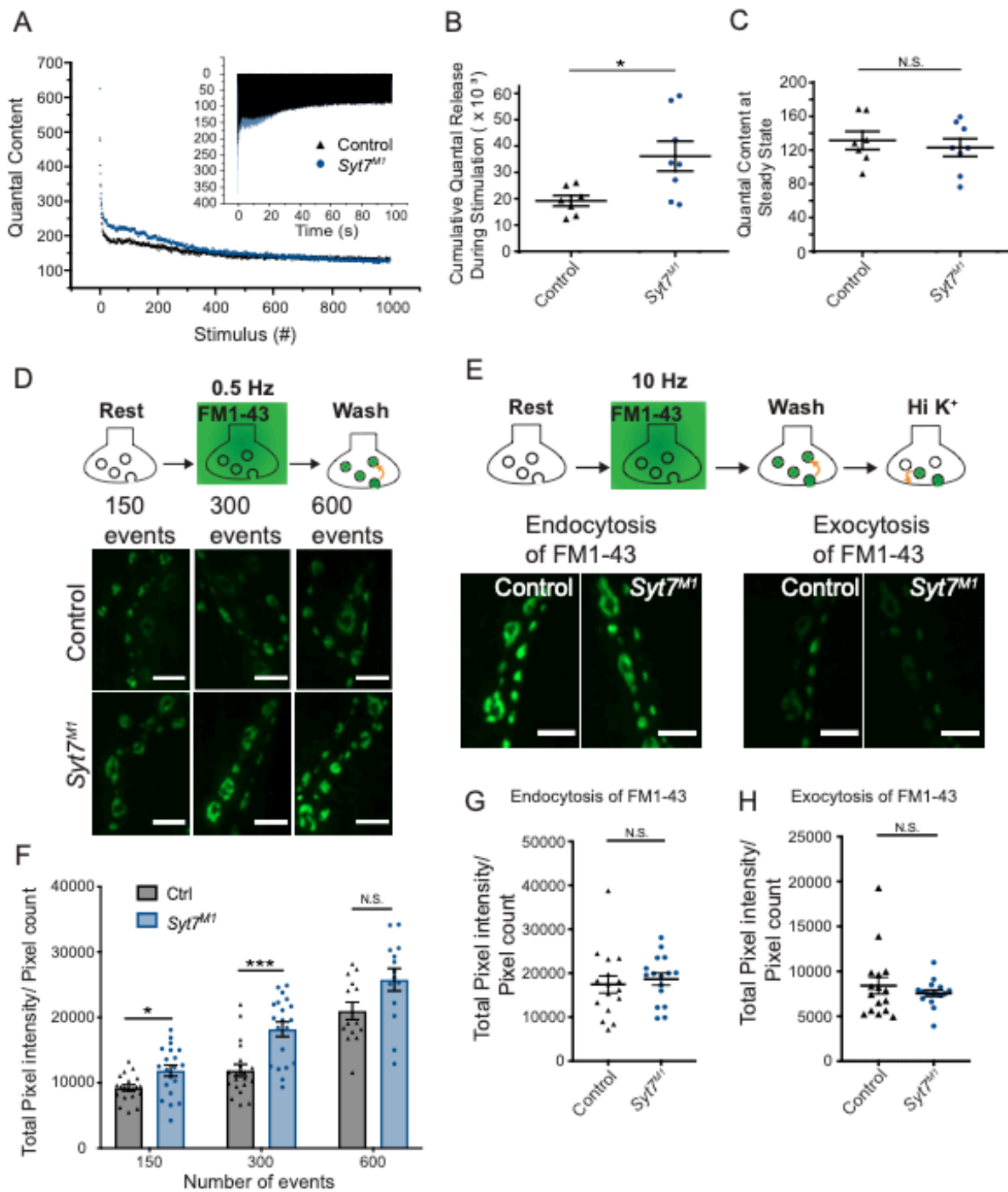


Figure 9. *Syt7* mutants have a larger releasable pool of SVs and normal endocytosis. (A) Representative mean eEJC quantal content determined by mEJC charge during 1000 stimuli at 10 Hz in 2 mM Ca^{2+} in control (black) and *Syt7^{M1}* (blue). The inset shows representative eEJC traces in control (black) and *Syt7^{M1}* (blue). (B) Quantification of average cumulative quanta released during the 1000 stimuli at 10 Hz tetanic stimulation in control (black, $19.21\text{K} \pm 2.88\text{K}$, $n=7$) and *Syt7^{M1}* (blue, $36.18\text{K} \pm 5.67\text{K}$, $n=8$). (C) Quantification of average quantal content at steady-state release at the end of the 10 Hz stimulation in control (black, 131.54 ± 10.71 , $n=7$) and *Syt7^{M1}* (blue, 123.05 ± 10.47 , $n=8$). Statistical significance for B and C was determined with a Mann-Whitney unpaired t-test. (D) FM1-43 loading in control and *Syt7^{M1}* larvae at muscle 6/7 NMJs in 2 mM Ca^{2+} following 150, 300 or 600 stimuli delivered at 0.5 Hz. (E) FM1-43 loading with 500 stimuli at 10 Hz in 2 mM Ca^{2+} and FM1-43 unloading with high K^+ (90 mM) in control and *Syt7^{M1}* larvae at muscle 6/7 NMJs. (F) Quantification of FM1-43 loading following 150, 300 or 600 stimuli delivered at 0.5 Hz. (G) Quantification of FM1-43 loading after 500 stimuli at 10 Hz. (H) Quantification of FM1-43 unloading with high K^+ (90 mM). Statistical significance was determined with Student's t-test for F-H. Scale bar = $5\mu\text{m}$.

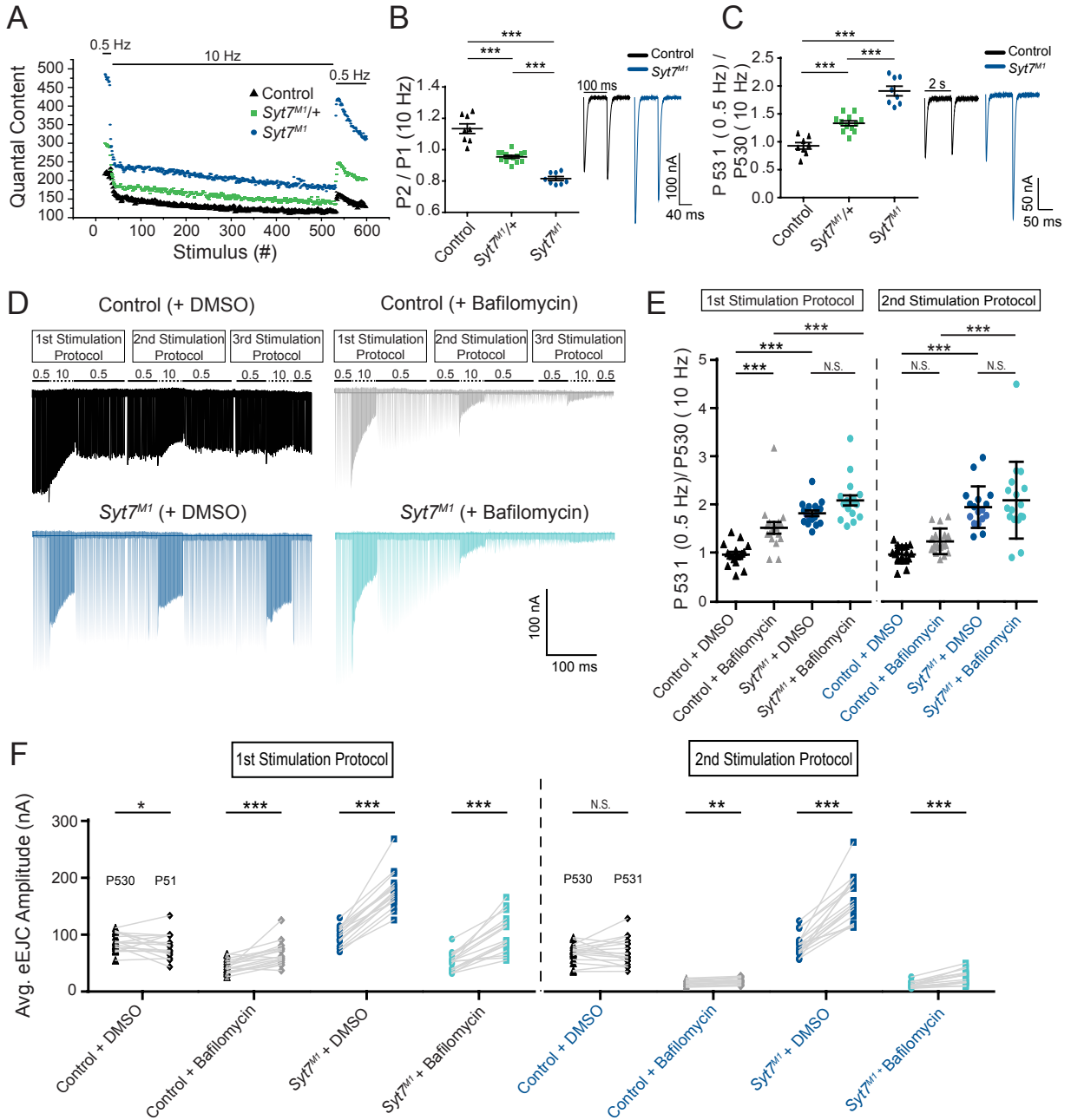


Figure 10. *Syt7* mutants have enhanced refilling of the RRP that does not require endocytosis.

(A) Average eEJC quantal content during the indicated stimulation protocol in 2 mM external Ca^{2+} for control (black), *Syt7^{MI/+}* (green) and *Syt7^{MI}* (blue). (B) Quantification of P2/P1 ratio (P1 = 1st response to 10 Hz, P2 = 2nd response to 10 Hz) in control (black, 1.13 ± 0.03 , n=8), *Syt7^{MI/+}* (green, 0.95 ± 0.009 , n=14) and *Syt7^{MI}* (blue, 0.82 ± 0.01 , n=8). Representative eEJC traces of P1 and P2 for control (black) and *Syt7^{MI}* (blue) are shown on the right. (C) Quantification of P531/P530 ratio (P530 is the last response to 10 Hz and P531 is the 1st response to 0.5 Hz stimulation delivered 2 seconds after P530) in control (black, 0.93 ± 0.06 , n=8), *Syt7^{MI/+}* (green, 1.33 ± 0.04 , n=12) and *Syt7^{MI}* (blue, 1.91 ± 0.09 , n=8). Representative eEJC traces of P530 and P531 for control (black) and *Syt7^{MI}* (blue) are shown on the right. (D) Representative eEJC traces for control with DMSO (black) or 4 μM bafilomycin (gray) and *Syt7^{MI}* with DMSO (dark blue) or 4 μM bafilomycin (light blue) in 2 mM external Ca^{2+} with the indicated stimulation protocol repeated three times. (E) Quantification of P531/P530 for the indicated genotypes (1st stimulation protocol: Control + DMSO, 0.98 ± 0.056 , n=17; Control + bafilomycin, 1.53 ± 0.12 , n=17; *Syt7^{MI}* + DMSO, 1.83 ± 0.058 , n=17; *Syt7^{MI}* + bafilomycin, 2.10 ± 0.11 , n=17; 2nd stimulation protocol: Control + DMSO, 0.97 ± 0.045 , n=17; Control + bafilomycin, 1.25 ± 0.064 , n=17; *Syt7^{MI}* + DMSO, 1.95 ± 0.10 , n=17; *Syt7^{MI}* + bafilomycin, 2.09 ± 0.19 , n=17). Statistical significance was determined with a one-way Anova with Sidak's multiple comparisons test. (F) Quantification of mean eEJC amplitudes for P530 and P531 for the indicated genotypes (1st stimulation protocol: P530 in Control + DMSO, 87.39 ± 3.85 , n=17; P531 in Control + DMSO, 80.22 ± 5.25 , n=17; P530 in Control + bafilomycin, 44.68 ± 2.80 , n=17; P531 in Control + bafilomycin, 66.26 ± 5.03 , n=17; P530 in *Syt7^{MI}* + DMSO, 97.62 ± 4.04 , n=17; P531 in *Syt7^{MI}* + DMSO, 177.34 ± 7.80 , n=17; P530 in *Syt7^{MI}* + bafilomycin, 52.44 ± 3.83 , n=17; P531 in *Syt7^{MI}* + bafilomycin, 102.50 ± 8.07 , n=17; 2nd stimulation protocol: P530 in Control + DMSO, 68.21 ± 3.97 , n=17; P531 in Control + DMSO, 70.05 ± 5.95 , n=17; P530 in Control + bafilomycin, 15.09 ± 1.26 , n=17; P531 in Control + bafilomycin, 18.15 ± 1.34 , n=17; P531 in *Syt7^{MI}* + DMSO, 82.89 ± 4.64 , n=17; P531 in *Syt7^{MI}* + DMSO, 163.52 ± 9.74 , n=17; P530 in *Syt7^{MI}* + bafilomycin, 11.98 ± 1.26 , n=17; P531 in *Syt7^{MI}* + bafilomycin, 24.71 ± 3.00 , n=17). Statistical significance was determined with a Student's paired t-test.

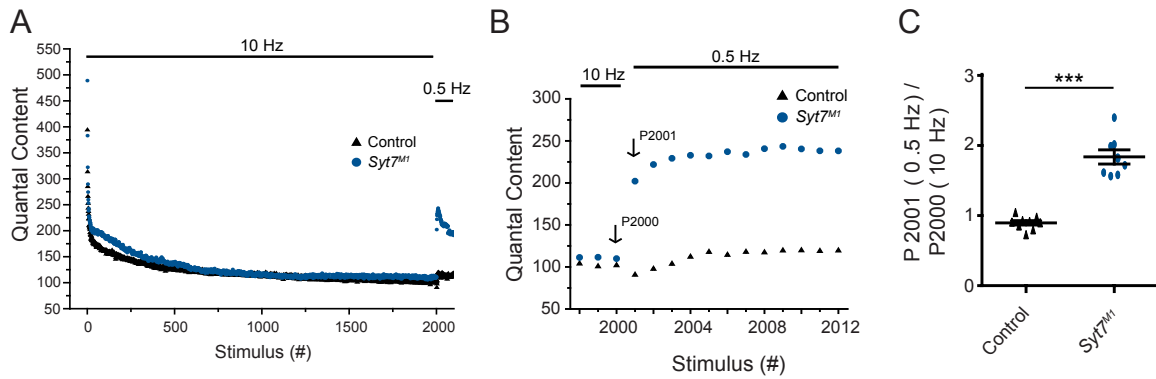


Figure 10 – figure supplement 1. Enhanced recovery after termination of 10 Hz stimulation in *Syt7* mutants. (A) Average eEJC quantal content to 2000 stimuli at 10 Hz stimulation at 3rd instar segment A3 muscle 6 in 2 mM external Ca²⁺ for control (black) and *Syt7^{MI}* (blue). (B) Representative average quantal content of the last 3 responses to 10 Hz and the 1st 12 responses to 0.5 Hz stimulation. P2000 = last response to 10 Hz stimulation, P2001 = 1st response to 0.5 Hz stimulation 2 seconds after P2000. (C) Quantification of P2001/P2000 ratio for control (black, 0.90 ± 0.03 , n=9) and *Syt7^{MI}* (blue, 1.84 ± 0.10 , n=8). Statistical significance was determined with a Mann-Whitney unpaired t-test.

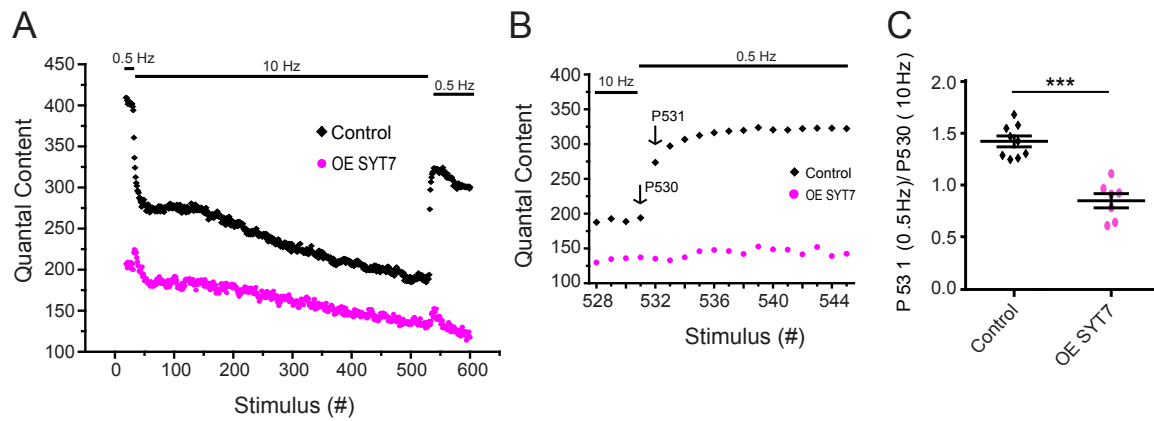


Figure 10 – figure supplement 2. SYT7 overexpression reduces RRP refilling following 10 Hz stimulation. (A) Representative average eEJC quantal content for the indicated stimulation in 2 mM external Ca^{2+} in control (black) and *elav^{C155}-GAL4; UAS-Syt7* (OE SYT7, magenta). (B) Representative average quantal content for the last 4 responses during 10 Hz and the 1st 14 responses during 0.5 Hz in control (black) and OE SYT7 (magenta). (C) Quantification of P531/P530 ratio for control (black, 1.43 ± 0.052 , $n=9$) and OE SYT7 (magenta, 0.85 ± 0.068 , $n=7$). Statistical significance was determined with a Mann-Whitney unpaired t-test.

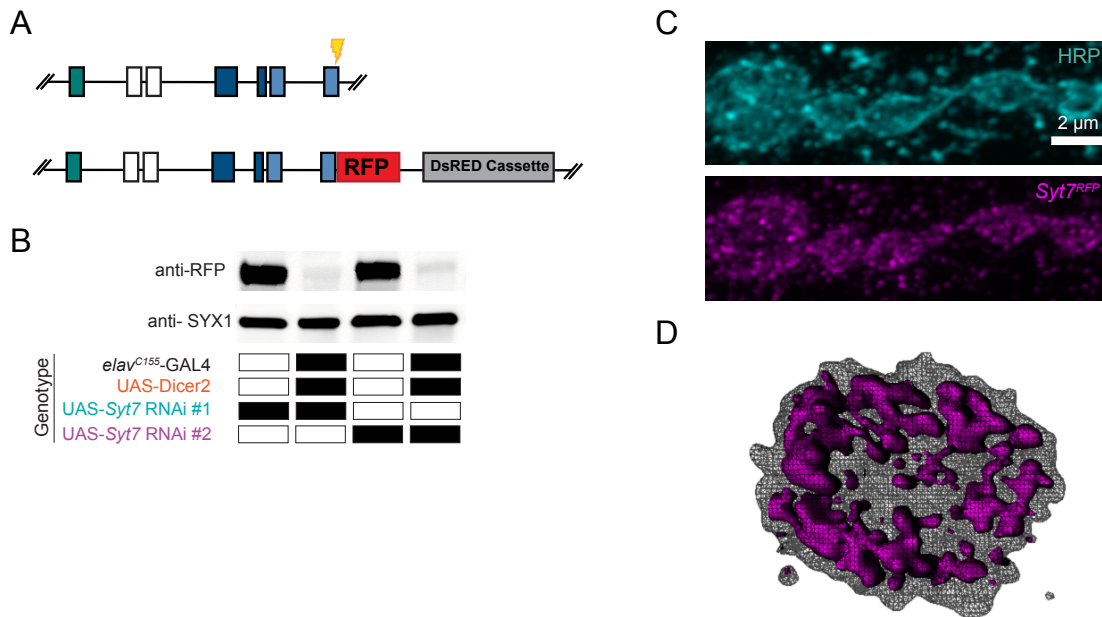


Figure 11. Tagging and location of endogenous SYT7. (A) CRISPR strategy used to insert RFP in frame at the *Syt7* 3' end to generate SYT7^{RFP}. Exon coloring is the same as Figure 1D. The guide RNA cleavage site is displayed in yellow. (B) Two *Syt7* UAS-RNAi lines (#1 and #2) were used to pan-neuronally knockdown SYT7^{RFP}. Western analysis of head extracts probed with anti-RFP (top panel) from SYT7^{RFP} adults following pan-neuronal knockdown of SYT7: lane 1: *UAS-Syt7* RNAi#1; SYT7^{RFP}: lane 2: *elav^{C155}-GAL4*, *UAS-Dicer2*; *UAS-Syt7* RNAi#1; SYT7^{RFP}: lane 3: *UAS-Syt7* RNAi#2; SYT7^{RFP}: lane 4: *elav^{C155}-GAL4*, *UAS-Dicer2*; *UAS-Syt7* RNAi line#2; SYT7^{RFP}. SYX1 antisera was used as a loading control (bottom panel). (C) Immunocytochemistry with anti-HRP (top) and anti-RFP (bottom) in SYT7^{RFP} 3rd instar larvae at muscle 6/7 NMJs. SYT7^{RFP} staining is abundant in the presynaptic terminal, with a few postsynaptic membrane compartments also labeled. (D) 3D rendering of the terminal bouton (left) from above. The SYT7^{RFP} intra-terminal compartment is labeled in magenta, with HRP-labeled plasma membrane indicated with a grey mesh. Scale bar = 2 μ m.

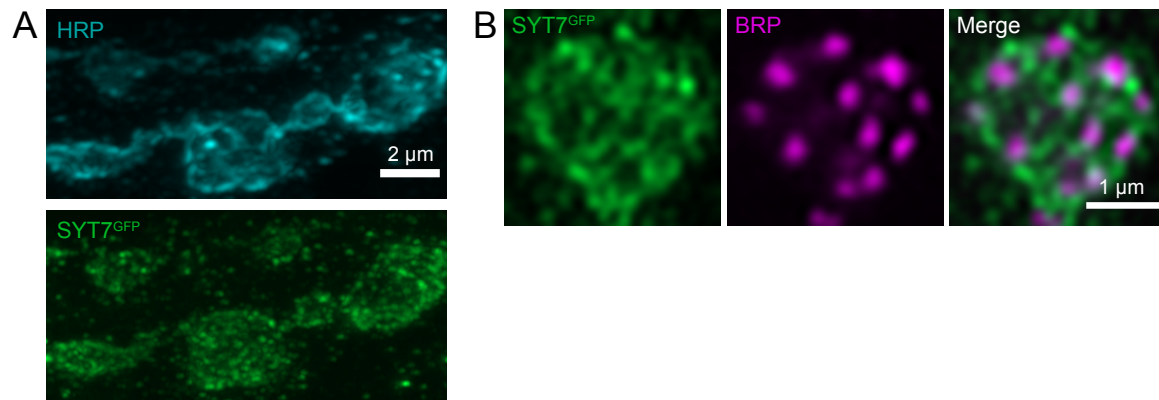


Figure 11 – figure supplement 1. Location of SYT7^{GFP} within synaptic boutons. (A) Immunocytochemistry with anti-HRP (top) and anti-GFP (bottom) in SYT7^{GFP} 3rd instar larvae at muscle 6/7 NMJs. SYT7^{GFP} staining, like SYT7^{RFP}, localizes throughout the presynaptic terminal. Scale bar = 2 μm. (B) Synaptic bouton immunolabeled with anti-BRP and anti-GFP in SYT7^{GFP} larvae. SYT7 surrounds but does not co-localize with BRP-labeled AZs, similar to other previously described peri-AZ proteins. Scale bar = 1 μm.

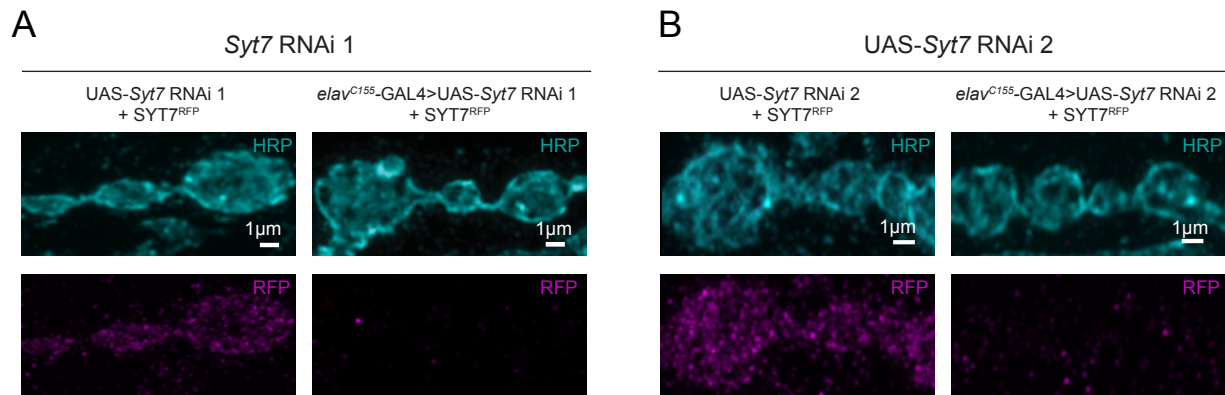


Figure 11 – figure supplement 2. Knockdown of SYT7^{RFP} with *Syt7* RNAi eliminates RFP immunostaining. (A) Immunocytochemistry with anti-HRP (cyan) and anti-RFP (magenta) in SYT7^{RFP} 3rd instar larvae without (left) or with *elav*^{C155}-GAL4, UAS-Dicer2; UAS-*Syt7* RNAi#1. (B) Immunocytochemistry with anti-HRP and anti-RFP in SYT7^{RFP} without (left) or with *elav*^{C155}-GAL4, UAS-Dicer2; UAS-*Syt7* RNAi#2 (right). Neuronal knockdown of SYT7^{RFP} eliminates presynaptic and most postsynaptic SYT7 staining, suggesting a small fraction of SYT7^{RFP} may undergo exosome-mediated transfer, as shown for SYT4. The majority of SYT7 protein resides in the presynaptic terminal. Scale bar = 2 μm.

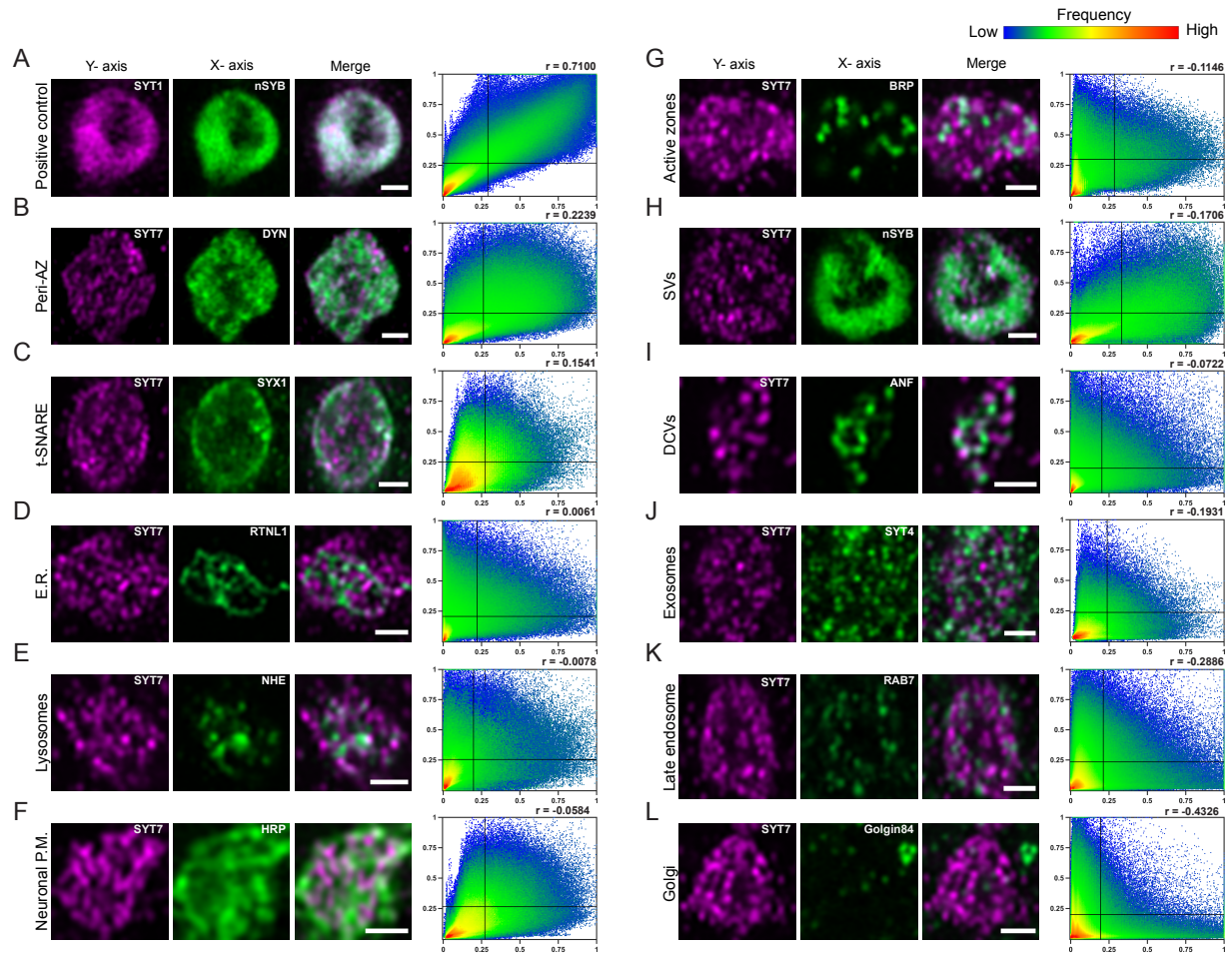


Figure 12. Localization of SYT7 in presynaptic terminals. Immunostaining for the indicated proteins in each panel was performed at 3rd instar larval muscle 6/7 NMJs. Staining for all panels except A were done in the SYT7^{RFP} endogenously tagged background using anti-RFP to label the SYT7 compartment, with the merged image shown on the right. The Pearson correlation coefficient (r) calculated from the cytofluorogram co-localization plots is shown on the upper right. All images are from single confocal planes. **(A)** Co-localization of the SV proteins SYT1 (left, magenta, anti-SYT1 antisera) and nSYB (middle, green, endogenous nSYB^{GFP}) as a positive control. The remaining panels show boutons co-stained for SYT7^{RFP} (left, magenta, anti-RFP antisera) and the indicated compartment marker (middle, green): **(B)** Dynamin (anti-DYN antisera); **(C)** SYX1 (anti-SYX1 antisera); **(D)** Reticulin like-1 (*elav^{C155}-GAL4; UAS-RTNL1-GFP*); **(E)** lysosomal Na⁺/H⁺ exchanger 1 (*elav^{C155}-GAL4; UAS-NHE-GFP*); **(F)** HRP (anti-HRP antisera); **(G)** BRP (anti-BRP Nc82 antisera); **(H)** nSYB (nSYB^{GFP}); **(I)** Atrial natriuretic peptide (*elav^{C155}-GAL4; UAS-ANF-GFP*); **(J)** SYT4 (endogenously tagged SYT4^{GFP-2M}); **(K)** RAB7 (anti-RAB7 antisera); and **(L)** Golgin84 (anti-GOLGIN84 antisera). Co-localization plots were generated with normalized pixel intensity of stacked images of 10-24 type Ib boutons from 3 animals per genotype, with the color representing the frequency of data points as shown in the right scale bar. The vertical line on the X-axis indicates the threshold used to identify pixels above background for the compartment stain. The horizontal line on the Y-axis represents the threshold used to identify pixels above background for SYT7. Scale bar = 1 μ m.

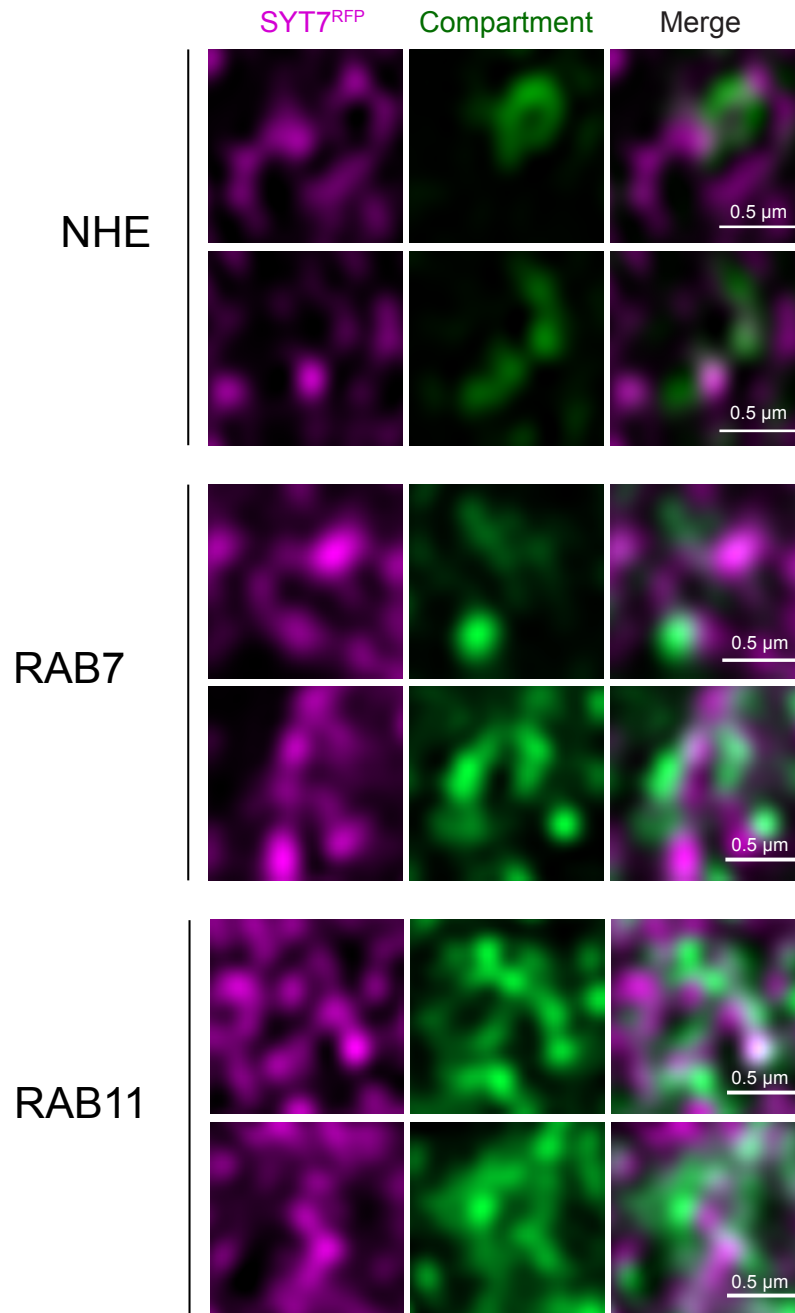


Figure 12 – figure supplement 1. SYT7 tubules reside in proximity to multiple presynaptic compartments. Immunostaining for endogenously-tagged SYT7^{RFP} (label) and a lysosomal marker (NHE), a late endosomal marker (RAB7) and a peri-AZ endosomal protein (RAB11). The merged image is shown on the right. Scale bar = 0.5 μ m.

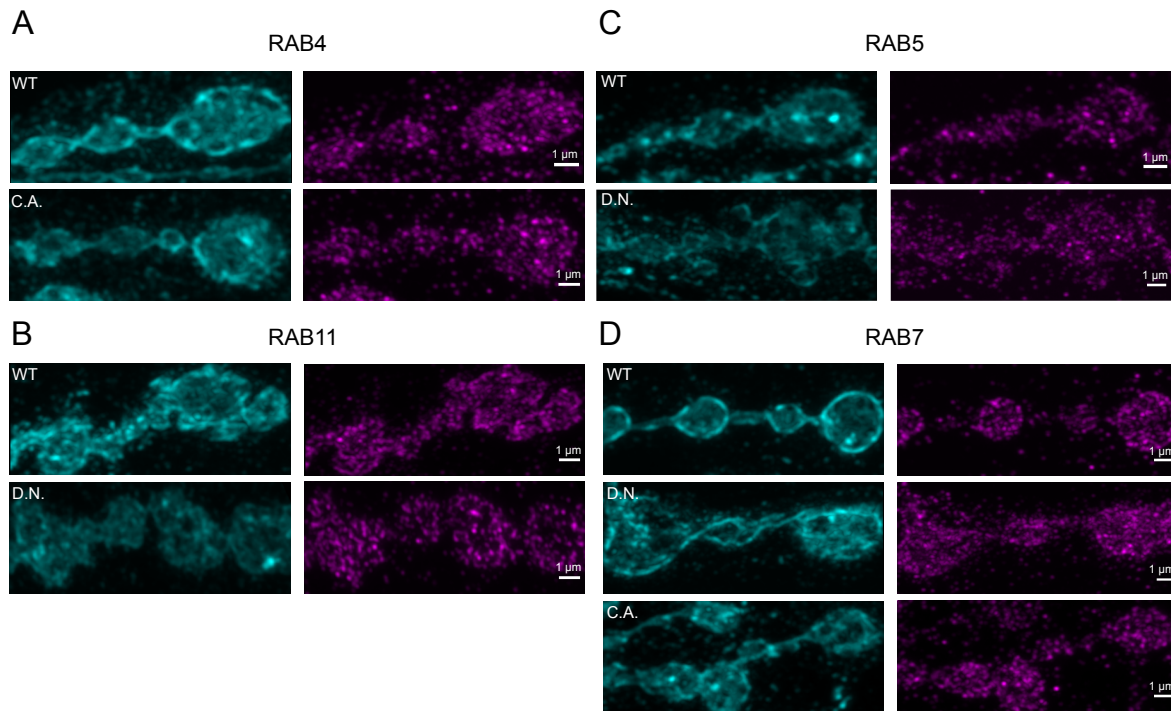


Figure 12 – figure supplement 2. SYT7 localization is not altered by specific RAB protein manipulations. Dominant-negative (D.N), constitutively-active (C.A.) or wildtype (WT) RAB4, RAB5, RAB7 and RAB11 were expressed from UAS constructs with *elav^{C155}*-GAL4 in the SYT7^{RFP} background. Immunostaining with anti-HRP and anti-RFP to label the SYT7 compartment is shown for each manipulation. Several manipulations resulted in extremely reduced larval viability and could not be analyzed. Scale bar = 1 μ m.

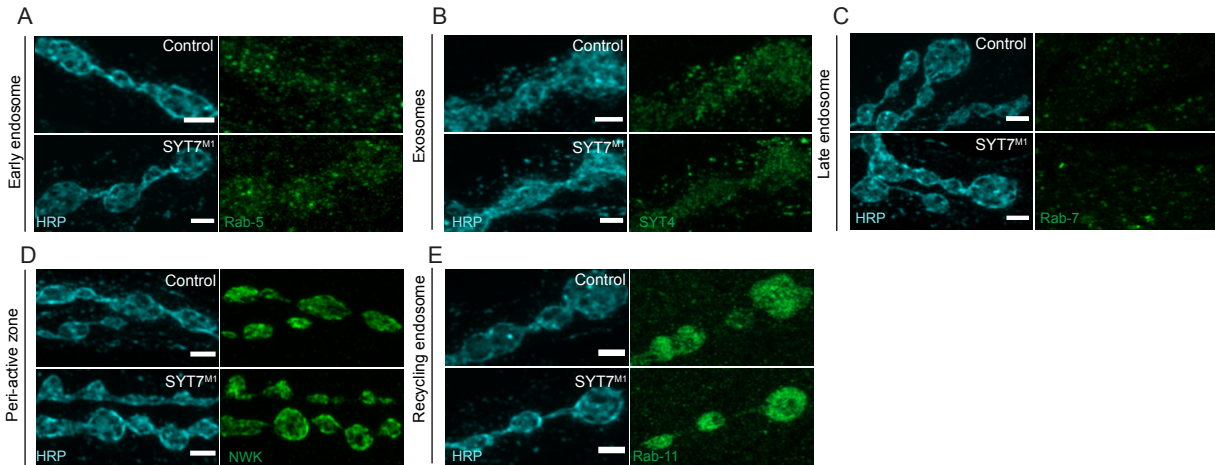


Figure 12 – figure supplement 3. Localization of compartment-specific markers in *Syt7* mutants. Immunocytochemistry with anti-HRP (cyan) and anti-GFP (green) in control and *Syt7^{M1}* 3rd instar larvae to label: **(A)** endogenously-tagged RAB5; **(B)** endogenously-tagged SYT4 (*SYT4^{GFP-2M}*); **(C)** RAB7 (anti-RAB7 antisera); **(D)** NWK (anti-NWK antisera); and **(E)** endogenously tagged RAB11. No changes were observed in *Syt7^{M1}* mutants. Scale bar = 1 μm.

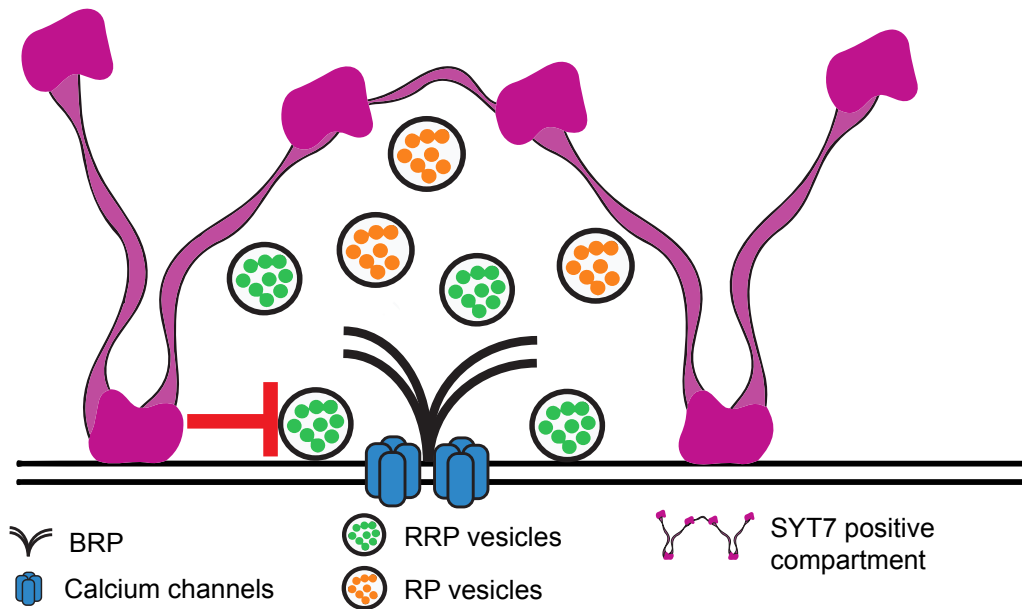


Figure 12 – figure supplement 4. Model for SYT7 localization and function. SYT7 functions to decrease the fusogenicity of SVs in the RRP and slow refilling of the RRP following stimulation. SYT7 localizes to internal tubular membranes within the peri-AZ network. This location places SYT7 at a key node to modulate SV re-entry into the RRP in a Ca^{2+} -dependent manner by interfacing with other membrane compartments and the SV sorting machinery at peri-AZs.

Chapter 3: Characterization of the differential SYT7 expression in tonic versus phasic neurons and the trafficking properties of mutant C2 domain SYT7 proteins.

Mónica C. Quiñones-Frías, Yulia Akvergenova and J. Troy Littleton

The Picower Institute for Learning and Memory, Department of Biology, Massachusetts
Institute of Technology, Cambridge, MA 02139

The majority of the work was performed by Mónica C. Quiñones-Frías. Release probability mapping was performed by Yulia Akvergenova. This work is unpublished.

Introduction

Neurons rely on the regulated secretion of neurotransmitter-filled synaptic vesicles (SVs) to transfer information at specialized junctions called synapses through a process known as neurotransmission (Südhof and Rizo, 2011). Neurons control the amount of SV fusion by modulating synaptic strength through a phenomenon known as synaptic plasticity. Neurons can rapidly enhance or decrease synaptic strength through the short-term plasticity mechanisms of facilitation or depression, respectively. Intrinsic properties that set active zone release probability (P_r) in each neuron help determine if a synapse will exhibit facilitation or depression (Regehr, 2012; Zucker and Regehr, 2002). In other words, the proteins expressed at each synapse help define the electrophysiological properties observed in that neuron to regulate SV fusion during nerve stimulation. Strong active zones with high P_r are associated with depression, while weaker low P_r sites generally undergo facilitation.

Muscle contraction at the larval *Drosophila* neuromuscular junction (NMJ) is regulated by two glutamatergic motor neurons called Ib and Is that innervate each muscle (Kurdyak et al., 1994). During a stimulation train, these two neurons exhibit distinct electrophysiological properties. Ib neurons are similar to other tonic neurons and tend to facilitate, while Is neurons are more phasic in nature and depress (Kurdyak et al., 1994; Newman et al., 2017). The two motoneuron subclasses also differ in their axon terminal size, active zone density, postsynaptic density and SV size (Kittel and Heckmann, 2016; Menon et al., 2013; Newman et al., 2017). The highly stereotyped nature of the *Drosophila* NMJ provides an ideal model to identify proteomic differences that contribute to the unique morphological and electrophysiological properties observed in Ib and Is neurons.

Here we characterize the role of the Synaptotagmin family member, SYT7, and its role in regulating neurotransmission in Is and Ib terminals at *Drosophila* NMJs. SYTs are a family of membrane trafficking proteins that contain a transmembrane domain, a short variable linker and 2 C2 domains, termed C2A and C2B (Perin et al., 1991). C2 domains contain loops with negatively charged residues that bind to calcium. Upon calcium binding, these loops penetrate membranes to promote exocytosis of SVs (Bai et al., 2004; Chapman, 2008; Chapman and Davis, 1998; Chapman and Jahn, 1994; Davletov and Südhof, 1993; Fernandez et al., 2001; Li et al., 1995; Ubach et al., 1998; Wang et al., 2016; Zhang et al., 1998). SYT7 has been found to regulate the asynchronous phase of neurotransmitter release during an evoked response (Bacaj et al., 2013; Chen et al., 2017; Luo et al., 2015; Luo and Südhof, 2017; Wen et al., 2010). SYT7 is also known to regulate facilitation and vesicle replenishment (Chen et al., 2017; Jackman et al., 2016; Liu et al., 2014; Luo and Südhof, 2017).

As described in Chapter 2, we discovered that SYT7 controls these forms of short-term plasticity by setting active zone P_r . Loss of SYT7 leads to enhanced release and reduced facilitation, while overexpression of SYT7 reduces initial P_r and enhances facilitation. Given the dose-dependent control of P_r by the synaptic levels of SYT7, the protein represents an attractive target for controlling short-term plasticity across different neuronal classes. Heterogeneity of SYT7 function across neurons could arise from local posttranslational modification of SYT7 at synapses or differential expression of SYT7 globally across neuronal subclasses. In particular, reduced levels of SYT7 is likely to give synapses with more phasic properties (higher initial P_r active zones that depress), while normal levels or overexpression of SYT7 would favor tonic release properties (lower initial P_r sites that facilitate).

In this chapter, I describe preliminary data that suggest SYT7 levels indeed contribute to the distinct synaptic properties of tonic and phasic motoneurons in *Drosophila*. In particular, we found that SYT7 is expressed at 40% lower levels in Is terminals compared to Ib terminals at *Drosophila* NMJs. This difference in expression of SYT7 between Ib and Is terminals could differentially regulate release probability at each synapse given our observation that SYT7 controls neurotransmission in a dose-dependent manner. We indirectly measured exocytosis by quantifying the levels of FM1-43 uptake during stimulation to measure SV cycling in Is and Ib synapses. Is terminals have higher vesicle recycling than Ib terminals in control. In contrast, SV recycling was increased only in Ib terminals of *Syt7* mutants (*Syt7^{M1}*) while it remained unchanged at Is terminals. These findings suggest SYT7 can differentially regulate SV fusion at Ib and Is terminals. To extend our studies of SYT7, we also began a series of structure-function studies to test the role of calcium binding residues in each C2 domain. We found that disruption of C2 domain calcium binding can lead to abnormal trafficking and stability of SYT7.

Results

SYT7 is differentially expressed at Ib and Is nerve terminals

Previously we found that SYT7 regulates neurotransmission in a dose-dependent manner at the *Drosophila* NMJ. The absence of SYT7 leads to an increase in neurotransmitter release, while overexpression suppresses release. Since Is and Ib terminals exhibit different synaptic release properties, we wondered if SYT7 was differentially expressed across these two neuronal subclasses and contributed to their distinct release probabilities. To test this, we measured the endogenous levels of SYT7 at Is and Ib terminals in muscle 4. At muscle 4, Is and Ib terminals are spatially separated on the muscle, allowing for unequivocal quantification of SYT7 levels at synapses of each neuronal subtype (**Figure 1A**). Neuronal membranes were labeled with HRP and an endogenous SYT7^{RFP} CRISPR-tagged line was used to report the protein levels of SYT7 in Ib and Is terminals. Fluorescence intensity was normalized to neuronal volume because Is and Ib neurons differ in size. We found that Is terminals express 40% less SYT7 compared to Ib terminals (**Figure 1B**). We did not observe differences in the expression of the synaptic vesicle protein, synaptobrevin (nSYB), between Is and Ib terminals (**Figure 1C**). These findings suggest release probability in Is and Ib neurons could be defined by the levels of SYT7 at nerve terminals.

FM1-43 uptake experiments indicate only Ib terminals are affected in *Syt7* mutants (*Syt7^{M1}*)

Differential expression of SYT7 in Ib and Is terminals could set the release probability observed at each neuron. If so, we would predict that loss of SYT7 might differently affect synaptic properties of each neuron. To test the effects of SYT7 loss in Is and Ib motoneurons, FM1-43 dye uptake experiments were used to measure SV recycling in *Syt7^{M1}* mutants. FM1-43 is a lipophilic

dye that binds to membranes and is endocytosed during nerve stimulation. FM1-43 uptake is measured after stimulation, providing an indirect measure of exocytosis that can be mapped specifically to Ib versus Is synapses. FM1-43 dye was incubated while nerve terminals were stimulated at 0.5 Hz for 5 min (**Figure 2A**). In control, Ib terminals uptake significantly less FM1-43 than Is (**Figure 2B**, $p=0.0012$; Ib control: 9012 ± 287.5 , $n=6$ AZs from larvae; Is control: 12531 ± 531.7 , $n=12$ AZs from 6 larvae), consistent with the well-known differences in these motoneuron types (stronger synapses in the phasic Is neuron). In contrast, no significant difference was observed in the uptake of FM1-43 at Ib and Is terminals in *Syt7^{M1}* (**Figure 2B**, $p=0.7348$; Ib *Syt7^{M1}*: 12531 ± 531.7 , $n=10$ AZs from 6 larvae; Is *Syt7^{M1}*: 13922 ± 1388 , $n=10$ AZs from 6 larvae). Compared to control, FM1-43 uptake was only significantly increased in Ib terminals of *Syt7^{M1}* (**Figure 2B**, $p=0.0043$; control: 9012 ± 287.5 , $n=12$ AZs from 6 larvae; *Syt7^{M1}*: 12531 ± 531.7 , $n=12$ AZs from 6 larvae), as uptake remained unchanged in Is NMJs (**Figure 2B**, $p=0.9754$; control: 14511 ± 1410 , $n=10$ AZs from 6 larvae; *Syt7^{M1}*: 13922 ± 1388 , $n=10$ AZs from 6 larvae). These results indicate Ib tonic synapses have increased exocytosis in *Syt7* mutants, while Is terminals are unaffected by the loss of SYT7. We conclude that differential expression of SYT7, where it is much higher in Ib motoneurons, contributes to the lower release probability observed in Ib terminals.

Calcium binding loops of SYT7 have a redundant role in SYT7 trafficking to nerve terminals

To further understand how SYT7 regulates neurotransmission, mutant isoforms of SYT7 were generated to perform structure-function studies, similar to previous work carried out in the lab on SYT1 (Guan et al., 2017; Lee and Littleton, 2015). To test the role of calcium binding to each C2 domain in SYT7, aspartic and glutamic residues in the calcium binding loops were

neutralized by mutating them to asparagine and glutamine, respectively (**Figure 3**). I generated UAS lines with neutralizing mutations in C2A (C2A*), in C2B (C2B*), or in both C2 domains (C2A*C2B*). All UAS lines were inserted in the same attP chromosomal insertion docking site to ensure equal mRNA expression of all constructs. The transgenes were also tagged with a C-terminal Myc to allow visualization of the proteins by immunocytochemistry and western blotting.

Mutant SYT7 proteins under UAS control were expressed with the neuronal driver *elav-GAL4* to compare expression to the wildtype protein at nerve terminals and in the ventral nerve cord (VNC). Neuronal overexpression of SYT7 C2A* or C2B* mutant proteins revealed the proteins localized to the VNC and NMJ (**Figure 4A-B**). SYT7 C2A* expression level was reduced compared to controls, but additional quantification will be required to define the extent to which mutating the C2A calcium binding sites disrupt SYT7 stability and/or localization. Although SYT7 C2B* mutant proteins trafficked to synapses, we observed the formation of aggregates that were not found following expression of control or C2A* SYT7. In contrast to mutations in only one of the C2 domains, SYT7 C2A*C2B* double mutant proteins failed to traffic to nerve terminals and were only observed in neuronal cell bodies (**Figure 4B**). These data indicate mutation of calcium binding loops in both the C2A and C2B domain alter the ability of SYT7 to fold and/or traffic to nerve terminals. Mutation of only one of the C2 domains in SYT7 is better tolerated, and the protein localizes to synapses. However, these mutant proteins also reduce expression (C2A*) or are aggregation prone (C2B*), restricting a detailed structure-function study with these versions. In the future, mutating only 1 or 2 of the calcium-binding aspartate residues, as was done for SYT1 studies, will need to be performed to generate more subtle disruptions that may have less deleterious effects on protein stability.

To determine if SYT7 function requires tethering to a membrane compartment through its transmembrane domain, I generated UAS lines containing only the cytosolic portion of SYT7 (Δ TD SYT7). I also replaced the transmembrane domain of SYT7 with a myristoylation domain, hoping to tether SYT7 to the plasma membrane (Myr-SYT7) through this lipid anchor. Similar approaches were done for SYT1 and these mutant SYT1 proteins trafficked to nerve terminals (Lee and Littleton, 2015). In contrast, I observed no expression of cytosolic or myristoylated SYT7 at NMJs or within the ventral nerve cord following pan-neuronal overexpression of these lines. These results suggest these mutant versions of SYT7 are likely to be degraded. Western analysis of head extracts confirm that Myr-SYT7 is degraded in contrast to the SYT7C2A*, C2B* and C2A*C2B* versions (**Figure 5**).

I also generated an UAS line containing human SYT7 (H. SYT7) to test for rescue of *Drosophila Syt7* mutants and potential conservation of SYT7 function from *Drosophila* to humans. Pan-neuronal expression of H. SYT7 localized to terminals in muscles 6-7, but very low expression was observed at muscle 4, in contrast to D. SYT7 (**Figure 4C**). The transport of H. SYT7 did not mimic that of D. SYT7, preventing an analysis of potentially shared functional synaptic properties.

Discussion

Here we characterized the differential expression of SYT7 in Ib and Is neurons and the trafficking properties of mutant C2 domain SYT7 proteins at *Drosophila* NMJs. Our findings suggest that differential expression of SYT7 in Is and Ib terminals may control release probability differences between these neurons. We also found that calcium binding residues in C2 domains appear redundant for trafficking SYT7 to nerve terminals, but are also required for normal stability of the protein.

Differential expression of SYT7 may regulate release probability at Is and Ib terminals

We previously observed that SYT7 negatively regulates neurotransmitter release in a dose-dependent manner. We found that Ib terminals express 40% more SYT7 than Is terminals. Since Ib has a lower release probability compared to Is, we hypothesized that release probability of Ib would increase more than Is in *Syt7* mutants (**Figure 6**). Indeed, we found that SYT7 suppresses vesicle cycling to a greater extent in Ib synapses compared to Is. This is parallel to an observed increase in release probability at active zones in *Syt7^{MI}* Ib terminals (**Figure 6**). Interestingly, the release probability observed in *Syt7^{MI}* Ib terminals increases to match the release probability observed at control Is terminals. We hypothesize that release probability at active zones in *Syt7^{MI}* Is terminals is likely to remain unchanged or only mildly increase because we did not observe a significant change in FM1-43 cycling at Is terminals of *Syt7* mutants. If so, this finding would suggest that release probability in Is neurons is unlikely to be affected to the same degree as Ib terminals following loss of SYT7, given its lower expression at Is synapses in control. To further test if SYT7 regulates release probability at Is synapse, it will be interesting to overexpress the protein only at Is terminals. We would predict this experimental manipulation should have a very

strong effect and decrease release probability and vesicle cycling when it is upregulated in Is neurons. Differential expression of SYT7 at terminals in Ib and Is might be set transcriptionally or post-translationally. If *Syt7* transcripts are equal in Is and Ib, SYT7 could become “diluted” in Is terminals given Is targets multiple muscles while Ib only targets a single muscle (Hoang and Chiba, 2001). This could be tested by measuring the levels of SYT7 at Is terminals in *Syt7*^{M1} heterozygotes and SYT7 overexpression. SYT7 protein levels may also be actively regulated post-translationally within specific neuronal subclasses, leading to differences in protein turnover and activity at terminals. Others have shown that mammalian SYT7 levels are post-transcriptionally modulated by γ -secretase proteolytic activity and APP, linking it to SV trafficking defects in Alzheimer’s disease (Barthet et al., 2018).

Mutations in calcium binding loops of SYT7’s C2 domains have a redundant role in trafficking it to nerve terminals

We attempted to perform a structure function analysis of SYT7 as previously done for SYT1 (Lee and Littleton, 2015). Neutralizing mutations in both C2 domains of SYT1 did not alter the localization of SYT1. In contrast, neutralizing mutations in both C2 domains of SYT7 abolished trafficking to nerve terminals. Interestingly, neutralizing mutations in only one C2 domain allowed some targeting of SYT7 to terminals, suggesting the C2 domains may have a redundant role in trafficking the protein. Mutations in calcium binding residues in each C2 domain of mammalian SYT7 abolishes calcium-dependent oligomerization of the protein (Fukuda et al., 2002; Fukuda and Mikoshiba, 2000). SYT1 oligomers have been shown to be important for calcium regulation of exocytosis. Consequently, disrupting calcium-dependent oligomerization in SYT7 could impair its trafficking to terminals. We hypothesized that rescue experiments with

mutant C2A* SYT7 in the *Syt7^{M1}* background would not rescue the SYT7 phenotype, as the C2A domain has been suggested to play a major role in exocytosis in the rodent SYT7 protein, in contrast to C2B (Bacaj et al., 2013; Jackman et al., 2016; Voleti et al., 2017). The aggregates we observe in SYT7 C2B* expressing animals may result in dominant effects on membrane trafficking. SYT7 contacts various trafficking compartments and disruption of such trafficking could lead to aberrant accumulation of the protein. In SYT1, neutralizing mutations in calcium residues in the C2B domain have a dominant negative effect and disrupts neurotransmission even in the presence of wild-type SYT1. It will be interesting to test if dominant negative effects on SV trafficking also occur in mutant SYT7 C2B* animals.

Materials and Methods

Drosophila stocks

Drosophila melanogaster were cultured on standard medium at 22-25°C. Genotypes used in the study include: *elav^{C155}-GAL4* (Bloomington Drosophila Stock Center (BDSC)#8765), SYT7^{RFP} (generation described in Chapter 2) and nSYB^{GFP} (generation described in Chapter 2).

Mutant SYT7 UAS lines

C2 domain mutations were synthesized with Genewiz (South Plainfield, NJ, USA). Site directed mutagenesis was used to delete the transmembrane domain of SYT7 to generate Δ TD SYT7 and Myr-SYT7. All mutant SYT7 isoforms were cloned into pBID (Addgene, #35190) and plasmids were injected into embryos of *y¹w⁶⁷c²³*; P{CaryP}attP2 (BDSC# 8622) by Best Gene Inc (Chino Hills, CA, USA).

FM1-43 uptake and release assays

3rd instar wandering larvae were dissected in Ca²⁺-free HL3.1 and axons were severed from the CNS. Axon bundles were stimulated with a suction electrode in 1.5 mM CaCl₂ HL3.1 solution containing 2 μ M of the lipophilic dye FM 1-43FX (F35355; Thermo Fisher Scientific, Waltham, MA, USA). Dye loading was performed at 0.5 Hz for 5 minutes (150 events). After stimulation, samples were washed for 2 min in Ca²⁺ free HL3.1 containing 100 μ M Advacep-7 (Sigma; A3723) to help remove non-internalized FM 1-43 dye. Image stacks from muscle 6/7 at segment A3 were obtained using a spinning disk confocal with a 63X water immersion objective. Mean FM1-43

intensity at the NMJ was quantified using the Volocity 3D Image Analysis software (Quorum Technologies Inc., Puslinch, Ontario, CAN).

Western analysis and immunocytochemistry

Western blotting of adult head lysates (1 head/lane) was performed using standard laboratory procedures with rabbit anti-Myc (GTX103436; GeneTex) at 1:3000. Visualization and quantification were performed with a LI-COR Odyssey Imaging System (LI-COR Biosciences, Lincoln, MA, USA). Secondary antibodies for Westerns included Alexa Fluor 680-conjugated goat anti-rabbit IgG (1:5000, Invitrogen; A21109).

Immunostaining was performed on wandering stage 3rd instar larvae dissected in Ca^{2+} -free HL3.1 and fixed for 17 min in Ca^{2+} -free HL3.1 containing 4% PFA. Fixed larvae were blocked and permeabilized overnight in PBS containing 0.25% Saponin, 2.5% normal goat serum (NGS), 2.5% bovine serum albumin (BSA) and 0.1% sodium azide. Fixed larvae were incubated with primary antibody at 4°C for 24 hrs and with secondary antibodies for 1.5 hrs at room temperature. Fixed larvae were mounted in ProLong® Diamond Antifade Mountant (#P36970; Thermo Fisher Scientific, Waltham, MA, USA). Antibodies used for immunolabeling were: mouse anti-Myc (9E10; DSHB), rabbit anti-GFP at 1:1000 (#G10362; Thermo Fisher Scientific, Waltham, MA, USA), and DyLight 649 conjugated anti-HRP at 1:1000 (#123-605-021; Jackson Immuno Research, West Grove, PA, USA). Secondary antibodies used for AZ and bouton counting were used at 1:1000: goat anti-rabbit Alexa Fluor Plus 555 (A32732; ThermoFisher) and goat anti-rabbit Alexa Fluor Plus 488 (A32731; ThermoFisher). Immunoreactive proteins were imaged on a ZEISS LSM 800 microscope with Airyscan using a 63X oil immersion objective.

Statistical analysis

Statistical analysis and graphing were performed with either Origin Software (OriginLab Corporation, Northampton, MA, USA) or GraphPad Prism (San Diego, CA, USA). Statistical significance was determined using specific tests as indicated in the text. Appropriate sample size was determined using GraphPad Statmate. Asterisks denote p-values of: *, $P \leq 0.05$; **, $P \leq 0.01$; and ***, $P \leq 0.001$. All measurements are shown as mean \pm SEM.

Optical quantal imaging and P_r mapping

P_r mapping was performed on a Zeiss Axio Imager 2 equipped with a spinning-disk confocal head (CSU-X1; Yokagawa, JAPAN) and ImagEM X2 EM-CCD camera (Hamamatsu, Hamamatsu City JAPAN) as previously described (Akbergenova et al., 2018). Myristoylated-GCaMP6s was expressed with 44H10-LexAp65 (provided by Gerald Rubin). Postsynaptic densities were visualized by expression of GluRIIA-RFP under its endogenous promoter (provided by Stephan Sigrist). An Olympus LUMFL N 60X objective with a 1.10 NA was used to acquire GCaMP6s imaging data at 8 Hz. 3rd instar larvae were dissected in Ca²⁺-free HL3 containing 20 mM MgCl₂. After dissection, preparations were maintained in HL3 with 20 mM MgCl₂ and 1.0 mM Ca²⁺ for 5 minutes. Motor nerves were stimulated every three seconds for GCaMP6s mapping. The time and location of Ca²⁺ events were imported into Excel or Matlab for further analysis. The number of observed GCaMP events per AZ was divided by the number of stimuli to calculate AZ P_r .

References

1. Bacaj T, Wu D, Yang X, Morishita W, Zhou P, Xu W, Malenka RC, Südhof TC. 2013. Synaptotagmin-1 and synaptotagmin-7 trigger synchronous and asynchronous phases of neurotransmitter release. *Neuron* 80:947–59. doi:10.1016/j.neuron.2013.10.026
2. Bai J, Tucker WC, Chapman ER. 2004. PIP 2 increases the speed of response of synaptotagmin and steers its membrane-penetration activity toward the plasma membrane. *Nat Struct Mol Biol* 11:36–44. doi:10.1038/nsmb709
3. Barthet G, Jordà-Siquier T, Rumi-Masante J, Bernadou F, Müller U, Mülle C. 2018. Presenilin-mediated cleavage of APP regulates synaptotagmin-7 and presynaptic plasticity. *Nat Commun* 9:4780. doi:10.1038/s41467-018-06813-x
4. Chapman ER. 2008. How Does Synaptotagmin Trigger Neurotransmitter Release? *Annu Rev Biochem* 77:615–641. doi:10.1146/annurev.biochem.77.062005.101135
5. Chapman ER, Davis AF. 1998. Direct interaction of a Ca²⁺-binding loop of synaptotagmin with lipid bilayers. *J Biol Chem* 273:13995–14001. doi:10.1074/jbc.273.22.13995
6. Chapman ER, Jahn R. 1994. Calcium-dependent interaction of the cytoplasmic region of synaptotagmin with membranes. Autonomous function of a single C2-homologous domain. *J Biol Chem* 269:5735–5741.
7. Chen C, Satterfield R, Young SM, Jonas P. 2017. Triple Function of Synaptotagmin 7 Ensures Efficiency of High-Frequency Transmission at Central GABAergic Synapses. *Cell Rep* 21:2082–2089. doi:10.1016/j.celrep.2017.10.122
8. Davletov BA, Südhof TC. 1993. A single C2 domain from synaptotagmin I is sufficient for high affinity Ca²⁺/phospholipid binding. *J Biol Chem* 268:26386–26390.
9. Fernandez I, Araç D, Ubach J, Gerber SH, Shin OH, Gao Y, Anderson RGW, Südhof TC, Rizo J. 2001. Three-dimensional structure of the synaptotagmin 1 C2B-domain: Synaptotagmin 1 as a phospholipid binding machine. *Neuron* 32:1057–1069. doi:10.1016/S0896-6273(01)00548-7
10. Fukuda M, Katayama E, Mikoshiba K. 2002. The calcium-binding loops of the tandem C2 domains of synaptotagmin VII cooperatively mediate calcium-dependent oligomerization. *J Biol Chem* 277:29315–29320. doi:10.1074/jbc.M201697200
11. Fukuda M, Mikoshiba K. 2000. Calcium-Dependent and -Independent Hetero-Oligomerization in the 645:637–645.
12. Guan Z, Bykhovskaia M, Jorquera RA, Sutton RB, Akbergenova Y, Littleton JT. 2017. A synaptotagmin suppressor screen indicates SNARE binding controls the timing and Ca²⁺ cooperativity of vesicle fusion. *Elife* 6:1–30. doi:10.7554/eLife.28409
13. Hoang B, Chiba A. 2001. Single-cell analysis of Drosophila larval neuromuscular synapses. *Dev Biol* 229:55–70. doi:10.1006/dbio.2000.9983
14. Jackman SL, Turecek J, Belinsky JE, Regehr WG. 2016. The calcium sensor synaptotagmin 7 is required for synaptic facilitation. *Nature* 529:88–91. doi:10.1038/nature16507
15. Kittel RJ, Heckmann M. 2016. Synaptic vesicle proteins and active zone plasticity. *Front Synaptic Neurosci* 8:8. doi:10.3389/fnsyn.2016.00008
16. Kurdyak P, Atwood HL, Stewart BA, Wu C-F. 1994. Differential physiology and morphology of motor axons to ventral longitudinal muscles in larval Drosophila. *J Comp Neurol* 350:463–472. doi:10.1002/cne.903500310
17. Lee J, Littleton JT. 2015. Transmembrane tethering of synaptotagmin to synaptic vesicles

- controls multiple modes of neurotransmitter release. *Proc Natl Acad Sci* 112:201420312. doi:10.1073/pnas.1420312112
18. Li C, Ullrich B, Zhang JZ, Anderson RGW, Brose N, Südhof TC. 1995. Ca²⁺-dependent and -independent activities of neural and non-neural synaptotagmins. *Nature* 375:594–599. doi:10.1038/375594a0
 19. Liu H, Bai H, Hui E, Yang L, Evans CS, Wang Z, Kwon SE, Chapman ER. 2014. Synaptotagmin 7 functions as a Ca²⁺-sensor for synaptic vesicle replenishment. *Elife* 2014:1–18. doi:10.7554/eLife.01524.001
 20. Luo F, Bacaj T, Südhof TC. 2015. Synaptotagmin-7 Is Essential for Ca²⁺-Triggered Delayed Asynchronous Release But Not for Ca²⁺-Dependent Vesicle Priming in Retinal Ribbon Synapses. *J Neurosci* 35:11024–33. doi:10.1523/JNEUROSCI.0759-15.2015
 21. Luo F, Südhof TC. 2017. Synaptotagmin-7-Mediated Asynchronous Release Boosts High-Fidelity Synchronous Transmission at a Central Synapse. *Neuron* 94:826–839.e3. doi:10.1016/j.neuron.2017.04.020
 22. Menon KP, Carrillo RA, Zinn K. 2013. Development and plasticity of the Drosophila larval neuromuscular junction. *Wiley Interdiscip Rev Dev Biol* 2:647–670. doi:10.1002/wdev.108
 23. Newman ZL, Hoagland A, Aghi K, Worden K, Levy SL, Ho Son J, Lee LP, Isacoff EY. 2017. Input-Specific Plasticity and Homeostasis at the Drosophila Larval Neuromuscular Junction. *Neuron* 93:1388–1404.e10. doi:10.1016/j.neuron.2017.02.028
 24. Perin MS, Brose N, Jahn R, Südhof TC. 1991. Domain structure of synaptotagmin (p65). *J Biol Chem* 266:623–629.
 25. Regehr WG. 2012. Short-term presynaptic plasticity. *Cold Spring Harb Perspect Biol* 4:1–19. doi:10.1101/cshperspect.a005702
 26. Südhof TC, Rizo J. 2011. Synaptic vesicle exocytosis. *Cold Spring Harb Perspect Biol* 3. doi:10.1101/cshperspect.a005637
 27. Ubach J, Zhang X, Shao X, Südhof T, Rizo J. 1998. Ca²⁺ binding to synaptotagmin: how many Ca²⁺ ions bind to the tip of a C2 domain? *EMBO J* 17:3921–3930.
 28. Voleti R, Tomchick DR, Südhof TC, Rizo J. 2017. Exceptionally tight membrane-binding may explain the key role of the synaptotagmin-7 C2A domain in asynchronous neurotransmitter release. *Proc Natl Acad Sci U S A* 114:E8518–E8527. doi:10.1073/pnas.1710708114
 29. Wang S, Li Y, Ma C. 2016. Synaptotagmin-1 C2B domain interacts simultaneously with SNAREs and membranes to promote membrane fusion. *Elife* 5:e14211. doi:10.7554/eLife.14211
 30. Wen H, Linhoff MW, McGinley MJ, Li GL, Corson GM, Mandel G, Brehm P. 2010. Distinct roles for two synaptotagmin isoforms in synchronous and asynchronous transmitter release at zebrafish neuromuscular junction. *Proc Natl Acad Sci U S A* 107:13906–13911. doi:10.1073/pnas.1008598107
 31. Zhang X, Rizo J, Südhof TC. 1998. Mechanism of phospholipid binding by the C2A-domain of synaptotagmin I. *Biochemistry* 37:12395–12403. doi:10.1021/bi9807512
 32. Zucker RS, Regehr WG. 2002. Short-Term Synaptic Plasticity. *Annu Rev Physiol* 64:355–405. doi:10.1146/annurev.physiol.64.092501.114547

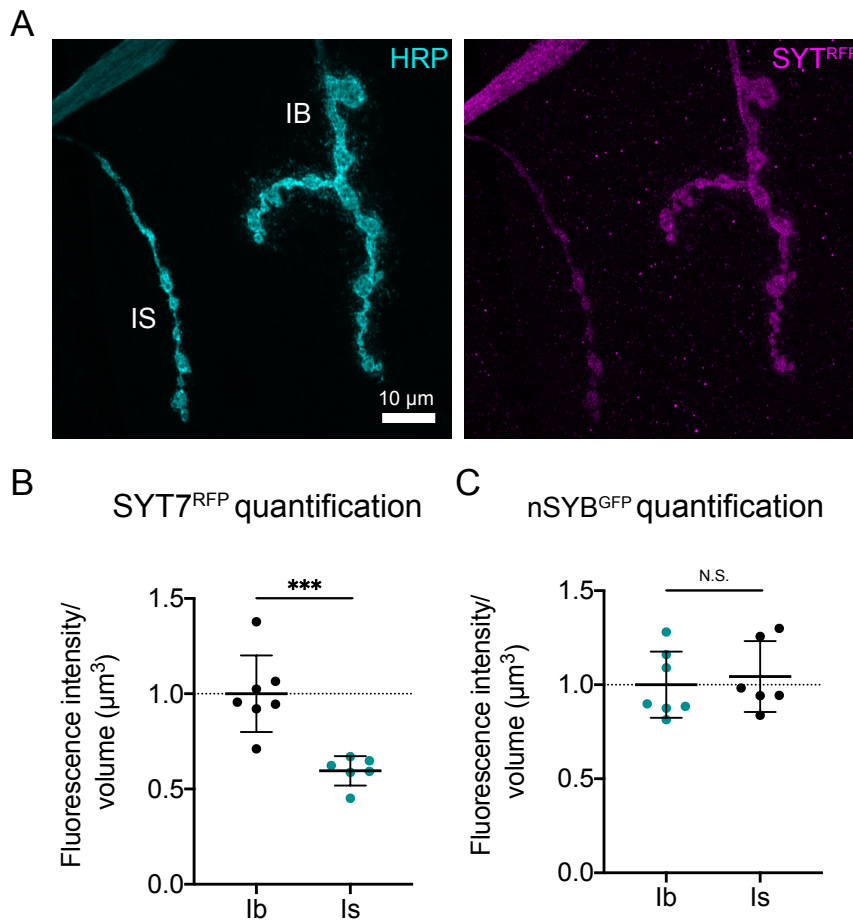


Figure 1. Differential expression of SYT7 in Ib and Is neurons. (A) Neurons in muscle 4 were labeled with HRP (cyan) and RFP (magenta) to label neuronal membranes and SYT7^{RFP}, respectively. Is and Ib terminals are indicated. (B) Quantification of SYT7^{RFP} expression in Ib and Is terminals normalized to the mean of Ib (dashed line). (C) Quantification of nSYB^{GFP} expression in Ib and Is terminals normalized to the mean of Ib (dashed line). Scale bar = 10μm.

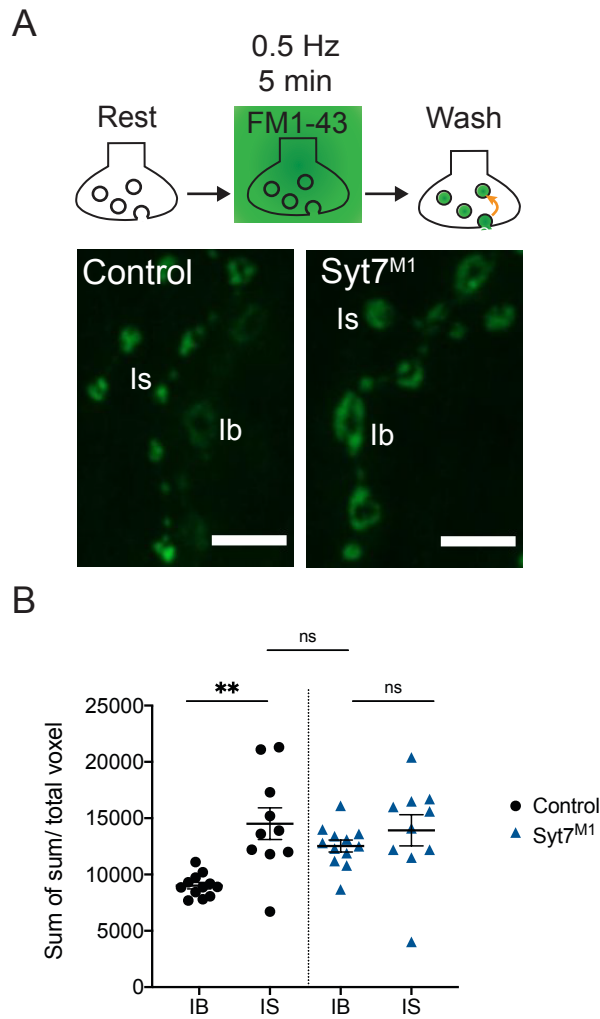


Figure 2. FM1-43 uptake is increased at Ib terminals of *Syt7* mutants. (A) (Top) FM1-43 was incubated in HL3.1 during nerve stimulation at 0.5 Hz for 5 min. Samples were washed and then imaged. (Bottom) Representative images of loaded terminals with FM1-43 in control and *Syt7* mutants with Is and Ib neurons labeled. (B) Quantification of FM1-43 loaded in control (black) and *Syt7* mutants (blue). Scale bar = 5 μ m.

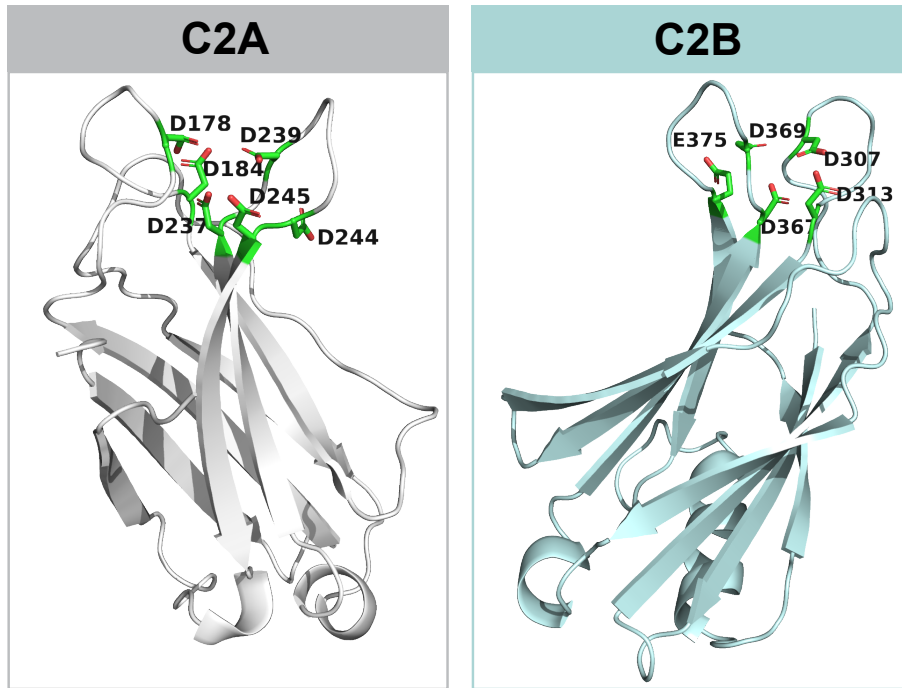


Figure 3. Calcium binding residues in C2A and C2B of Drosophila SYT7. This is a homology model of Drosophila SYT7 generated from a published structure of mammalian SYT7 (Voleti et al., 2017). Negative residues in C2A and C2B that bind calcium are highlighted. These residues were mutated to generate C2A*, C2B* and C2A*C2B*.

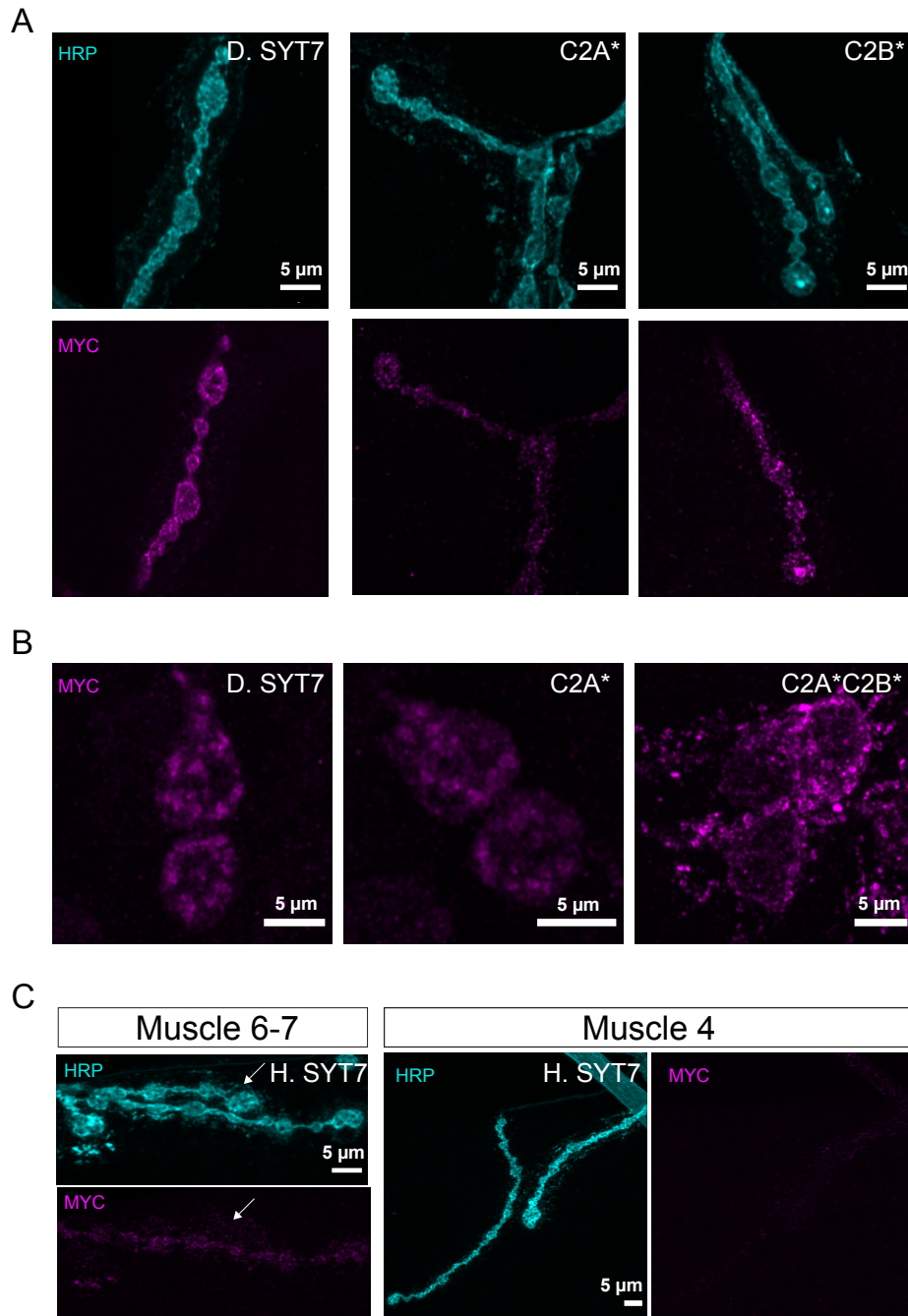


Figure 4. Trafficking is altered in mutant isoforms of SYT7 . (A) Immunocytochemistry of *Drosophila* 3rd instar larva muscle 6-7 with HRP (cyan) and MYC (magenta) following neuronal overexpression of *Drosophila* wildtype SYT7 (left), C2A* SYT7 (middle) and C2B* SYT7 (right). (B) Immunocytochemistry of neuronal cell bodies in 3rd instar larval ventral nerve cords with MYC (magenta) following neuronal overexpressing of SYT7 (left), C2A* (middle) and C2B* (left). (C) Immunocytochemistry of 3rd instar larval muscle 6-7 (left) and muscle 4 (right) with HRP (cyan) and MYC (magenta) after neuronal overexpression of H. SYT7. Arrow highlights the absence of SYT7. Scale bar = 5 μ m.

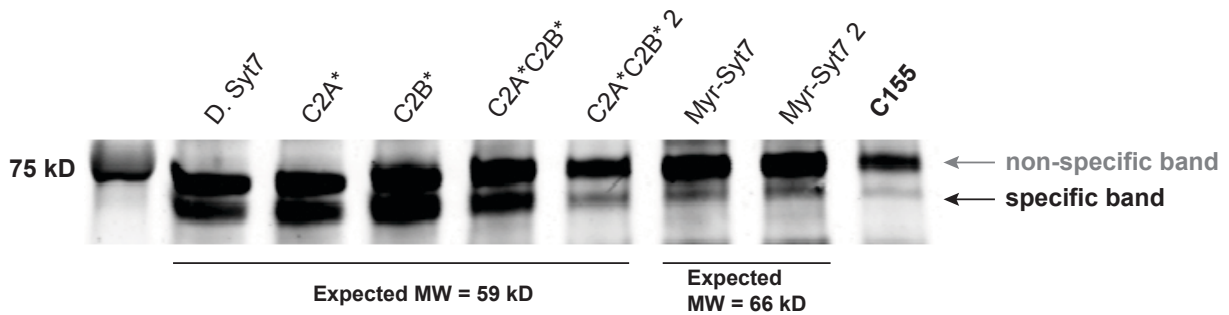


Figure 5. Removal of the transmembrane domain lead to degradation of SYT7. Western blot of head extracts with anti-Myc from neuronal overexpression of SYT7 isoforms: lane 1: *elav-Gal4*, UAS-D. Syt7 Myc; lane 2: *elav-Gal4*, UAS-C2A* Syt7 Myc; lane 3: *elav-Gal4*, UAS-C2B* Syt7 Myc; lane 4: *elav-Gal4*, UAS-C2A*C2B* Syt7 Myc; lane 5: *elav-Gal4*, UAS-C2A*C2B* Syt7 Myc #2; lane 6: *elav-Gal4*, UAS-Myr-Syt7 Myc; lane 7: *elav-Gal4*, UAS-Myr-Syt7 #2; lane 8: *elav-Gal4* (negative control). The expected molecular weight (MW) for D. SYT7, C2A*, C2B*, C2A*C2B* and C2A*C2B* 2 is 59 kD. The expected molecular weight (MW) for Myr-SYT7 and Myr-SYT7 2 is 66 kD. Two non-specific band were observed in the negative control but expression of D. SYT7, C2A*, C2B* and C2A*C2B* intensified this band suggesting expression of these constructs.

Chapter 4: Conclusions and Future Directions

Mónica C. Quiñones-Frías

Main Conclusions

In Chapter 2, I describe our characterization of the role of Synaptotagmin 7 (SYT7) in neurotransmission at the *Drosophila* neuromuscular junction (NMJ). I generated *Syt7* mutants and endogenously tagged versions using the CRISPR-Cas9 system to examine the role of SYT7 in neurotransmission and its localization at synapses. Our findings suggest *Syt7* mutants have increased release probability, a larger readily releasable SV pool and faster SV replenishment compared to controls. Compared to control synapses that facilitate at endogenous extracellular calcium levels, *Syt7* mutant terminals display depression. These phenotypes are dose-dependent suggesting that the levels of SYT7 at synapses tightly regulates neurotransmitter release and short-term synaptic plasticity. We propose that the defects in asynchronous release and facilitation, and others observe in *Syt7* mutants, occur as a consequence of increased release probability. In other words, these results do not indicate SYT7 serves as the calcium sensor that mediates facilitation and asynchronous release. Our localization studies also indicate SYT7 is not enriched at active zones as reported in mammals, but instead SYT7 regulates SV fusion from a tubular compartment in the peri-active zone region. Although its unknown at present how SYT7 regulates SV fusion from this compartment, we found that it interfaces with several membrane trafficking compartments that are positioned to control multiple aspects of SV trafficking. Future work is required to identify if there are genetic interactions between membrane trafficking compartments and SYT7 that are essential for regulating SV availability and replenishment. We conclude that SYT7 negatively regulates neurotransmitter release from the peri-active zone and that there other calcium sensors beyond SYT1 and SYT7 also regulate SV fusion at the *Drosophila* NMJ.

In Chapter 3, I described the characterization of differential expression of SYT7 at tonic (Ib) and phasic (Is) neurons and the trafficking properties of mutant C2 domain SYT7 proteins at *Drosophila* NMJs. Our preliminary results suggest that SYT7 levels are higher at Ib tonic synapses, consistent with their lower release probability and facilitation properties. In contrast, SYT7 expression is reduced at Is terminals, which in many ways behave like SYT7 heterozygote mutants that show higher release probability and depress during strong stimulation. We also found that calcium binding residues in SYT7's C2 domains appear redundant for trafficking the protein to nerve terminals, and are also required for normal stability of the protein.

Future Directions

Rescue experiments with C2 domain mutants to test calcium-dependent roles of SYT7 in regulating SV trafficking

C2 domains in SYTs have been shown to differentially regulate SV fusion. C2 domains bind to membranes in a calcium-dependent manner with varying kinetics and have different affinities to calcium (Bhalla et al., 2005; Hui et al., 2005). Structure-function studies of SYT1 and SYT7 have suggested specific roles for each C2 domain in regulating neurotransmission. In SYT1, the C2B domain is essential for regulating synchronous release, while the C2A domain primarily inhibits asynchronous fusion (Desai et al., 2000; Guan et al., 2017; Mackler et al., 2002; Schupp et al., 2016; Yoshihara et al., 2010; Zhou et al., 2015). In contrast, the C2A domain in mammalian SYT7 plays a major role in regulating SV release in facilitation and asynchronous release, while C2B plays a minor role (Bacaj et al., 2013; Jackman et al., 2016). The contribution of each C2 domain in SYT7 in regulating SV replenishment remains unknown (Liu et al., 2014).

To test the role of each C2 domain in SYT7 at the *Drosophila* NMJ, electrophysiology recordings could be performed in *Syt7* mutants overexpressing C2 domain mutant isoforms such as those described in Chapter 3. If *Drosophila* SYT7 behaves in a similar manner to mammalian SYT7, rescue experiments with neuronal over-expression of a calcium insensitive C2A domain SYT7 should fail to rescue the *Syt7* mutant phenotype. Other studies have not reported that the C2B domain of SYT7 is essential to regulate SV fusion, but biochemical studies show that its essential for calcium-dependent oligomerization of SYT7 (Fukuda et al., 2002; Fukuda and Mikoshiba, 2000). In *Drosophila*, we observe that calcium insensitive C2B SYT7 aggregates in nerve terminals. Electrophysiology recordings in *Syt7^{MI}* with neuronal overexpression of calcium insensitive C2B SYT7 may reveal that this isoform has a dominant negative effect in neurotransmission. We also observed that abolishing calcium binding in both C2 domains completely eliminated SYT7 expression at nerve terminals. This mutant isoform contains 11 mutations that could disrupt the stability of the protein. Previous studies have found that single amino acid changes in the loops of SYT1 and SYT7 can abolish calcium binding (Lee and Littleton, 2015). Generation of new UAS lines with less mutations in each C2 domain might allow testing for the role of a completely calcium insensitive SYT7 protein that gets properly trafficked to nerve terminals. All lines generated to study the effects of C2 domains should be inserted in the same attP site in the genome to assure expression levels are equal, given the extreme dose-dependent effects we have observed with reduced or increased SYT7 levels.

Molecular mechanism of SYT7 mediated SV replenishment

In Chapter 2, we observed that the levels of SYT7 in neurons is crucial to regulate spontaneous and evoked SV fusion. If SYT7 levels are high, neurotransmitter release is

suppressed. In contrast, if SYT7 levels are low, neurotransmitter release is enhanced. We also observed a fast recovery after high frequency stimulation in *Syt7* mutants that was suppressed by neuronal overexpression of SYT7. This recovery is independent of endocytosis as we observed that blocking neurotransmitter-refilling of newly endocytosed SVs in *Syt7* mutants with bafilomycin still show increased SV recovery compared to control. SYT7 could regulate SV fusion by physically binding to SVs upon calcium influx. The more SYT7 at nerve terminals, the more SVs it could bind. This might explain the dose-dependent phenotype. SYT7 has been shown to bind to membranes containing phosphatidylcholine and phosphatidylserine that are present at the plasma membrane and synaptic vesicles (Bhalla et al., 2005; Hui et al., 2005; Takamori et al., 2006). SYT7 has a high affinity for calcium and can bind to membranes longer than any other SYT, which would allow it to potentially restrict SVs from entering the readily releasable pool during an evoked response (Bhalla et al., 2005; Hui et al., 2005).

SYT7 might also regulate the replenishment of the readily releasable pool in a manner similar to Synapsin. Synapsin becomes phosphorylated during an action potential to release synaptic vesicles and replenish the recycling and readily-releasable pool (Denker and Rizzoli, 2010; Rizzoli, 2014). If SYT7 is preventing the entry of SVs into the readily releasable pool, a *Synapsin/Syt7* double mutant should block the enhanced replenishment phenotype observed in *Syt7* mutants during a train stimulation. During a train stimulation, SYT7 is activated to prevent the fast depletion of synaptic vesicles liberated by phosphorylated Synapsin. In other words, Synapsin acts as an activator of replenishment and SYT7 as a replenishment blocker to regulate the size of the readily releasable pool during an evoked response.

If SYT7 is acting as a calcium sensor to regulate the replenishment of SVs, SYT7 would become active during nerve stimulation and be inactive at rest. This might explain why we did not observe any defects in the SV density and SV number near active zones in *Syt7* mutants because these experiments were performed at rest. These experiments could be repeated after stimulating nerve terminals of *Syt7* mutants to measure SV density and SV distribution at active zones. We would expect to see a significant decrease in SV density and SV distribution at boutons of *Syt7* mutants compared to control following stimulation. If SYT7 is regulating the replenishment of SVs from the recycling and reserve pool, we should expect depletion of SVs near the plasma membrane in *Syt7* mutants. In contrast, if SYT7 is overexpressed, we would expect to see more SVs near active zones after stimulation because SYT7 prevents the fusion of SVs. We might also uncover defects in membrane trafficking compartments by the appearance of abnormal vesicular compartments in *Syt7* mutants after stimulation. Since SYT7 interfaces with many of these membrane trafficking compartments, such interactions might be essential during activity and not at rest.

Synapse dependent role of SYT7 in regulating release probability at tonic (Ib) and phasic (Is) neurons

In Chapter 3, I describe my observation that SYT7 is differentially expressed between Is and Ib nerve terminals. SYT7 might be differentially expressed because of differences in transcriptional regulation of the *Syt7* gene or protein turnover within each neuron. We can use gene trap lines that carry a GAL4 driver generated by the Gene Disruption Project to measure the expression levels of SYT7 at cell bodies in Is and Ib neurons. There are 2 gene traps in the *Syt7* gene that can be tested to measure the expression levels of SYT7 by indirectly measuring the

expression of UAS-GFP or UAS-RFP. To identify Is and Ib, we have generated neuronal specific drivers that use the LexA-lexAop system to drive expression of lexAop-GFP or lexAop-RFP in Is or Ib neurons, allowing transcriptional evaluation of the levels of *Syt7* through *in situ* hybridization or RNA profiling. If SYT7 levels are comparable between Is and Ib terminals it suggests that the turnover of SYT7 in Is is higher than Ib. To test this hypothesis, we can pulse expression of SYT7 in motor neurons using GAL80^{ts}. At room temperature, GAL80^{ts} suppresses GAL4 and prevents it from binding to the UAS promoter to drive expression of transgenes. Heat shock relieves GAL4 from GAL80^{ts} and can induce the expression of transgenes. This will require optimization using western blot to identify how long it takes to induce expression of SYT7 and a positive control such as GFP. The OK6-GAL4 driver should be used because it drives equal expression between Is and Ib terminals. Once the heat shock protocol is optimized, the expression of SYT7 should be monitored over time to determine the turnover at Is and Ib terminals. If turnover of SYT7 is faster in Is, we should see less expression of SYT7 compared to Ib. If SYT7 levels are never the same between Is and Ib terminals, it suggests that SYT7 is trafficked at lower rates in Is.

Preliminary experiments suggest that different levels of SYT7 might regulate release probability observed at Ib and Is neurons at the *Drosophila* NMJ. In Chapter 3, I describe my assays of exocytosis by indirectly measuring the endocytosis of FM1-43 in Is and Ib terminals. This assay is significantly less sensitive than electrophysiology recordings or optical imaging of SV release at active zones to generate release probability maps. To perform electrophysiology recordings at Is or Ib terminals only, channelrhodopsin could be expressed using single neuronal drivers available in the lab to stimulate one neuron at a time. We hypothesize that both neurons will have increased neurotransmitter release in *Syt7* mutants, but Ib neurons will exhibit a greater

effect compared to Is neurons. In addition, the size of Is active zones and calcium influx should also be quantified to determine if Is terminals in *Syt7* mutants exhibit any changes as observed in Ib terminals.

SYT7 compartment at rest and during stimulation

Studying how SYT7 and other compartments interact *in vivo* might provide insights into how SYT7 regulates SV fusion. The endogenous GFP and RFP tags used in Chapter 2 are too dim to perform *in vivo* experiments. To increase fluorescence intensity of endogenously tagged SYT7, we generated a Split-GFP SYT7 to perform *in vivo* experiments (Appendix 1). There are many RFP tagged lines that could be used to label SVs, active zones, endosomes, lysosomes and many other compartments to study the interaction of these compartments and SYT7 *in vivo*. For example, we could measure if SYT7 and SVs increase their co-localization during stimulation. If they do, it suggests SYT7 might increase its affinity to SVs during activity. Follow-up experiments would require generating mutants that disrupt these interactions and perform electrophysiology recordings to identify how they regulate neurotransmission.

References

1. Bacaj T, Wu D, Yang X, Morishita W, Zhou P, Xu W, Malenka RC, Südhof TC. 2013. Synaptotagmin-1 and synaptotagmin-7 trigger synchronous and asynchronous phases of neurotransmitter release. *Neuron* 80:947–59. doi:10.1016/j.neuron.2013.10.026
2. Bhalla A, Tucker WC, Chapman ER. 2005. Synaptotagmin Isoforms Couple Distinct Ranges of Ca²⁺, Ba²⁺, and Sr²⁺ Concentration to SNARE-mediated Membrane Fusion. *Mol Biol Cell* 16:4755–4764. doi:10.1091/mbc.e05-04-0277
3. Denker A, Rizzoli SO. 2010. Synaptic vesicle pools: An update. *Front Synaptic Neurosci* 2:1–12. doi:10.3389/fnsyn.2010.00135
4. Desai RC, Vyas B, Earles CA, Littleton JT, Kowalchuck JA, Martin TFJ, Chapman ER. 2000. The C2B domain of synaptotagmin is a Ca²⁺-sensing module essential for exocytosis. *J Cell Biol* 150:1125–1135. doi:10.1083/jcb.150.5.1125
5. Fukuda M, Katayama E, Mikoshiba K. 2002. The calcium-binding loops of the tandem C2 domains of synaptotagmin VII cooperatively mediate calcium-dependent oligomerization. *J Biol Chem* 277:29315–29320. doi:10.1074/jbc.M201697200
6. Fukuda M, Mikoshiba K. 2000. Calcium-Dependent and -Independent Hetero-Oligomerization in the 645:637–645.
7. Guan Z, Bykhovskaia M, Jorquera RA, Sutton RB, Akbergenova Y, Littleton JT. 2017. A synaptotagmin suppressor screen indicates SNARE binding controls the timing and Ca²⁺ cooperativity of vesicle fusion. *Elife* 6:1–30. doi:10.7554/eLife.28409
8. Hui E, Bai J, Wang P, Sugimori M, Llinas RR, Chapman ER. 2005. Three distinct kinetic groupings of the synaptotagmin family: candidate sensors for rapid and delayed exocytosis. *Proc Natl Acad Sci U S A* 102:5210–4. doi:10.1073/pnas.0500941102
9. Jackman SL, Turecek J, Belinsky JE, Regehr WG. 2016. The calcium sensor synaptotagmin 7 is required for synaptic facilitation. *Nature* 529:88–91. doi:10.1038/nature16507
10. Lee J, Littleton JT. 2015. Transmembrane tethering of synaptotagmin to synaptic vesicles controls multiple modes of neurotransmitter release. *Proc Natl Acad Sci* 112:201420312. doi:10.1073/pnas.1420312112
11. Liu H, Bai H, Hui E, Yang L, Evans CS, Wang Z, Kwon SE, Chapman ER. 2014. Synaptotagmin 7 functions as a Ca²⁺-sensor for synaptic vesicle replenishment. *Elife* 2014:1–18. doi:10.7554/eLife.01524.001
12. Mackler JM, Drummond JA, Loewen CA, Robinson IM, Reist NE. 2002. The C2B Ca²⁺-binding motif of synaptotagmin is required for synaptic transmission in vivo. *Nature* 418:340–344. doi:10.1038/nature00846
13. Rizzoli SO. 2014. Synaptic vesicle recycling: Steps and principles. *EMBO J* 33:788–822. doi:10.1002/embj.201386357
14. Schupp M, Malsam J, Rüter M, Scheutrow A, Wierda KDB, Söllner TH, Sørensen JB. 2016. Interactions between SNAP-25 and synaptotagmin-1 are involved in vesicle priming, clamping spontaneous and stimulating evoked neurotransmission. *J Neurosci* 36:11834–11836. doi:10.1523/JNEUROSCI.1011-16.2016
15. Takamori S, Holt M, Stenius K, Lemke EA, Grønborg M, Riedel D, Urlaub H, Schenck S, Brügger B, Ringler P, Müller SA, Rammner B, Gräter F, Hub JS, De Groot BL, Mieskes G, Moriyama Y, Klingauf J, Grubmüller H, Heuser J, Wieland F, Jahn R. 2006. Molecular Anatomy of a Trafficking Organelle. *Cell* 127:831–846. doi:10.1016/j.cell.2006.10.030
16. Yoshihara M, Guan Z, Littleton JT. 2010. Differential regulation of synchronous versus

asynchronous neurotransmitter release by the C2 domains of synaptotagmin 1. *Proc Natl Acad Sci U S A* 107:14869–14874. doi:10.1073/pnas.1000606107

17. Zhou Q, Lai Y, Bacaj T, Zhao M, Lyubimov AY, Uervirojnangkoorn M, Zeldin OB, Brewster AS, Sauter NK, Cohen AE, Soltis SM, Alonso-Mori R, Chollet M, Lemke HT, Pfuetzner RA, Choi UB, Weis WI, Diao J, Südhof TC, Brunger AT. 2015. Architecture of the synaptotagmin-SNARE machinery for neuronal exocytosis. *Nature* 525:62–67. doi:10.1038/nature14975

**Appendix: Increasing *in vivo* fluorescence of endogenous SYT7
using the Split-GFP system**

Mónica C. Quiñones-Frías and J. Troy Littleton

The Picower Institute for Learning and Memory, Department of Biology, Massachusetts
Institute of Technology, Cambridge, MA 02139

This work was performed by Mónica C. Quiñones-Frías. This work is unpublished.

Results

Generation of *Syt7*^{7xGFP11}

The endogenous CRISPR-tagged RFP and GFP tagged SYT7 lines are too dim to perform live imaging, though they can be used for fixed staining with anti-RFP and anti-GFP antisera. To create a system that would allow dynamic imaging of SYT7 localization, and potential shifts in SYT7 movement during the synaptic vesicle cycle, the Split-GFP system was used to improve the endogenous fluorescence of SYT7. GFP is a beta barrel protein made from 11 beta-strands. GFP can be separated into two fragments that only fluoresce when brought together. GFP is split from beta strands 1-10 (GFP1-10) and 11 (GFP11) (Cabantous et al., 2005). GFP 11 is a short peptide of 16 amino acids that is cloned into the protein of interest. Multiple GFP 11 tags can be introduced into the protein of interest to increase the number of GFPs assembled on the protein of interest (Kamiyama et al., 2016). To tag the C-terminus of SYT7, seven GFP11 tags were introduced before the stop codon of the *Syt7* locus using CRISPR to generate an endogenously tagged line (*SYT7*^{7xGFP11}). *Drosophila* strains overexpressing GFP1-10 with *elav*-Gal4 were crossed to *SYT7*^{7xGFP11} animals. In the absence of endogenously tagged *SYT7*^{GFP11}, we did not detect fluorescence at nerve terminals when GFP1-10 was overexpressed in neurons (not shown). When expressed together, endogenous SYT7 labeling was observed in larval neuromuscular junctions of live animals (**Figure 1A**).

Activity does not seem to drive remodeling of the SYT7 compartment

Understanding the dynamics of the SYT7 compartment could provide clues into how the protein regulates neurotransmitter release at the larval *Drosophila* NMJ. The structure of the SYT7

compartment might change during activity to interact with other compartments, like active zones, to regulate neurotransmitter release. The Split-GFP system was used to label SYT7 *in vivo*. At rest, the SYT7 compartment appears to be dynamic, with movements of the brightest puncta within the terminal (**Figure 1A**). To test if activity alters mobility of the SYT7 compartment, the preparation was stimulated with high potassium for 1 min. An image was taken before and after stimulation for comparison. Although bleaching was detected, the structure of the compartment overall did not appear to be altered (**Figure 1B**).

SYT7 localization in the presynaptic terminal is not disrupted by acute alterations to the actin cytoskeleton

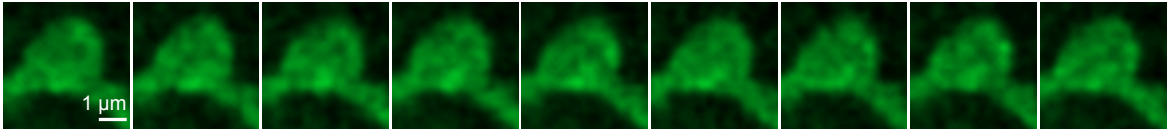
The SYT7 compartment appeared to be highly dynamic at rest. This suggests that it could be associated with the cytoskeleton. To test this hypothesis, the Split-GFP system was used to label SYT7 *in vivo* in the presence of the actin polymerization blocker, latrunculin. Treatment with latrunculin for 15 min did not appear to affect the distribution of SYT7^{7xGFP11} at nerve terminals (**Figure 2A**). As a positive control, actin was labeled using a transgenic Actin^{GFP} strain and actin patches were visualized throughout the nerve terminal during the experiment (**Figure 2B**). Treatment with latrunculin for 15 min disrupted actin localization throughout the terminal and significantly reduced the intensity of Actin^{GFP} at nerve terminals (**Figure 2C**). These data indicate that the SYT7 compartment is quite mobile with presynaptic terminals, but this mobility is not obviously altered by enhancing synaptic activity or disrupting the actin cytoskeleton.

References

1. Cabantous S, Terwilliger TC, Waldo GS. 2005. Protein tagging and detection with engineered self-assembling fragments of green fluorescent protein. *Nat Biotechnol* **23**:102–107. doi:10.1038/nbt1044
2. Kamiyama D, Sekine S, Barsi-Rhyne B, Hu J, Chen B, Gilbert LA, Ishikawa H, Leonetti MD, Marshall WF, Weissman JS, Huang B. 2016. Versatile protein tagging in cells with split fluorescent protein. *Nat Commun* **7**. doi:10.1038/ncomms11046

A

Before stimulation



B

After 10 Hz stimulation for 50 seconds

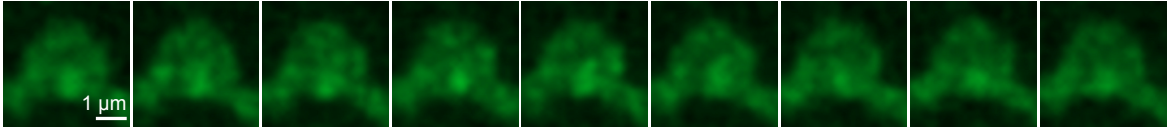


Figure 1. SYT7^{7xGFP11} before and after 10 Hz stimulation for 6 seconds. (A) SYT7^{7xGFP11} appears to have some dynamics but it does not rearrange rapidly. (B) The same bouton was imaged after 10 Hz stimulation and appears to have a similar labeling pattern to SYT7^{7xGFP11} at rest. Scale bar = 1 μ m.

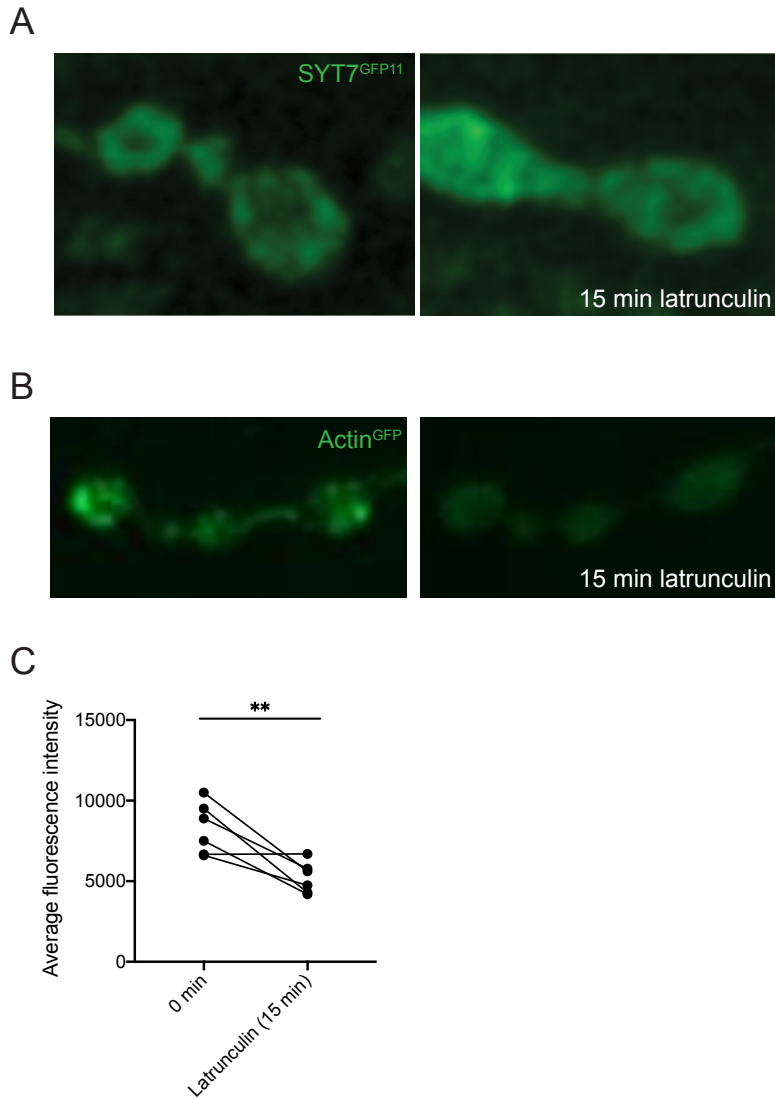


Figure 2. SYT7^{7xGFP11} after latrunculin treatment. (A) SYT7^{7xGFP11} without latrunculin treatment (left) and after 15 min latrunculin treatment (right). (B) Actin^{GFP} without latrunculin treatment (left) and after 15 min latrunculin treatment (right). (C) Quantification of Actin^{GFP} before and after latrunculin treatment. Actin^{GFP} staining is significantly reduced after latrunculin treatment. **, $p \leq 0.01$.